

**MOLECULAR CHARACTERIZATION OF RUBELLA VIRUS NONSTRUCTURAL
PROTEINS AND VIRAL RNA SYNTHESIS**

By

Yuying Liang

B. Sc., Sichuan University, P. R. China, 1992

M. Sc., Shanghai Institute of Biochemistry, Academia Sinica, 1995

A thesis submitted in partial fulfillment of the requirements for the degree of Doctor of
Philosophy in the Faculty of Graduate Studies, Genetics Program

We accept this thesis as conforming to the required standard

The University of British Columbia

© Yuying Liang. 1999 September 2000.

In presenting this thesis in partial fulfilment of the requirements for an advanced degree at the University of British Columbia, I agree that the Library shall make it freely available for reference and study. I further agree that permission for extensive copying of this thesis for scholarly purposes may be granted by the head of my department or by his or her representatives. It is understood that copying or publication of this thesis for financial gain shall not be allowed without my written permission.

Department of Genetics Graduate Program

The University of British Columbia
Vancouver, Canada

Date Oct 3, 2000

ABSTRACT

Rubella virus (RV) is a single-strand positive RNA virus. Its 9762-nucleotide (nt) genomic RNA contains two large open reading frames (ORFs) at the 5'- and 3'-termini, encoding nonstructural and structural proteins, respectively. The nonstructural proteins (NSPs) are first translated as a 200-kDa polyprotein (p200), which undergoes a single proteolytic cleavage into p150 and p90 by an intrinsic protease, the RV nonstructural protease (NS-pro).

The purpose of this thesis work is to characterize RV NSPs and viral RNA synthesis at the molecular level, including the characterization of the RV NS-pro domains, the roles of NSPs in viral RNA synthesis, and the regulatory mechanism for viral RNA synthesis.

RV NS-pro is an M-group papain-like cysteine protease (PCP) with both *trans*- and *cis*-cleavage activities. Employing an *in vitro* translation system, I mapped the regions of NS-pro required for *trans*- and *cis*- activities, and demonstrated the importance of an X domain in *trans*-cleavage activity. RV NS-pro catalytic region was also predicted to have a papain-like folding from primary and secondary structure analyses.

The time course of RV RNA synthesis was precisely determined. Synthesis of negative-strand RNA stops after 10 h postinfection (hpi), and subsequently switches to highly efficient synthesis of positive-strand RNAs (genomic and subgenomic RNA). The roles of respective NSPs and the underlying regulatory mechanism for RV RNA synthesis were investigated by mutational analysis and complementation experiments. Processing of p200 was found to be crucial for virus replication. Uncleaved p200 was shown to be functional in negative-strand RNA synthesis but not for positive-strand RNA. In contrast, the complex formed by the

cleavage products p150/p90 is not an active replicase for negative-strand RNA, but is required for the efficient generation of positive-strand RNAs. Syntheses of both negative- and positive-strand RV RNAs were found to be *cis*-preferential from complementation experiments.

A mechanism for RV NSP translation, processing and RV RNA replication was proposed. Newly translated p200 functions in *cis* to synthesize a full-length negative-strand RNA. The subsequent processing of p200 into p150/p90 converts this replicase into one with positive-strand RNA specificity, which functions in *cis* to produce genomic and subgenomic RNA efficiently.

TABLE OF CONTENTS

ABSTRACT.....	ii
LIST OF TABLES	vi
LIST OF FIGURES	vii
LIST OF ABBREVIATIONS.....	viii
ACKNOWLEDGEMENTS	x
1. INTRODUCTION.....	1
1.1. Rubella virus (RV) biology.....	1
1.1.1. Classification.....	1
1.1.2. Clinical aspects.....	1
1.1.3. Virion structure and virion proteins	2
1.1.4. Genome organization and sequence information.....	4
1.1.5. Replication features and infection cycles	6
1.1.6. Attachment, entry and uncoating	7
1.1.7. RV nonstructural proteins (NSPs).....	8
1.1.8. Replication complexes and viral RNA synthesis	9
1.1.9. Expression and processing of RV structural proteins (SPs)	10
1.1.10. Virus assembly and budding.....	13
1.2. Viral encoded papain-like cysteine proteases (PCPs)	16
1.2.1. Viral proteases.....	16
1.2.2. The papain-like cysteine protease (PCP) family	17
1.2.3. The M-, and L- group PCPs.....	18
1.2.4. Alphavirus NS protease	19
1.2.5. RV NS protease (NS-pro).....	20
1.3. Replication of positive-strand RNA viruses	20
1.3.1. RNA replication studies on some model positive-strand RNA viruses: poliovirus, BMV, and alphavirus.	21
1.3.2. Common replication strategies of positive-strand RNA viruses.....	27
1.3.3. <i>Cis</i> -preferential replication	30
2. PROJECT RATIONALE AND THESIS OBJECTIVES	33
3. MATERIALS AND METHODS	35
3.1. Materials and supplies.....	35
3.2. Methods	35
3.2.1. Growth of cells and viruses	35
3.2.2. Propagation of bacterial strains.....	36
3.2.3. Preparation of competent cells and transformation.....	36
3.2.4. Mini preparation of plasmid DNA	36
3.2.5. Restriction endonuclease digestions and DNA modifications.....	37
3.2.6. Polymerase Chain Reaction	38
3.2.7. Plasmid Construction.....	39
3.2.8. <i>In vitro</i> transcription.	46
3.2.9. <i>In vitro</i> translation	47
3.2.10. Vero cells transfected by RNA transcripts using Lipofectin.	47
3.2.11. BHK-21 cells transfected by RNA transcripts using electroporation	48

3.2.12.	Plaque assay and virus growth analysis.....	48
3.2.13.	Metabolic labeling.....	49
3.2.14.	Immunoprecipitation	49
3.2.15.	Total RNA preparation	50
3.2.16.	RNase protection assay (RPA).....	50
3.2.17.	Electrophoresis	53
3.2.18.	Image analysis and cleavage efficiency comparison.....	54
3.2.19.	Sequence analysis.....	55
4.	RESULTS AND DISCUSSIONS.....	56
4.1.	Characterization of domains involved in cis- and trans-cleavage activities of RV	
NS-pro	56
4.1.1.	Processing of RV NSP by <i>in vitro</i> translation.....	56
4.1.2.	Construction of truncated NS-pro cDNA clones.	59
4.1.3.	Defining the NS-pro domain required for <i>trans</i> cleavage.	61
4.1.4.	Domains required for <i>cis</i> cleavage.....	64
4.1.5.	Effect of N-terminal regions on cleavage efficiency.....	66
4.1.6.	Secondary structure prediction for RV NS-pro.....	69
4.1.7.	Discussion I.....	72
4.2.	Effects of NSP cleavage on virus replication and RNA synthesis.....	76
4.2.1.	Construction of mutants.....	76
4.2.2.	Effects of mutations on NSP processing.	77
4.2.3.	Effects of mutations on virus growth.	79
4.2.4.	Effects of mutations on viral RNA synthesis.....	83
4.2.5.	Discussion II	91
4.3.	Molecular characterization of RV RNA synthesis	96
4.3.1.	RV RNA replication is <i>cis</i> -preferential.	96
4.3.2.	Time course of RV RNA synthesis.	103
4.3.4.	Discussion III	105
5.	SUMMARY AND PERSPECTIVE.....	110
	REFERENCES.....	112

LIST OF TABLES

Table 1. Sequence information on oligonucleotide primers used in this work.	40
Table 2. Mutations created at the catalytic site and around the cleavage site.	77
Table 3. Effects of RV NSP cleavage mutants on virus replication.	80
Table 4. Comparison of the relative amounts of RNAs produced in the WT and mutants.....	89

LIST OF FIGURES

Figure 1. Genome organization of RV and SIN.	5
Figure 2. Replication strategy of RV.	10
Figure 3. Predicted membrane topology of the RV SPs.....	12
Figure 4. Poliovirus genome organization.....	22
Figure 5. Genome organization of brome mosaic virus (BMV).....	24
Figure 6. Locations of PCR primers for serial deletions on RV genome.....	41
Figure 7. Locations of PCR primers for site-directed mutagenesis on RV genome.	45
Figure 8. Probes used in RNase protection assay (RPA) and the relative positions and lengths of the protected regions.	51
Figure 9. RV NSP processing in <i>in vitro</i> translation systems with or without addition of Zn ²⁺	57
Figure 10. RV p200(G1301S) and p150 cleave substrate protein in <i>trans</i>	59
Figure 11. Plasmids and protease-encoding constructs.....	60
Figure 12. <i>In vitro</i> translation of protease constructs (A ₃₄₈ /G ₁₃₀₁ , M ₈₂₇ /G ₁₃₀₁ , V ₉₂₀ /G ₁₃₀₁ , A ₉₇₄ /G ₁₃₀₁ , A ₁₀₂₀ /G ₁₃₀₁ , and G ₁₁₀₂ /G ₁₃₀₁) and examination of their <i>trans</i> -cleavage activities.	62
Figure 13. <i>In vitro</i> translation of protease constructs (V ₉₂₀ /H ₁₂₉₀ , V ₉₂₀ /V ₁₂₉₅ , V ₉₂₀ /P ₁₂₉₆ , V ₉₂₀ /L ₁₂₉₇ , and V ₉₂₀ /R ₁₂₉₉) and examination of their <i>trans</i> -cleavage activities.	63
Figure 14. Autolytic processing of protease constructs V ₉₂₀ /I ₁₇₇₃ , A ₉₇₄ /I ₁₇₇₃ , A ₁₀₂₀ /I ₁₇₇₃ , and G ₁₁₀₂ /I ₁₇₇₃	65
Figure 15. Cleavage efficiencies of protease constructs.	68
Figure 16. Comparison of primary and secondary structures between RV NS-pro and papain.	71
Figure 17. Functional domains of RV NS-pro and comparison with complete papain sequence.	73
Figure 18. Effects of mutations on NSP processing in an <i>in vitro</i> translation system.	78
Figure 19. Comparison of processing ratios between the WT and mutant NSPs.....	79
Figure 20. Immunoprecipitation of RV-specific SPs from cells transfected by WT and mutant RNAs.....	81
Figure 21. Growth curves of the WT, G1300A, and R1299A mutant viruses.	83
Figure 22. Sensitivity of RPA for detection of both positive- and negative-strand RV RNAs.	85
Figure 23. RNA analysis of the WT and mutant constructs.....	88
Figure 24. Comparison of WT and mutant G1301S on the levels of negative-strand RNA synthesis.	90
Figure 25. <i>Trans</i> complementation of RV replication.	98
Figure 26. Schematic diagrams of constructed replication-defective mutants.	99
Figure 27. Synthesis of positive-strand RNA is <i>cis</i> -preferential.	102
Figure 28. Accumulated amounts of viral RNAs during virus infection.	104
Figure 29. Proposed mechanism for RV NSP translation, processing, and viral RNA synthesis.	109

LIST OF ABBREVIATIONS

A	absorbance
ATCC	American Type Culture Collection
ATP	adenosine triphosphate
BHK	baby hamster kidney cell line
BMV	brome mosaic virus
bp	base pair
BSA	bovine serum albumin
BVDV	Bovine viral diarrhea virus
CIP	calf intestinal alkaline phosphatase
CRS	congenital rubella syndrome
cpm	count per minute
CTP	cytidine triphosphate
DI	defective-interfering
DMEM	Dulbecco's modified Eagle's medium
DMSO	dimethyl sulfoxide
DNA	deoxyribonucleic acid
DNase	deoxyribonuclease
dNTPs	deoxynucleoside triphosphates
DTT	dithiothreitol
EAV	equine arteritis virus
EDTA	ethylene diaminetetraacetic acid
EM	electron microscopy
EMBL	European Molecular Biology Laboratory
ER	endoplasmic reticulum
FCS	fetal calf serum
FMDV	the foot-and-mouth virus
GTP	guanosine triphosphate
h	hour
hpi	hour post infection
HAV	hypovirulence-associated virus
HI	hemagglutination inhibition
ICTV	International Committee on Taxonomy of Viruses
IRES	Internal ribosomal entry site
kb	kilobase
kDa	kilodalton
kV	kilovolt
Lpro	leader protease
M	molar
m.o.i	multiplicity of infection
MEM	minimal essential medium
mg	milligram
MHV	Mouse hepatitis virus
min	minute
ml	milliliter
mM	millimolar

MOPS	3-[N-morpholino]-propanesulfonic acid
ng	nanogram
NIH	National Institutes of Health
nm	nanometer
NSP	nonstructural protein
NS-pro	nonstructural protease
nt	nucleotide
OD ₂₆₀	absorbance at 260 nm wavelength
ORF	open reading frame
PAGE	polyacrylamide gel electrophoresis
PBS	phosphate-buffered saline
PCP	papain-like cysteine protease
PCR	polymerase chain reaction
PEG	polyethylene glycol
PFU	plaque forming unit
pg	picogram
PIPES	piperazine-N, N'-bis[2-ethane-sulfonic acid]
PMSF	phenylmethylsulfonyl fluoride
RdRp	RNA-dependent RNA polymerase
RNA	ribonucleic acid
RNase	ribonuclease
RPA	RNase protection assay
rpm	rotation per minute
RRV	Ross River virus
RT	room temperature
RV	rubella virus
s	second
S	Svedberg unit
SDS	sodium dodecyl sulfate
SFV	Semliki Forest Virus
SIN	Sindbis Virus
SL	stem-loop
SP	structural protein
ss	single-stranded
TM	transmembrane domain
Tris	trishydroxymethylaminomethane
ts	temperature sensitive
TYMV	turnip yellow mosaic virus
ug	microgram
UTP	uridine triphosphate
UTR	untranslated region
VLP	Virus-like particle
WT	wild type
YFV	yellow fever virus

ACKNOWLEDGEMENTS

First, I would like to thank my supervisor, Dr. Shirley Gillam, for giving me an opportunity to pursue the graduate study, for her advice, support, and encouragement throughout.

I would also like to thank members in my supervisory committee, Drs. Caroline Astell, Peter Candido, and Ann Rose for their advice, suggestion, and discussions.

Thank you to Jiansheng, Dawei, Zhiyong (Joe), Karen, and Hanwei for all the helps, and to many people in the B.C. Research Institute for a wonderful working environment.

I was supported by the studentship award from BC Research Institute for Children's and Woman's Health.

This thesis is dedicated to my parents.

1. INTRODUCTION

1.1. *Rubella virus (RV) biology*

1.1.1. Classification

Rubella virus (RV) is the single member of the *Rubivirus* genus of the *Togaviridae* family, which consists of two genera – *Alphavirus* and *Rubivirus* (Francki *et al.*, 1991). Members of this family are small enveloped viruses with a single-strand positive RNA genome. The *Alphavirus* genus contains 27 distinct arthropod-transmitted viruses, which can replicate in both arthropod and vertebrate hosts. In contrast, the only known natural reservoir for RV is in humans and RV has no known invertebrate host. Extensive studies have been carried out on the structure and replication of *Sindbis virus* (SIN), the prototype of alphaviruses (for a review, see Strauss and Strauss, 1994).

1.1.2. Clinical aspects

RV is the causative agent of a benign disease, German measles (also known as rubella, 3-day measles) characterized by symptoms including maculapapular rash, lymphadenopathy, low-grade fever, conjunctivitis, sore throat, and arthralgia (for a review see Wolinsky, 1996). The major health concern with RV is its teratogenicity. The incidence of birth defects in babies born to women infected during the first trimester approaches 80%. The birth defects, collectively known as congenital rubella syndrome (CRS), involve heart defects, cataracts, deafness, and mental retardation (Frey, 1994). Immunization of infants and susceptible women of childbearing age against RV infection has dramatically reduced the incidence of both rubella and CRS. However, RV remains a significant human pathogen as shown by the resurgence of

rubella despite a vaccination program, the significant incidence of joint involvement (transient arthralgia and arthritis, chronic arthritis) following virus infection or vaccination, and its association with chronic diseases including autoimmune diseases (Frey, 1994).

1.1.3. Virion structure and virion proteins

RV is a small spherical particle of 60-70 nm diameter (Bardeletti *et al.*, 1975). Thin-section electron microscopy of the virion reveals a 30-35 nm electron-dense core surrounded by an electron-lucent zone between the core and the virion envelope (Murphy *et al.*, 1968; Murphy, 1980). The central core, suggested to have a $T = 3$ icosahedral symmetry (Frey, 1994), contains a single copy of an RNA genome protected by multiple copies of capsid protein. On the lipid bilayer envelope, the glycoproteins form rather poorly resolvable 6- to 8-nm surface spikes (Trudel *et al.*, 1980). Following degradation of virions, spherical subunits that form hexagonal and pentagonal arrays were observed, possibly representing an end-on view of the virion spike (Payment *et al.*, 1975; Frey, 1994). It is unknown whether the glycoproteins on the RV envelope form a similar $T = 4$ icosahedral lattice to those of alphavirions (Strauss and Strauss, 1994).

RV is composed of three structural proteins (SP), the capsid protein C and two envelope glycoproteins, E1 and E2 (Oker-Blom *et al.*, 1983; Clarke *et al.*, 1987). The non-glycosylated C protein has 299 amino acids and is rich in proline and arginine residues (Clarke *et al.*, 1987; Frey and Marr, 1988). The cluster of positively-charged residues may be involved in binding to the genomic RNA in nucleocapsids. With a molecular mass of 35 kDa, C migrates as a doublet on polyacrylamide gel electrophoresis, the lower band being of greater intensity than the upper one (Oker-Blom *et al.*, 1983; Marr *et al.*, 1991). In addition, the capsid protein in virions has

been reported to be a disulfide-linked dimer (Waxham and Wolinsky, 1983; Baron and Forsell, 1991). Nevertheless, dimerization of capsid protein does not seem to be required for virus particle formation (Lee *et al.*, 1996).

From the deduced sequence, the large surface glycoprotein E1 is a 412-amino-acid protein and migrates as a discrete band of 58 kDa (Clarke *et al.*, 1987). Monoclonal antibodies against E1 exhibit hemagglutination inhibition (HI) and/or neutralization activity, suggesting that E1 contains hemagglutination activity and neutralization domains (Green and Dorsett, 1986; Gerna *et al.*, 1987; Ho-Terry and Cohen, 1985; Trudel *et al.*, 1985; Umino *et al.*, 1985; Waxham and Wolinsky, 1983, 1985b). Although most monoclonal antibodies against E1 recognize non-linear epitopes, the linear epitopes recognized by some anti-E1 monoclonal antibodies have been mapped. Epitopes that react with monoclonal antibodies specific for hemagglutination and neutralization have been defined between amino acids 245 and 285 (Terry *et al.*, 1988), and between amino acids 202 and 283 (Wolinsky *et al.*, 1991). Chaye *et al.* (1992) further mapped the hemagglutination epitope to amino acids between 214 and 240, and two neutralization epitopes to amino acids between 214 and 233, and between 219 and 233, respectively.

E2, the heavily glycosylated envelope protein, migrates as a smear between 42 and 54 kDa (Oker-Blom *et al.*, 1983). These forms of E2 derive from a single protein (deduced 281 amino acids) with different extents of glycosylation (Clarke *et al.*, 1987; Waxham and Wolinsky, 1985b). The biological role of E2 remains obscure, although it appears to contain one neutralization epitope (Green and Dorsett, 1986) and a strain-specific epitope (Dorsett *et al.*, 1985). E2 is required for cell surface expression of E1 (Hobman *et al.*, 1990). Very few E2-specific monoclonal antibodies are isolated compared to the large number of E1-specific when mice are immunized with whole RV (Green and Dorsett, 1986; Waxham and Wolinsky, 1983),

possibly due to poor immunogenicity of E2 in native virions. In fact, E2 epitopes seem to be buried under E1 in the glycoprotein spike complexes (Ho-Terry and Cohen, 1984; Katow and Sugiura, 1988a; Waxham and Wollinsky, 1985a; Green and Dorsett, 1986).

In the alphavirions, E1 and E2 form a heterodimer by noncovalent bonds and three heterodimers form each surface spike (Vogel *et al.*, 1986; Anthony and Brown, 1991). Although the structure of the RV surface spikes has not been defined, there is evidence that E1 and E2 form a complex in the virion. E1-E2 heterodimers were observed when virions were disrupted with nonionic detergent (Dorsett *et al.*, 1985; Baron and Forsell, 1991) as well as when E1 and E2 were coexpressed from cDNA constructs (Baron and Forsell, 1991). A small fraction of the glycoproteins in the virion is disulfide-linked, including E1-E1 homodimer and E1-E2 heterodimer (Waxham and Wolinsky, 1983; Dorsett *et al.*, 1985). Moreover, the E1-E1 homodimers seem to be present in a complex with E2 since they can be immunoprecipitated by both anti-E1 and anti-E2 antiserum (Baron and Forsell, 1991).

1.1.4. Genome organization and sequence information

The RV genome (Fig. 1) is a single-strand positive RNA of 9762 nucleotides (nt) (Pugachev *et al.*, 1997a) encoding two large open reading frames (ORFs). The 5'-proximal nonstructural protein-ORF (NSP ORF) from nt 41 to nt 6388 encodes nonstructural proteins involved in viral RNA synthesis (Pugachev *et al.*, 1997a; Yao *et al.*, 1998); the 3'-proximal structural protein-ORF (SP ORF) from nt 6512 to nt 9701 encodes structural proteins required for virus assembly (Clarke *et al.*, 1987; Dominguez *et al.*, 1990; Pugachev *et al.*, 1997).

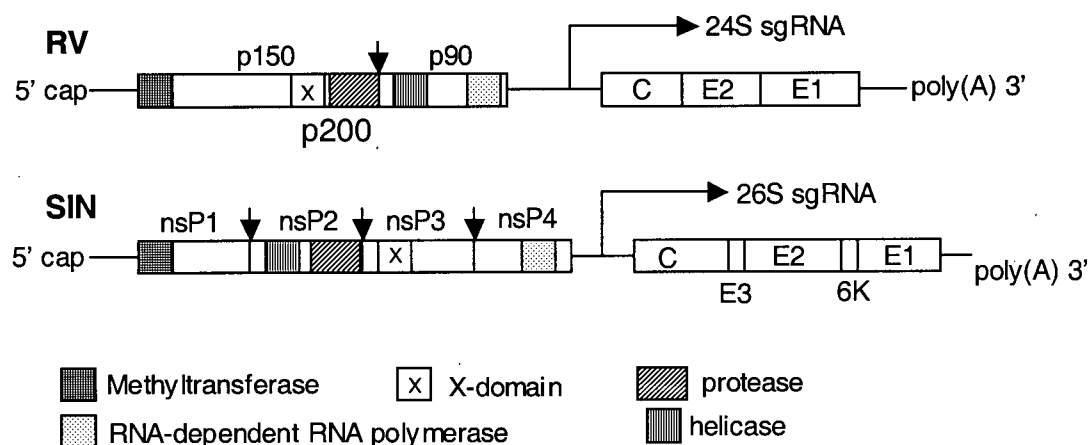


Figure 1. Genome organization of RV and SIN.

Both genomes contain two large ORFs, NSP and SP ORFs, at the 5' and 3' ends, respectively. NSPs of the two viruses are first translated as polyprotein precursors, which are processed into final cleavage products by virus-encoded proteases. RV NSP polyprotein p200 is cleaved once into p150 and p90, whereas SIN NSP is cleaved into four final products, nsP1 to nsP4. RV and SIN NSPs share a conserved domain with unknown function called the X domain. Four conserved enzyme motifs identified in a number of positive-strand RNA viruses, the methyltransferase, protease, helicase and RNA-dependent RNA polymerase (RdRp), were also identified in RV and SIN. However, the order of these domains in RV differs from that of SIN. SPs of both viruses are translated as polyproteins from subgenomic RNAs, which are produced during virus infection, and posttranslationally cleaved into C, E2 and E1, with an additional two small peptides E3 and 6K in SIN. (Modified from Frey, 1994).

The 5' and 3' ends of the RV genome can bind specific host proteins (Pogue *et al.*, 1993; Nakhasi *et al.*, 1994; Chen and Frey, 1999) and are presumed to be critical *cis* elements for viral RNA synthesis. The 5' end contains a 14-nt single-stranded leader (ss-leader) followed by a stem-and-loop structure [5'(+)SL] (nt 15 to nt 65), the complement of which at the 3' end of the negative-strand RNA [3'(-)SL] has been proposed to function as a promoter for synthesis of positive-strand genomic RNA. Pugachev and Frey (1998) examined the effects of the 5' end structure on virus replication by making mutations and deletions in an infectious cDNA clone. It was revealed that the AA dinucleotide at nt 2 and 3 is of critical importance whereas mutations in the other positions caused variable but not lethal effects. In general, mutations

within the stem had a more profound effect on viral phenotype than did mutations in either the ss-leader or upper loop. The 5'(+)SL was found to be important for efficient translation of the NSP ORF. In contrast, positive-strand RNA synthesis was unaffected by the 5'(+)SL mutations as well as the ss-leader mutations, which argues against the proposed function of the 3'(-)SL as a promoter for initiation of the genomic positive-strand RNA.

The 3' end of the RV genome contains four SL structures. SL1 and SL2 are both located in the E1 coding region, while SL3 and SL4 are within the 59-nt 3'-untranslated region (UTR) preceding the poly(A) tract. SL2 is a structure shown to interact with human calreticulin (Singh *et al.*, 1994), an autoantigen potentially involved in RV RNA replication and pathogenesis. Site-directed mutagenesis of the 3' UTR with an RV infectious cDNA clone (Chen and Frey, 1999) revealed that most of the 3' UTR is required for viral viability except for the 3'-terminal 5 nt and the poly(A) tract, although poly(A) was rapidly regenerated during subsequent replication. Maintenance of the overall SL3 structure, the 11-nt single-stranded sequence between SL3 and SL4 and the sequences forming SL4 were all important for viral viability. In contrast to a previous proposal, maintenance of the SL2 stem rather than the U-U bulge was critical in calreticulin binding. However, mutations in the SL2 stem or the U-U bulge gave rise to viable viruses when introduced into an infectious cDNA clone, indicating that binding of calreticulin to SL2 is independent of viral viability.

1.1.5. Replication features and infection cycles

Compared to the rapid and efficient replication of alphavirus, RV infection has a long latency period, slow replication cycle, and low virus production (Hemphill *et al.*, 1988). Differences in the replication features between RV and alphavirus are summarized as follows. (1) Alphavirus

can infect a wide range of host cells, including an acute, usually short-duration infection in vertebrates and a persistent lifelong infection in arthropods. This situation is mirrored in cell culture (Strauss and Strauss, 1994). RV replicates in a number of primary cell cultures and continuous cell lines of vertebrates, but fails to infect mosquitoes (Tesh and Rosen, 1975). (2) Alphavirus infection reaches a peak by 4 to 8 h after a 2 to 3-h latent period, whereas RV infection has a latent period of 24 h and reaches peak level by 48 to 72 h. (3) Alphavirus can grow to high titers (10^9 PFU/ml) in cultured vertebrate cells. In contrast, RV normally grows to a very low titer in most cell lines except for Vero and BHK-21 cells, the two most used permissive cell lines to grow RV with a titer of 10^7 - 10^8 PFU/ml (Frey, 1994). (4) Alphavirus infection shuts down host RNA and protein synthesis, whereas inhibition of host protein synthesis by RV infection is indistinguishable until 40 hpi and reaches 40% at 44 hpi (Hemphill *et al.*, 1988).

Some other features of RV replication include the profound inhibitory effects of interferon α and γ on the synthesis of viral RNAs and proteins, and the time-dependent inhibition by actinomycin D and α -amanitin (Nakhasi *et al.*, 1988).

1.1.6. Attachment, entry and uncoating

RV attaches to susceptible cells rapidly, mostly within 1 h. The RV receptor on the host cell surface has not been identified. It is believed that RV enters cells through receptor-mediated endocytosis. The low pH environment of endosomes triggers the fusogenic activity of the viral glycoproteins, causing fusion of the virus membrane with the endosomal membrane and resulting in the release of the viral nucleocapsid into the cytoplasm. Consistent with this hypothesized entry mechanism, exposure of the RV glycoproteins to low pH causes a fusogenic

activity (Katow and Sugiura, 1988b). Katow and Sugiura (1988a) suggested that RV E1 plays a vital role in membrane fusion. Sequence analysis revealed an internal hydrophobic domain within E1, which was shown to be involved in membrane fusion by site-directed mutagenesis (Yang *et al.*, 1998). The mechanism for uncoating of the genome from nucleocapsid remains obscure. C protein was found to undergo a conformational change at low pH that renders it hydrophobic (Mauracher *et al.*, 1991), indicating that a low pH environment may also trigger the uncoating process.

1.1.7. RV nonstructural proteins (NSPs)

The uncoated RV genome first serves as the mRNA for the translation of NSPs. A 200-kDa polyprotein, p200, is first produced and processed by intrinsic protease activity into the 150-kDa N-terminal product (p150) and the 90-kDa C-terminal product (p90) (Bowden and Westaway, 1984; Chen *et al.*, 1996; Forng and Frey, 1995; Marr *et al.*, 1994; Yao *et al.*, 1998). Sequence analysis has predicted four conserved enzyme motifs in the NSP sequence, ordered from the N terminus to the C terminus as methyltransferase, protease, helicase and RNA-dependent RNA polymerase (RdRp) (Fig. 1) (Frey, 1994; Koonin and Dolja, 1993). Therefore, the cleavage product p150 carries methyltransferase (Rozanov *et al.*, 1992) and protease (Gorbalenya *et al.*, 1991) motifs on the N and C termini respectively, whereas p90 contains helicase (Gorbalenya *et al.*, 1990) and RdRp motifs (Kamer and Argos, 1984) on the N and C termini, respectively. These four enzyme motifs have also been identified in a number of animal and plant positive RNA viruses, possibly representing universal enzymatic requirements for their viral RNA synthesis (Koonin and Dolja, 1993; Strauss and Strauss, 1994). The protease domain is discussed in more details in section 1.2. The exact role of each RV NSP in viral RNA synthesis remains to be determined.

1.1.8. Replication complexes and viral RNA synthesis

Replication complexes are formed as membrane-bound cytoplasmic vacuoles to synthesize viral RNA during RV infection (Lee *et al.*, 1992, 1994). From immunogold labeling electron microscopy (EM) studies, Magliano *et al.* (1998) identified these membrane-bound structures as virus-modified lysosomes. The replication complexes presumably consist of RV NSPs and host factors. However, no successful isolation of functional replication complexes has been reported. Several host factors specifically binding to the 5' and 3' ends of RV RNA have been identified (Pogue *et al.*, 1993; Nakhasi *et al.*, 1991, 1994) and might be components of replication complexes. Two host proteins, 59 and 52 kDa in size, specifically interact with the RV 5'(+)SL RNA (Pogue *et al.*, 1993), and were identified as Ro/SSA-associated antigens (Nakhasi *et al.*, 1994). The 3'(-)SL structure (complementary negative-strand equivalent of the 5'-(+)SL) is thought to serve as a promoter for the initiation of positive-strand RNA synthesis, although this hypothesis was not confirmed from mutational analysis (Pugachev and Frey, 1998). Nevertheless, three cytosolic proteins with relative molecular masses of 97, 79, and 56 kDa were found to bind specifically to the 3'(-)SL structure (Nakhasi *et al.*, 1991). Host protein binding specifically to the 3' end was found to be a homologue of human calreticulin (Nakhasi *et al.*, 1994), and the binding site was mapped to SL2 (Singh *et al.*, 1994). In addition, Chen and Frey (1999) identified three 3'-end RNA-protein complexes by gel mobility shift assay, and detected six host protein species, with molecular masses of 120, 80, 66, 55, 48, and 36 kDa, interacting with the 3'-UTR.

RV employs a similar RNA replication mechanism to alphavirus (Fig. 2). Upon infection, NSPs are translated from input genomic RNA and form functional replication complexes with host

factors to replicate viral RNA. A full-length negative-strand RNA is first produced on the template of input genomic RNA and serves as the template for the replication of 40S positive-strand genomic RNA and for the transcription of 24S subgenomic RNA, which is initiated at an internal site (U₆₄₃₆) in the negative-strand RNA (Hemphill *et al.*, 1988; Pugachev *et al.*, 1997a).

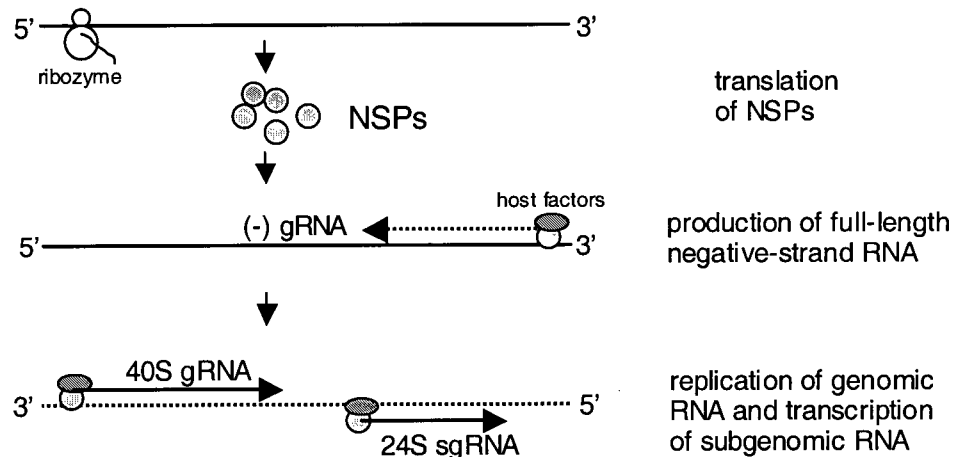


Figure 2. Replication strategy of RV.

Upon infection, NSP is translated from the input genomic RNA and associates with host factors to form replication complexes, which function to replicate viral RNAs. First, a full-length negative-strand RNA is produced and serves as the intermediate for the replication of positive-strand genomic RNA and transcription of subgenomic RNA (Modified from Wolinsky, 1996).

1.1.9. Expression and processing of RV structural proteins (SPs)

RV SPs are translated from the 24S subgenomic RNA as a 110-kDa polyprotein in the order of NH₂-C-E2-E1-COOH (Fig. 1) (Oker-Blom, 1984; Clarke *et al.*, 1987). The p110 is processed into C, E2, and E1, the latter two being further posttranslationally modified during intracellular transport. C is a cytoplasmic protein, whereas E1 and E2 are type I membrane glycoproteins, consisting of an N-terminal large ectodomain, a single transmembrane domain near the C-

terminus, and a short C-terminal cytoplasmic tail (Clarke *et al.*, 1987; Hobman and Gillam, 1989; Hobman *et al.*, 1988; Singer *et al.*, 1987).

RV capsid protein differs from alphavirus capsid protein in the mechanism of its cleavage from the precursor. Alphavirus capsid protein is an autoprotease and releases itself from the polyprotein precursor within the cytoplasm (Aliperti and Schlesinger, 1978; Melancon and Garoff, 1987). In contrast, RV capsid protein does not contain protease activity, and its release from the polyprotein precursor is mediated by host signal peptidase, a luminal enzyme that cleaves signal peptide from proteins following translocation (Clarke *et al.*, 1988; McDonald *et al.*, 1991). The cleavage between C and E2 occurs after the signal sequence of E2, a stretch of hydrophobic amino acids at the C-terminus of capsid protein. The signal sequence of E2 is inserted into the ER membrane and mediates the translocation of E2 into the ER (Hobman and Gillam, 1989; Suomalainen *et al.*, 1990). The C-terminal transmembrane domain of E2 stops the translocation and anchors E2 to membrane (Clarke *et al.*, 1987; Vidgren *et al.*, 1987). Translocation of E1 is mediated by a hydrophobic signal sequence located immediately after the E2 transmembrane domain, and continues until the C-terminal transmembrane domain of E1 is anchored to membrane (Hobman *et al.*, 1988). The cleavage between E2 and E1 occurs just after the E1 signal sequence (Qiu *et al.*, 1994b). The topology of each SP is schematically shown in Fig. 3.

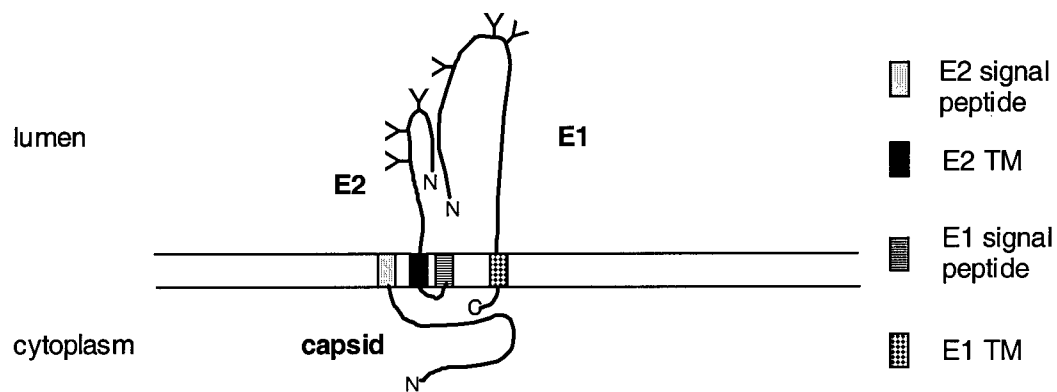


Figure 3. Predicted membrane topology of the RV SPs.

Capsid is a cytosolic protein whereas E2 and E1 are membrane bound with the bulk of their N-termini projecting into the lumen of microsomes. The hydrophobic signal peptides of E2 and E1 (shaded and striped rectangles, respectively) are thought to remain attached to the carboxyl termini of capsid and E2, respectively. E2 and E1 are anchored in the lipid bilayer via a transmembrane domain (TM) near their carboxyl termini (blank and checkered rectangles, respectively). Both E2 and E1 contain three N-linked glycans (Y). The cytoplasmic domain of E2 is a short hydrophilic loop between its TM and the signal peptide of E1. In contrast, E1 has a carboxyl-terminal cytoplasmic tail (C) of 13 amino acids, which may interact with capsid protein. The carboxyl (C) and amino (N) termini of the proteins are indicated (Hobman *et al.*, 1994).

Both E1 and E2 are posttranslationally modified by glycosylation and acylation during the transport from ER through Golgi complex to plasma membrane. High-mannose, hybrid-type, and complex-type N-linked glycans have been found in both E1 and E2 from virions (Sanchez and Frey, 1991), whereas O-linked oligosaccharides are observed only in E2 (Lundstrom *et al.*, 1991; Sanchez and Frey, 1991). Generally, oligosaccharides on glycoproteins play a role in initiation and maintenance of correct folding, protecting polypeptides against proteolysis, and influencing the antigenicity and immunogenicity of glycoproteins (Ng *et al.*, 1990; Gallagher *et al.*, 1992). E2 contains three functional N-linked glycosylation sites. Removal of any site results in slower glycan processing and lower stability, suggesting that mutated E2 proteins are not properly folded and transported, and are rapidly degraded (Qiu *et al.*, 1992b). Moreover,

removal of more than one glycosylation site blocks E2 from cell surface expression (Hobman *et al.*, 1994).

E1, containing hemagglutination and major neutralization epitopes, has three functional N-glycosylation sites (Hobman *et al.*, 1991). The single glycosylation mutants (G1, G2, and G3), but not the double mutant (G2G3) or the triple mutant (G1G2G3), were found to be capable of inducing neutralization antibodies (Qiu *et al.*, 1992a). However, the failure of G1 mutant in producing hemagglutinin inhibition antibody suggested an important role of oligosaccharide at the G1 site in hemagglutination activity (Qiu *et al.*, 1992a).

Formation of E1-E2 heterodimer is required for transport of E1 to the Golgi complex and to the cell surface (Hobman *et al.*, 1990). E2 can be transported to the plasma membrane in the absence of E1 (Hobman and Gillam, 1989). In contrast, unassembled subunits of E1 are arrested in a post-ER, pre-Golgi compartment (Hobman *et al.*, 1992), and require coexpression of E2 for release and targeting to the Golgi complex and to the cell surface (Baron *et al.*, 1992; Hobman *et al.*, 1993). An internal hydrophobic domain within E1 is found to be important in the noncovalent E1-E2 interaction (Yang *et al.*, 1998). Only a small proportion of E1 and E2 is transported to the cell surface. In fact, the bulk of E1 and E2 accumulate in the Golgi-like compartments, facilitating the intracellular budding of virions (Bardeletti *et al.*, 1979; Bowden and Westaway, 1985; Hobman *et al.*, 1990; Payment *et al.*, 1975).

1.1.10. Virus assembly and budding

Assembly of enveloped RNA virus includes encapsidation, the formation of nucleocapsid by specific interactions between capsid protein and genomic RNA, and budding, the acquisition of

viral envelope derived from viral glycoprotein-modified cell membrane. Encapsidation signal, which confers the capability of efficient binding to RNA by capsid protein, has been identified in SIN (Frolova *et al.*, 1997; Owen and Kuhn, 1996), SFV (White *et al.*, 1998), RRV (Frolova *et al.*, 1997), and other viruses. Encapsidation by RV capsid protein is specific for 40S positive-strand genomic RNA (Oker-Blom *et al.*, 1984). A region between nt 330 and nt 617 was identified to bind capsid protein specifically. Further deletion studies narrowed this down to 29 nt between nt 347 and nt 375 (Liu *et al.*, 1996). However, it is unknown whether this sequence is sufficient for genomic RNA packaging. On the other hand, an arginine-rich domain on capsid protein between amino acids 28 and 56 interacted specifically with RV RNA. Nevertheless, other region(s) may also be involved in efficient RNA binding, since the domain between amino acids 28 and 56 has lower RNA binding affinity than intact capsid protein (Liu *et al.*, 1996).

RV virions have been shown to bud from a variety of sites including the Golgi complex, intracellular vacuoles, and plasma membrane (Lee *et al.*, 1992; Murphy, 1980). The intracellular budding of RV is supported by studies on virus-like particles (VLPs), in which all three SPs expressed in mammalian cells were targeted predominantly to the Golgi complex with only a small proportion of E1 and E2 detectable on the plasma membrane, and facilitated the budding of VLPs from these sites (Hobman *et al.*, 1990; Qiu *et al.*, 1994a).

Proteins involved in the budding of enveloped viruses vary (for a review see Garoff *et al.*, 1998). (1) For alphavirus (Simons and Garoff, 1980; Suomalainen *et al.*, 1992) and hepadnavirus (Bruss and Ganem, 1991), budding is driven by interactions between the viral transmembrane proteins and the internal virion components (core, capsid, or nucleocapsid). (2) Some viruses accomplish budding mainly by internal components. For example, core protein

(the Gag protein) of retroviruses (simian immunodeficiency virus, HIV-1) is able to form enveloped particles by itself (Delchambre *et al.*, 1989; Gheysen *et al.*, 1989). Budding of negative-strand RNA viruses (rhabdoviruses, orthomyxoviruses, and paramyxoviruses) is directed predominantly by the matrix protein, although spike proteins (not required absolutely) are also engaged in this process (Li *et al.*, 1993; Liu *et al.*, 1995; Liu and Air, 1993; Jin *et al.*, 1994; Justice *et al.*, 1995; Mebatsion *et al.*, 1996; Mitnaul *et al.*, 1996; Pattnaik *et al.*, 1986; Schnell *et al.*, 1994). (3) Budding of coronavirus particles depends solely on the envelope glycoproteins. Coexpression of the MHV envelope protein genes (S, M, and E) resulted in the release of membrane particles morphologically indistinguishable from authentic virions, suggesting that the membrane proteins can assemble into virtually *bona fide* envelopes without the nucleocapsid (Vennema *et al.*, 1996).

Like alphavirus, budding of RV also depends on the interactions between glycoproteins and capsid protein. VLPs morphologically indistinguishable from virus particles could be released by coexpression of the three SPs, capsid C, and glycoproteins E1 and E2, but not by expression or coexpression of any one or two of them (Qiu *et al.*, 1994a). Using mutational analysis, Yao and Gillam (1999) demonstrated that the E1 transmembrane domain and the cytoplasmic tail of 13 amino acids play an important role in late stages of virus assembly, possibly during virus budding, consistent with earlier studies (Hobman *et al.*, 1994) indicating that the E1 cytoplasmic domain may interact with nucleocapsids and that this interaction drives virus budding.

After budding into the lumen of the Golgi complexes, RV virions are released through microsome-mediated exocytosis. The E1 cytoplasmic domain was found to modulate virus

release in a sequence-dependent manner, possibly through interactions with other proteins (Yao and Gillam, 2000).

1.2. *Viral encoded papain-like cysteine proteases (PCPs)*

1.2.1. Viral proteases

In order to use their small coding capacity economically, viruses often encode proteins in the form of polyproteins that are processed into final products by host and viral encoded proteases. Viral proteases also function to cleave host cell proteins for the benefit of virus life cycles (Roehl *et al.*, 1997). Therefore, virus encoded proteases generally regulate viral gene expression and pathogenesis, and are often good targets for drug design.

There are four classes of proteases, named after the chemical nature of their catalytic sites, cysteine, serine, aspartate, and metallo-proteases. Each class can be further divided into protein families that have common origins and structural folding (Rawlings and Barrett, 1993).

RNA viral proteases have diverged to the point that sequence similarity between homologues can barely be detected except for the close vicinity of catalytic sites, possibly because of the high mutation rate of RNA viruses. Nevertheless, distant relationship between RNA viral proteases and cellular ones, mostly chymotrypsin-like or papain-like proteases, can still be detected from their common catalytic sites and similar three-dimensional structures. Viral encoded chymotrypsin-like proteases include proteases with different catalytic triads, such as Ser-His-Asp, Cys-His-Asp, and Cys-His-Glu, while adopting homologous folding to

chymotrypsin (Bazan and Fletterick, 1988; Gorbalenya *et al.*, 1989a; Choi *et al.*, 1991b; Allaire *et al.*, 1994; Matthews *et al.*, 1994). Viral encoded papain-like proteases are discussed below.

1.2.2. The papain-like cysteine protease (PCP) family

The PCP family include a group of cellular and viral proteases which employ the catalytic Cys and His dyad. Viral PCPs include members with highly variable protein size and sequence except for the close vicinity of catalytic residues (Gorbalenya *et al.*, 1991). Until recently, the relationship between viral and cellular papain-like proteases had been based on primary sequence analysis (Gorbalenya *et al.*, 1989b, 1991; Hardy and Strauss, 1989; Oh and Carrington, 1989) and predicted secondary structure (Skern *et al.*, 1998). The first crystal determination of a viral PCP, the foot-and-mouth disease virus (FMDV) leader protease (Lpro), confirmed the previous prediction that it adopts a modified compact version of the cellular papain folding (Guarne *et al.*, 1998).

Viral PCPs contain required residues of Cys and His, a single conservative change of which abolishes all protease activity, suggesting their roles in catalytic reaction (Hardy and Strauss, 1989; Chen *et al.*, 1996; Marr *et al.*, 1994). The involvement of Asn as the third catalytic sites, however, is not very clear. No Asn was absolutely required for alphavirus nsP2 protease activity (Strauss *et al.*, 1992).

Using the Schechter and Berger (1967) nomenclature for the description of cleavage sites, the amino acid residues of the N-terminal side of the cleaved bond are numbered P3, P2, P1 and those residues of the C-terminal side are numbered P1', P2', P3' (P1 or P1' near the cleaved bond). Alignment of the cleavage sites recognized by viral PCPs revealed some common

features. Most uniform is the presence of a residue with short side chain (Gly or Ala) in the P1 position. The P1' position is also usually a short-side-chain residue (Chen *et al.*, 1996).

1.2.3. The M-, and L- group PCPs

Two groups of viral PCPs have been distinguished on the basis of their positions in polyproteins and their processing behaviors (Gorbalenya *et al.*, 1991). Leader or L-group PCPs include potyvirus proteinase HC-Pro (Oh and Carrington, 1989), the FMDV Lpro (Piccone *et al.*, 1995), the p29 and p48 proteases of hypovirulence-associated virus (HAV) of chestnut blight fungus (Choi *et al.*, 1991a; Shapira and Nuss, 1991), the equine arteritis virus (EAV) nsP1 protease (Snijder *et al.*, 1992) and others. They are located at the N-terminus of the respective polyprotein and mediate a single cleavage at their own C termini (function in *cis*). These protease domains are located outside the domains directly involved in genome replication and expression.

Main or M-group PCPs include the NS protease of alphavirus (Hardy and Strauss, 1989), the murine coronavirus mouse hepatitis virus (MHV) PLP-1 (Baker *et al.*, 1993; Bonilla *et al.*, 1997), and RV NS protease (NS-pro) (Chen *et al.*, 1996; Yao *et al.*, 1998). They seem to be the main, and possibly the only enzymes responsible for the processing of the respective polyproteins, and function in both *cis* and *trans*. These protease domains are located in the central region of the polyprotein and therefore constitute parts of the molecules involved in genome replication and expression. It is interesting to note that an outside X domain (a novel conserved domain of unknown function) is associated with M-group PCPs. It is speculated that the X domain might function in regulating polyprotein processing. Elimination of the X domain from PLP-1 of MHV reduced cleavage by 22 to 63% (Bonilla *et al.*, 1995).

1.2.4. Alphavirus NS protease

Alphavirus NS protease was mapped to the C-terminal domain of nsP2, specifically from residue 460 to 807 in SIN, using an *in vitro* translation system (Hardy and Strauss, 1989). This NS protease functions both in *cis* and *trans* (Hardy and Strauss, 1989). Both sequence analysis (Hardy and Strauss, 1989) and mutational analysis (Strauss *et al.*, 1992) demonstrated alphavirus NS protease to be a viral M-group PCP, in which C₄₈₁ and H₅₅₈ form the catalytic dyad. A remarkable mutation, N614D, was found to enhance cleavage (Strauss *et al.*, 1992). Its effects on virus replication and viral RNA synthesis suggested a specific function of polyprotein P123 in negative-strand RNA synthesis (Lemm *et al.*, 1994). Regulation of viral RNA synthesis by NSP processing is discussed in section 1.3.1.3.

Both nsP2 and polyproteins containing nsP2 have been found to be active proteases, but the cleavage site preferences of different polyproteins are different (de Groot *et al.*, 1990). In general, (1) polyproteins containing nsP1 (i.e., P12, P123, or P1234) could not cleave the nsP2/nsP3 site, but cleave the nsP3/nsP4 site fairly efficiently and the nsP1/nsP2 site inefficiently; (2) only polyproteins containing nsP3 (i.e., P123, P1234, P23 and P234) could cleave the nsP3/nsP4 site; (3) polyproteins lacking nsP1 (i.e., P23 and P234), as well as nsP2 under some conditions, could cleave the nsP2/nsP3 site very efficiently; (4) the presence of nsP4 in the polyprotein does not affect cleavage specificity. These cleavage site preferences result in different processing pathways for NSPs early and late in infection (de Groot *et al.*, 1990). Early in infection, SIN genomic RNA is translated into P123 and P1234. P123 could not autoproteolyze and P1234 cleaves at the nsP3/nsP4 site in *cis*, resulting in the presence of P123 and nsP4. With the increase of P123, cleavage in *trans* of P123 at the nsP1/nsP2 site produces

proteases that are active in cleaving the nsP2/nsP3 site. By 3 to 4 hpi, cleavage of the nsP2/nsP3 site occurs so rapidly that the nascent polyprotein is cut to produce P12 and P34. P12 can be cleaved both in *cis* and *trans* into nsP1 and nsP2, whereas P34 is stable. Therefore, the major NSP proteins after 4 hpi are nsP1, nsP2, nsP3 (produced by termination at the opal termination codon), and P34. Things are a little different in SFV, which lacks an opal codon between nsP3 and nsP4, in which nsP3 is produced throughout. However, SFV was also shown (Takkinen *et al.*, 1991) to produce P123 only early in infection and to produce P12 and P34 late in infection, similarly to the case of SIN.

1.2.5. RV NS protease (NS-pro)

By comparative sequence analysis, Gorbalenya *et al.* (1991) proposed that RV NS-pro is an M-group PCP, and identified an X domain (from residue 834 to 940) adjacent to the RV NS-pro domain. Our previous studies demonstrated that RV NS-pro could function both in *cis* and in *trans* (Yao *et al.*, 1998), a feature consistent with M-group PCPs. The catalytic dyad residues of NS-pro, C₁₁₅₂ and H₁₂₇₃, have been proposed by sequence alignment (Gorbalenya *et al.*, 1991) and supported by site-directed mutagenesis (Chen *et al.*, 1996; Marr *et al.*, 1994). However, the lack of precisely mapped domain for NS-pro and its highly variable sequence from other PCPs make the structure and functions of NS-pro poorly characterized.

1.3. Replication of positive-strand RNA viruses

From the Sixth Report of the International Committee on Taxonomy of Viruses (ICTV) (Murphy *et al.*, 1995), viruses can be classified by genome structure into double-strand DNA

virus, single-strand DNA virus, double-strand RNA virus, single-strand positive RNA virus, single-strand negative RNA virus, DNA and RNA Reverse Transcribing Viruses, and the Subviral Agents. Among known viruses the single-strand positive RNA virus group is most abundant. Many of these cause human, animal, and plant diseases including encephalitis, hemorrhagic fevers, and hepatitis. Their genomic RNAs act directly as viral messenger RNA and are thus infectious. Replication of positive-strand RNA viruses is of fundamental interest to understanding their pathogenesis.

A variety of approaches has been employed in studying viral RNA replication. Biochemical analyses of viral-encoded NSPs provide details of their enzymatic features. Mutational analyses were used to study their replication, including temperature-sensitive (ts) mutants, isolated variants, and mutants constructed from infectious cDNA clones. *In vivo* and *in vitro* reconstituted systems were constructed to reflect authentic viral RNA replication by using RNA templates and expressed viral NSPs. These varied methods were employed to characterize viral NSPs, *cis* RNA elements, and host factors in the replication process. Below are examples of replication studies on some model viruses like poliovirus, brome mosaic virus (BMV), and alphavirus.

1.3.1. RNA replication studies on some model positive-strand RNA viruses: poliovirus, BMV, and alphavirus.

1.3.1.1. Poliovirus

Poliovirus is a member of the *Picornaviridae* family of positive-strand RNA viruses. The poliovirus genome (Fig. 4) is a 7500-nt positive-strand RNA with 5'-terminal covalently linked

protein VPg and 3'-terminal poly(A) sequence. It contains a single ORF, translated into a 220-kDa polyprotein and processed by intrinsic proteases into final cleavage products. Interestingly, initiation of translation of its genomic RNA is cap-independent and controlled by a long segment within the 5' non-translated region, termed the internal ribosomal entry site (IRES) (for a review, see Schmid and Wimmer, 1994). The proteins 1A, 1B, 1C, and 1D, located at the N-terminus of the polyprotein, are capsid proteins. The proteins 2A, 3C, and 3CD are proteases. 3B is VPg, covalently attached to the 5' end of all newly synthesized viral RNAs. Viral RNA replication requires 3D (the RdRp), and other viral proteins 2B, 2C, 3A, 3B, 3AB, and 3CD as well (for a review, see Wimmer *et al.*, 1993).

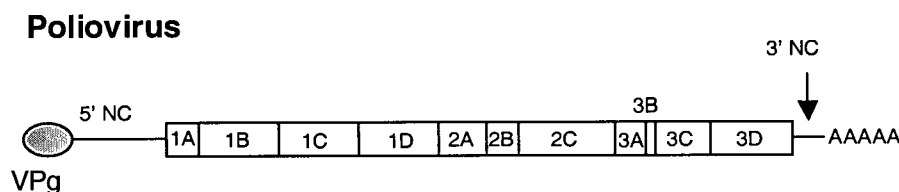


Figure 4. Poliovirus genome organization.

Molla *et al.* (1991) developed a cell-free, *de novo* system for the production of infectious poliovirus, in which newly synthesized proteins from poliovirion RNA using HeLa cell extract can replicate and encapsidate viral RNA to form infectious poliovirus. This is a complete system for studying poliovirus replication, i.e., translation, polyprotein processing, RNA replication, and virus assembly. This system efficiently yields virus titers of 4×10^7 PFU/ml and also reflects the authentic replication of poliovirus RNA, producing the VPg-linked RNAs asymmetrically with more positive than negative strands (Barton and Flanagan, 1993; Barton *et al.*, 1995; Barton *et al.*, 1996). The ability to form authentic, functional replication complexes

and infectious virus *in vitro* provides direct access to the replicative process. Using this system, initiation of negative-strand RNA synthesis was found to require the activity of a guanidine-inhibited viral protein 2C (Barton *et al.*, 1995; Barton and Flanagan, 1997). The switch from translation to initiation of negative-strand RNA synthesis was also characterized. The initiation of negative-strand synthesis appears to be coordinately regulated with the natural clearance of translating ribosomes to avoid the dilemma of ribosome-polymerase collisions (Barton *et al.*, 1999).

1.3.1.2. Brome mosaic virus (BMV)

BMV, the type of the *Bromovirus* genus, is a member of the alphavirus-like superfamily (Ahlquist, 1992). The BMV genome (Fig. 5) consists of three separately encapsidated RNAs, 1, 2, and 3. BMV RNAs do not contain the 3' poly(A) of cellular RNA, but have instead a tRNA-like structure, required for efficient negative-strand RNA synthesis (Dreher & Hall, 1988a, 1988b; Miller *et al.*, 1986; Sun *et al.*, 1996). RNAs 1 and 2 encode NSP 1a (109 kDa) and 2a (94-kDa), respectively, which are essential RNA replication factors. 1a contains domains implicated in RNA helicase and RNA capping functions (Ahola and Ahlquist, 1999; Kong *et al.*, 1999) and 2a contains an RdRp domain (Ahlquist, 1992). RNA3 encodes cell-to-cell movement and coat proteins. Coat protein is translated from a subgenomic RNA, RNA4, which initiates internally from the negative-strand RNA3 (Janda and Ahlquist, 1993).

Janda and Ahlquist (1993) found that yeast expressing the NSPs 1a and 2a supports BMV RNA replication and mRNA synthesis. This yeast system reproduces all known features of BMV RNA replication in natural plant hosts, including localization to the ER, dependence on 1a, 2a, and the same *cis* RNA signals, and similar ratios of positive- to negative-strand RNA

(Restrepo-Hartwig and Ahlquist, 1996, 1999; Janda and Ahlquist, 1993; Sullivan and Ahlquist, 1999; Krol *et al.*, 1999). This is a powerful system in characterizing viral NSPs (Chen and Ahlquist, 2000; Restrepo-Hartwig and Ahlquist, 1999), *cis* RNA elements (Sullivan and Ahlquist, 1999), and especially cellular factors essential for viral RNA replication (Diez *et al.*, 2000; Ishikawa *et al.*, 1997) in combination with yeast genetics.

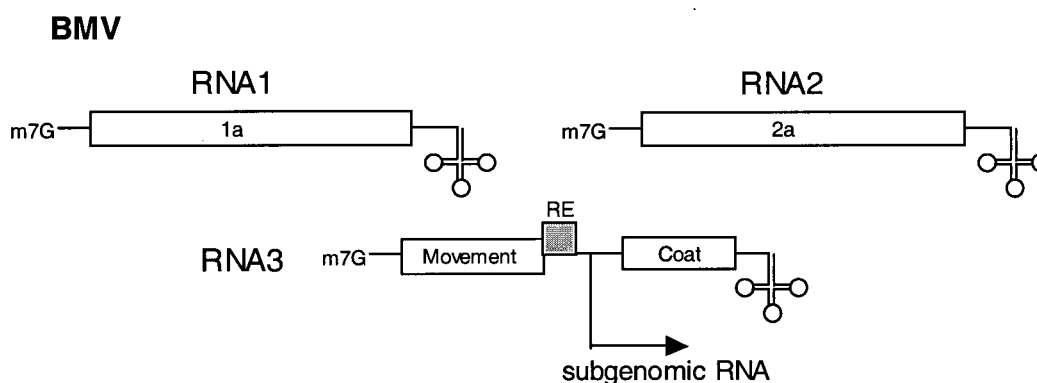


Figure 5. Genome organization of brome mosaic virus (BMV).

BMV genome contains three RNA molecules, each with 5' cap and 3' tRNA structure. The subgenomic RNA, translated into coat protein, is produced during virus infection (Diez *et al.*, 2000).

BMV replication was also studied from a biochemical approach. The partially purified RdRp from BMV-infected barley leaves allowed synthesis of negative-strand RNAs from input positive-strand templates in a sequence-specific manner (Miller *et al.*, 1986; Quadts and Jaspars, 1990; Kao and Sun, 1996), and also synthesized subgenomic RNA4 by initiating internally within the negative-strand RNA3 (Miller *et al.*, 1986). This *in vitro* system was used to analyze the initiation of negative-strand RNA synthesis, which starts at the penultimate cytidylate (Kao and Sun, 1996; Miller *et al.*, 1986), generates abortive initiation products (Sun *et al.*, 1996), and

requires the tRNA-like structure present at the 3' end (Chapman and Kao, 1999). It was also used to study the precise initiation of positive-strand RNA synthesis, in which a 27-nt RNA from BMV was found to direct correct initiation of genomic positive-strand RNA synthesis by the BMV replicase (Sivakumaran and Kao, 1999), and initiation of subgenomic RNA (Adkins *et al.*, 1997; Siegel *et al.*, 1997).

1.3.1.3. Alphaviruses

The *Alphavirus* genus, containing 27 currently recognized members, is the only other genus of the *Togaviridae* family in addition to *Rubivirus* (Calisher and Karabatsos, 1988; Strauss and Strauss, 1994). The alphavirus genome (Fig. 1) encodes two large ORFs. The 5'-terminal two-thirds of the genome encodes NSPs and the 3'-terminal one-third encodes SPs (for a review, see Strauss and Strauss, 1994). The NSPs of alphaviruses are translated from the input genomic RNA upon infection as one or two polyproteins, P123 or P1234, depending on the virus. Cleavage of these polyproteins into nsP1, nsP2, nsP3, nsP4, as well as a number of cleavage intermediates plays an important role in regulating viral RNA synthesis. The SPs are translated as a polyprotein from a 26S subgenomic RNA, and processed into the capsid protein C, the envelope proteins E1 and E2, and two small polypeptides E3 and 6K. Both the 49S genomic and the 26S subgenomic RNAs are capped and polyadenylated. During RNA replication, a full-length negative-strand RNA is produced that serves as a template for replication of the genomic RNA and for transcription of the subgenomic RNA. Synthesis of negative-strand RNA stops at 3 to 6 hpi whereas that of positive-strand RNAs (the 49S genomic and the 26S subgenomic RNAs) continues (Sawicki and Sawicki, 1980; Sawicki *et al.*, 1981). Several studies using different approaches characterized the underlying regulatory mechanism (Lemm and Rice, 1993a, 1993b; Lemm *et al.*, 1994, 1998; Shirako and Strauss, 1994).

Analyses of cleavage mutants suggest that virus replication is regulated by the extent of polyprotein cleavage. Mutant N614D has such a high protease activity to process nsP1/nsP2 and nsP2/nsP3 cleavage sites that polyprotein P123 cannot exist. This mutant was lethal at 37 °C, suggesting that P123 or an intermediate polyprotein was required for RNA synthesis (Strauss *et al.*, 1992). A further mutant, in which both nsP1/nsP2 and nsP2/nsP3 cleavage sites were blocked, allowing only P123 and nsP4 to be produced, carried out the early negative-strand RNA synthesis normally, while it had greatly impaired positive-strand RNA synthesis (Shirako and Strauss, 1994). Cleavage at the nsP3/nsP4 site to release nsP4 was found to be absolutely required as a mutation blocking this site was lethal (Shirako and Strauss, 1994). These results demonstrated that polyprotein P123 and nsP4 are required for negative-strand RNA synthesis, whereas cleavage products from P123 and nsP4 are responsible for efficient positive-strand RNA synthesis.

Lemm and Rice (Lemm and Rice, 1993a, 1993b; Lemm *et al.*, 1994) used a reconstitution system to identify the NSP requirements for RNA replication, in which various combinations of NSP cleavage products and intermediates expressed from vaccinia recombinants were tested for the ability to replicate a template RNA. They found that polyprotein P123 and nsP4 could support negative-strand RNA synthesis, whereas the four final cleavage products or any combination of polyproteins not including P123 could not. The requirement for P123 is further supported by the fact that a mutant polyprotein P123(N614D), which contains accelerated protease activity as described above, was inactive in RNA synthesis unless the nsP1/nsP2 and nsP2/nsP3 cleavage sites were blocked (Lemm and Rice, 1993b). The authentic nsP4 was also found to be necessary for RNA synthesis, and it can be supplied from cleavage of either P34 or

truncated forms of P34 or as a ubiquitin-nsP4 fusion protein rapidly cleaved in the cell (Lemm and Rice, 1993a, 1993b; Lemm *et al.*, 1994).

All these studies come to common conclusions. A model for the composition of replication complexes and the temporal regulation of negative- and positive-strand RNAs has thus been proposed (Lemm *et al.*, 1998). Alphavirus contains three forms of replication complexes, one formed by uncleaved P123 and nsP4 generating only negative-strand RNA, one composed of nsP1, P23, and nsP4 active in both negative-strand RNA and 49S positive-strand genomic RNA syntheses, and one consisting of the final cleavage products nsP1, nsP2, nsP3, and nsP4 producing only 49S positive-strand genomic RNA and subgenomic RNA. Therefore, cleavage at the 1/2 and 2/3 sites switches the template preference of the replication complex from negative- to positive-strand RNA and also inactivates negative-strand RNA synthesis, explaining the shutoff of negative-strand RNA synthesis after 4 to 6 hpi.

1.3.2. Common replication strategies of positive-strand RNA viruses

Studies on disparate groups of plant and animal positive strand RNA viruses have revealed remarkably similar replication strategies.

(1) Negative-strand RNA is the intermediate for the replication of genomic RNA and the transcription of subgenomic RNA. Upon infection, viral genomic RNA is first translated to generate replication factors that, along with host factors, form replication complexes to replicate viral RNA. Viral RNA replicates through a negative-strand RNA intermediate, produced first from the template of input genomic RNA and serves as the template for the replication of genomic RNA and/or the transcription of subgenomic RNA.

(2) Four conserved functional domains, methyltransferase, helicase, protease, and RdRp, have been identified within virus-encoded NSPs (Koonin and Dolja, 1993), suggesting that although the precise character of these and interacting host components varies for each virus they employ similar mechanisms for RNA replication. Methyltransferase is one of the enzyme activities needed for capping RNA transcripts (Bisaillon and Lemay, 1997; Rozanov *et al.*, 1992). Helicase is capable of enzymatically unwinding duplex RNA structures by disrupting the hydrogen bonds that hold the two strands together. This activity is coupled with the hydrolysis of an NTP by NTPase activity (for a review, see Kadare and Haenni, 1997). Protease processes nonstructural polyprotein to final products. RdRp is the enzyme responsible for the *de novo* synthesis of RNA from the end of an RNA template (for a review, see Buck, 1996; O'Reilly and Kao, 1998). All viral RdRps lack the proof-reading function of DNA polymerase, which leads to a high rate of random mutations during replication of viral RNAs.

(3) *Cis*-acting RNA sequences within 5' and 3'-ends, and internal regions of template RNA were identified as essential for RNA replication and transcription. Effects of these *cis* RNA elements on virus replication and viral RNA synthesis have been studied using mutational analysis. Both the secondary structure and the nucleotide sequence can be critical for recognition. Mutations of the stem-and-loop structure at the 5' end of RV [5'(+)SL] caused profound effects on viral phenotype (Pugachev and Frey, 1998). The 3' end of RV containing four stem-loop (SL) structures SL1 to 4 is important for virus viability (Chen and Frey, 1999). Four *cis* sequence elements have been identified in alphavirus RNAs; the first 44 nt and a 51-nt section in the coding region of nsP1 forming stem-loop structures, a 24-nt unit found within the junction between NSP and SP ORFs, and a 19-nt span at the 3' end (Strauss and Strauss, 1986). In a 27-nt promoter for positive-strand RNA synthesis of BMV, the nucleotide sequence rather

than the secondary structure was shown to be important for function (Sivakumaran *et al.*, 1999).

(4) Host factors are required participants in RNA replication. Direct and indirect evidence has confirmed that host factors (most likely proteins) are involved in positive-strand RNA virus replication. A number of SIN *ts* mutants were identified as host range dependent (Kowal and Stollar, 1981). Mutations in SIN RNA promoter elements affected RNA synthesis differently in different host cells (Kuhn *et al.*, 1990; Niesters and Strauss, 1990). Partially purified replication complexes from virus-infected cells contained cellular proteins (Andino *et al.*, 1990, 1993; Barton *et al.*, 1991). Many cellular proteins were found to bind specifically to the presumed promoter region of viral RNA (Blyn *et al.*, 1995; Ito and Lai, 1997; Furuya and Lai, 1993; Yu and Leibowitz, 1995; Nakhasi *et al.*, 1990, 1994; Pogue *et al.*, 1993; Tsuchihara *et al.*, 1997). Identified binding cellular proteins include autoantigen La and its homolog (Pardigon and Strauss, 1996; Pogue *et al.*, 1996; Svitkin *et al.*, 1994; Spangberg *et al.*, 1999), autoantigen calreticulin (Singh *et al.*, 1994), polypyrimidine tract-binding protein (Ito and Lai, 1997; Tsuchihara *et al.*, 1997), heterogeneous nuclear ribonucleoprotein A1 (Li *et al.*, 1997), and others.

(5) The process of viral RNA replication is well regulated, as shown by the switch of synthesis from negative- to positive-strand RNA and the asymmetric production of excess positive-strand RNAs over negative-strand RNA. Two regulatory mechanisms have been proposed. One involves the recruitment of additional host factors (Pogue *et al.*, 1994). The other possibility is that NSP cleavage results in distinct NSP components in replication complexes that possess different capabilities in the synthesis of different viral RNA species. A prominent example of the second mechanism is alphavirus as described above.

1.3.3. Cis-preferential replication

The genomes of positive-strand RNA virus contain essential *cis* sequence elements that act as recognition signals for viral RNA recognition and encodes NSPs participating in the replication process, normally in *trans*. Therefore, in complementation studies a replication-defective RNA template lacking a functional protein component can be rescued by a helper RNA expressing the active component in *trans*. However, mutations in some coding sequences of the viral genome are noncomplementable in *trans*, revealing their *cis*-acting functions. This has been reported for poliovirus (Novak and Kirkegaard, 1994), mouse hepatitis virus (MHV) (de Groot *et al.*, 1992), clover yellow mosaic virus (White *et al.*, 1992), cowpea mosaic virus (van Bokhoven *et al.*, 1993), turnip yellow mosaic virus (TYMV) (Weiland and Dreher, 1993), barley stripe mosaic virus (Zhou and Jackson, 1996), tomato bushy stunt virus (Scholthof and Jackson, 1997), tobacco etch virus (Mahajan *et al.*, 1996; Schaad *et al.*, 1996), and alfalfa mosaic virus (Neeleman and Bol, 1999). These *cis*-acting coding sequences are presumed to reflect a coupling between translation and replication of viral RNA or a *cis*-preferential function of the encoded protein in virus replication.

One of the three ORFs of TYMV encodes an NSP precursor, which is proteolytically processed into p150 and p70. Several genomic RNAs with different internal deletions and frameshift mutations failed to replicate detectably in the presence of wild-type helper genome, demonstrating that replication of TYMV RNA is strongly *cis*-preferential (Weiland and Dreher, 1993). The authors proposed a model in which the *cis*-preferential replication is due to the interaction of newly synthesized p150 and p70 preferentially with the RNA genome from which they have been made, resulting in the channeled formation of a replication initiation

complex in *cis*. The *cis* replication depends on the p150/p70 complex as an entity rather than on either protein alone.

Novak and Kirkegaard (1994) constructed amber mutations in the poliovirus genome and examined their rescue by wild-type proteins provided by a helper genome. Amber-suppressing cell lines were used to ensure that the defects in the amber mutants arose from failure to be translated, not from defects in RNA sequence or structure. An internal region of the poliovirus genome, located between coding region 2A-am66 and 3D-am28, was thus identified whose translation is required in *cis*. Such a requirement for translation in *cis* could, as proposed by the authors, result from either the preferential *cis* action of a protein, or a requirement for the act of ribosomal passage itself in *cis*. Several potential mechanisms were proposed by the authors to explain the *cis* action of a protein. (1) The newly synthesized protein is required for template establishment. A *cis*-acting protein might interact with the positive-strand RNA from which it is being translated to enable that RNA to be a template for negative-strand RNA synthesis. (2) Diffusion or integrity of protein could be restricted. Several poliovirus proteins and viral RNA synthesis were found to be associated with cytoplasmic membrane surfaces (Bienz *et al.*, 1990) that restrict the diffusion of a viral protein. In addition, a short-lived intermediate in processing of the polyprotein could be present at high concentration only near the RNA from which it was translated. (3) A viral RNA molecule was only transiently competent for both translation and template establishment. The RNA molecule from which a protein was translated would be one of the few RNA molecules in the vicinity available at that time as a template for RNA synthesis. On the other hand, two potential mechanisms for effects of ribosomal passage in *cis* on RNA replication were also proposed. (1) Ribosomal passage could alter the RNA structure in the *cis*-required region to facilitate negative-strand synthesis. (2) A ribosome-associated

protein or subcellular structure, required for RNA synthesis, can be obtained or used by the viral genome only while ribosomes pass through the *cis*-required region.

The benefits of *cis*-preferential replication of positive-strand RNA viruses were suggested (Weiland and Dreher, 1993; Novak and Kirkegaard, 1994) to facilitate the assembly of replication complexes when few viral RNAs and proteins are present, and to help prevent the replication of host RNAs or defective-interfering (DI) RNAs.

2. PROJECT RATIONALE AND THESIS OBJECTIVES

RV NSP cleavage is critical in viral RNA synthesis and the responsible enzyme, NS-pro, is an interesting viral PCP member for study. Because of the high diversity of primary sequence among PCP members, more information is needed for a clear understanding of this protease family. Like other M-group PCPs, RV NS-pro is located in the central region of polyprotein and the functional proteolytic domains of NS-pro, in either *cis*- or *trans*-cleavage activity, have not been defined. RV NS-pro also constitutes part of the domains mediating viral RNA synthesis. Therefore, characterization of NS-pro functional domains contributes not only to the knowledge of the viral PCP family, but also to the understanding of the biological roles of RV NSPs.

Viral RNA synthesis is a critical step for virus propagation. It is believed that RV NSPs, associated with host factors, form replication complexes to synthesize three RV-specific RNA species, full-length negative-strand RNA, 40S positive-strand genomic RNA and 24S subgenomic RNA (Frey, 1994; Wolinsky, 1996). The components of active replication complexes required for different viral RNA species have not been characterized, nor have the roles of p200, p150 and p90 in this process been studied. The synthetic process of different viral RNA species and the underlying regulatory mechanism are yet to be studied.

The purpose of this thesis is to characterize RV NSPs and viral RNA synthesis at the molecular level with the following specific objectives: (1) characterization of the domains involved in *cis*- and *trans*-cleavage activities of RV NS-pro and comparative analysis of NS-pro with papain in both primary and secondary structures; (2) investigation of the effects of NSP cleavage on virus

replication and viral RNA synthesis; (3) molecular characterization of viral RNA synthesis and its regulatory mechanism.

To characterize the related domains for NS-pro, a panel of in-frame deletion mutants from either the N- or C- terminus of the p150 coding region were constructed and their respective enzyme activities examined *in vitro*. Comparative analysis of RV NS-pro to papain were made using the ALIGN program for primary sequence analysis and the EMBL protein structure prediction service for secondary structure.

To study the effect of NSP cleavage on virus replication and viral RNA synthesis, site-directed mutations were introduced into an infectious cDNA clone at the protease catalytic site and around the cleavage site. The constructed NSP cleavage mutants were examined for NSP processing efficiency and the levels of virus replication and viral RNA synthesis.

To characterize RV RNA synthesis and regulatory mechanisms, the time courses of three viral RNAs were determined. *Trans*-complementation experiments were conducted to examine the respective roles of p200, p150, and p90 in synthesis of distinct viral RNA species.

These experiments lead to a better understanding of the structure and functions of RV NSPs and the process of RV RNA replication at the molecular level. Knowledge on this aspect not only contributes to the clarification of RV propagation and pathogenesis, but also provides a comparative model for studies on related positive-strand RNA viruses.

3. MATERIALS AND METHODS

3.1. *Materials and supplies*

DNA modifying enzymes and restriction endonucleases were purchased from Bethesda Research Laboratories (BRL), Promega, New England Biolabs, Boehringer Mannheim, Sigma, Pharmacia and United States Biochemical Corporation. All enzymes were used as specified by the manufacturer unless indicated otherwise. L-[³⁵S]methionine (10 mCi/ml) and α -[³⁵S]-CTP (12.5 mCi/ml) were from New England Nuclear (NEN). Tissue culture reagents were from Gibco BRL. GENECLAN (Bio101) was from Promega. Peptide antibodies raised against peptides located within RV NSPs were generated in this lab. Human polyclonal anti-rubella serum was provided by Dr A. Tingle (B.C. Children's Hospital, Vancouver, B. C.). BHK-21, Vero, and RV (M33 strain) were obtained from the American Type Culture Collection (ATCC).

3.2. *Methods*

3.2.1. Growth of cells and viruses

Vero cells were cultured in Eagle's minimum essential medium (MEM, Gibco BRL) supplemented with 5% fetal calf serum (FCS). BHK-21 cells were grown in MEM containing 10% FCS and 10% tryptose phosphate broth. RV (M33 strain) was propagated in Vero cells.

3.2.2. Propagation of bacterial strains

E. coli strain WM1100 was used for the propagation of recombinant clones. WM1100 containing recombinant plasmids were grown in $2 \times$ YT medium (16 g/l tryptone; 10 g/l Yeast extract; 5 g/l NaCl) containing 100 µg/ml ampicillin for selection of antibiotic resistance.

3.2.3. Preparation of competent cells and transformation

E. coli cells (1 ml) grown overnight were transferred into 100 ml of Psi broth (5 g/l Yeast extract; 20 g/l tryptone; 5 g/l magnesium sulfate, pH7.6) and incubated at 37 °C until OD₅₅₀ reached 0.48. Cells were incubated on ice for 15 min and pelleted by centrifuge at 5000 rpm at 4 °C for 5 min. The bacterial pellet was suspended in 40 ml of TfbI (30 mM potassium acetate; 100 mM rubidium chloride; 10 mM calcium chloride; 50 mM manganese chloride; 15% (v/v) glycerol, pH5.8) and incubated on ice for 15 min. Cells were pelleted, resuspended in 4 ml of TfbII (10 mM MOPS; 75 mM calcium chloride; 10 mM rubidium chloride; 15% (v/v) glycerol, pH6.5). Aliquots of prepared competent cells were stored at -70 °C.

For transformation, 50 µl of competent cells were incubated on ice with plasmid DNA or 5 µl of ligation reaction for 30 min. After a 90-sec heat shock at 42 °C, the transformation mixture was added 1 ml of $2 \times$ YT medium and recovered at 37 °C by gentle shaking before plating onto selective plates.

3.2.4. Mini preparation of plasmid DNA

Plasmid DNA mini-prep was performed by QIAprep Spin Plasmid Kit. Pelleted bacterial cells grown overnight were suspended in 250 µl of Buffer P1. Cells were lysed by adding 250 µl of Buffer P2 with gentle inversion. Chromosomal DNA and proteins were precipitated by 350 µl

of Buffer P3 added and thoroughly mixed. The solution was centrifuged at 12000 rpm for 5 min, and the supernatant was applied to QIAprep spin columns. The columns were centrifuged briefly and the flow-throughs were discarded. The columns were washed by 0.5 ml of Buffer PB, followed by 0.75 ml of Buffer PE. The DNA was eluted by 100 µl of H₂O and collected by centrifuging for 1 min. Buffers P1, P2, P3, PB, and PE were reagents provided by the kit.

A quick mini preparation of plasmids for screening by restriction enzyme digestion was done as follows. Colonies were inoculated in 3 ml of 2 × YT medium and grown overnight at 37 °C. Take 0.2 ml of cell culture, add 0.2 ml of solution II (1% SDS; 0.2 N NaOH) and mix gently. Add 0.2 ml of solution III (3M potassium acetate, pH5.5) and mix well. The reaction mixture was centrifuged at 14000 rpm for 2 min and the supernatant was transferred into 0.5 ml of isopropanol. The precipitated plasmids were collected by centrifuging at 14000 rpm for 1 min. After discarding supernatants completely, the pellet was resuspended by mixing (vortex) in 50 µl of TE buffer (10 mM Tris-HCl, pH 8.0; 1 mM EDTA) containing 10 µg/ml of RNase A. Use 5 µl for restriction enzyme digestion.

3.2.5. Restriction endonuclease digestions and DNA modifications

All restriction digestion reactions were performed according to assay conditions specified by the suppliers.

DNA fragments were ligated using T4 DNA ligase in 50 mM Tris-HCl (pH7.6), 10 mM MgCl₂, 1 mM ATP, 1 mM DTT, and 5% (v/v) PEG at 16 °C overnight.

DNA fragments with 5' overhangs were blunt ended with *E. coli* DNA polymerase I Klenow fragment in the same restriction enzyme digestion buffer and incubated for 30 min at RT.

DNA fragments with 3' overhangs were blunt ended with T4 DNA polymerase in the presence of 2 mM dNTPs in the same restriction enzyme digestion buffer and incubated for 20 min at 16 °C.

Removal of terminal 5' phosphates from DNA fragments was done using calf intestinal alkaline phosphatase (CIP) in 50 mM Tris-HCl (pH 9.0), 1 mM MgCl₂, 0.1 mM ZnCl₂, and 1 mM spermidine for 30 min at 37 °C (for fragments with 5' overhangs), or for 30 min at 37 °C followed by 45 min at 55 °C with additional CIP (for fragments with blunt ends or 3' overhangs). CIP reactions were terminated by phenol/chloroform extraction and DNA fragments were ethanol precipitated or recovered by GENECLAN (BIO 101).

Purification of DNA fragments from agarose gels was done using GENECLAN (BIO 101). Desired fragments were excised from ethidium bromide stained agarose gels and the gel matrix was solubilized in 3 volumes of saturated sodium iodide at 55 °C for 5 min. Glassmilk was incubated with agarose solution at 55 °C for another 5 min. The formed DNA-glass-bead complex was pelleted by brief centrifuging and washed three times with cold NaCl/ethanol/water solution. The DNA was eluted from the glass beads with H₂O by incubating at 55 °C for 3 min.

3.2.6. Polymerase Chain Reaction

PCR reactions were carried out in 25 cycles of 98°C for 30 s, 50°C for 2 min, and 70 °C for 2 min using either 2.5 U of *ExTaq* temperature-stable DNA polymerase (TaKaRa LA PCR kit) or Native *Pfu* DNA polymerase (Stratagene) in buffers provided by the manufacturers (10 mM

KCl, 10 mM (NH₄)₂SO₄; 20 mM Tris-Cl, pH 8.75; 2 mM MgSO₄; 0.1% TritonX-100; 100 µg/ml BSA) and supplemented with 8% dimethyl sulfoxide (DMSO). The resulting PCR fragments were purified with a QIAquick Spin PCR purification kit (QIAGEN).

3.2.7. Plasmid Construction.

An RV infectious cDNA clone (pBRM33) (Yao and Gillam, 1999) was used in the plasmid construction. Site-directed mutations and deletions were accomplished by PCR using primers that contain designed substitutions and restriction enzyme sites. All primer sequences and relative positions on the RV genome are given in Table 1.

Table 1. Sequence information on oligonucleotide primers used in this work.

Primers	Polarity ^a	Positions ^b	Amino acid changes	nucleotide sequences ^c
<i>PCR 5' and 3' primers</i>				
JSY-13	+	2770-2790		5' GCTGCTCGAGCGCGCCTACCG 3'
JSY-12	-	4220-4240		5' GTAGGTGGCGGCGTTCTTGAT 3'
JSY-16	-	1737-1757		5' GGTGGGCGGGGTGGCGGTAGA 3'
JSY-7	-	3584-3600		5' GCTTCGCTCAGGGCGCG 3'
<i>N-terminal deletion primers</i>				
YL-11	+	1082-1101		5' ATCCATGGCGTACTATAGCGAGCGCGT 3'
YL-30	+	2518-2533		5' ATATCCATGGACCCACCGCCT 3'
JSY-25	+	2798-2812		5'ATTCCCATGGTTCGCGCTAGCCGCC 3'
YL-25	+	2960-2977		5' ATTCCATGGCCACGCTGACGCACGCC 3'
YL-21	+	3098-3115		5' ATATCCATGGCGACCCCCCTCGGGGAT-3'
YL-22	+	3344-3361		5' ATATCCATGGGCATGTGCGGGAGTGAC-3'
<i>C-terminal deletion primers</i>				
YL-23	-	3893-3910		5' ATTAGGCCTTAGTGGGGGCGGTCCGAGAC 3'
YL-26	-	3908-3925		5'ATTAGGCCTTAGACCGCGAGCCAAAGGTG 3'
YL-28	-	3914-3928		5' ATTAGGCCTTAGGGGACCGCGAGCCA 3'
YL-27	-	3917-3931		5' ATTAGGCCTTACAGGGGGACCGCGAG 3'
YL-24	-	3920-3937		5' ATTAGGCCTTACCGAGACAGGGGGACCGC 3'
<i>Mutagenic primers</i>				
JSY-2	+	3482-3508	C1152S	5' GACCCAAACACCA G CTGGCTCCGCGCC 3'
JSY-3	-	3482-3508	C1152S	5' GGCGCGGAGCCAG C TGGTGTGTTGGGTC 3'
JSY-4	+	3929-3955	G1301S	5' CTGTCTCGGGGCAG C GGCACTTGTGCC 3'
JSY-5	-	3929-3955	G1301S	5' GGCACAAGTGCC G CTGCCCCGAGACAG 3'
YL-9	+	3929-3961	G1302stop	5'CTGTCTCGGGGCGGCTAAACTTGTGCCGCCACC3'
YL-10	-	3929-3961	G1302stop	5'GGTGGCGGCACAAGTTTAGCCGCCCCGAGACA3'
YL-15	+	3920-3952	R1299A	5'GCGGTCCCCCTGTCTGCAGGCGGCGGCACTTGT3'
YL-16	-	3920-3952	R1299A	5'ACAAGTGCCGCCCGCCT G CAGACAGGGGGACCGC3'
YL-13	+	3920-3952		5' GCGGTCCCCCTGTCTAGAGGCGGCGGCACTTGT 3'
YL-14	-	3920-3952		5' ACAAGTGCCGCCCGCCT CTAGAC AGGGGGACCGC 3'
YL-17	+	3941-3955	G1300A	5' CTGT CTAGAG CAAGGCGGCACTTGTGCC 3'
YL-18	+	3948-3958	G1301A	5' CTGTCTAGAGGCGCAGGCACTTGTGCCGCC 3'

^a polarity of primers on M33 genome. +, forward; -, backward.

^b Positions of primers on M33 genome.

^c Sequences of primers. The mutated nucleotides are in boldface. The restriction enzyme *Xba* I sites are underlined.

Truncated plasmids containing in-frame deletions from either the N- or C- terminus of p150

A series of in-frame deletions from either the N- or C-terminus of the p150 coding region were generated by amplifying the corresponding DNA fragment from pBR-150 (containing a stop codon between p150 and p90) using available restriction sites in RV cDNA and the *Nco* I site containing the initiation codon of p200. The relative positions of PCR primers on RV NSP ORF are schematically shown in Fig. 6.

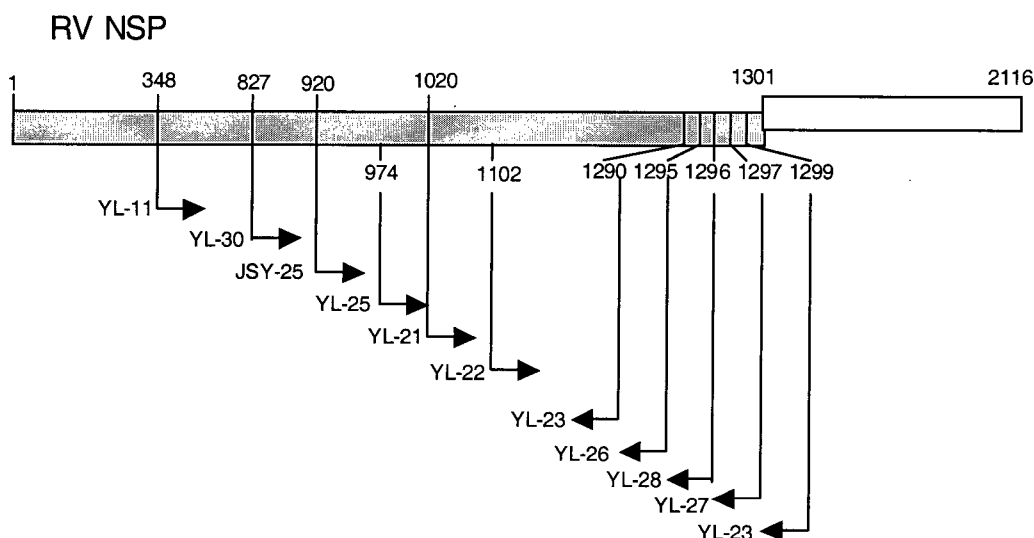


Figure 6. Locations of PCR primers for serial deletions on RV genome.

RV NSP ORF encodes a 200-kDa polypeptide (p200) to be processed into p150 (residues 1 to 1301) and p90 (residues 1302 to 2116). PCR primers used for making deletions from either end of p150 are shown by arrows, suggesting their polarities and relative amino acid positions on NSP ORF.

To make deletions from the N-terminus of p150, amplification reactions were carried out on pBR-150 DNA template using individual N-terminal deletion primers paired with an appropriate downstream 3'-end primer (Table 1 and Fig. 6). The N-terminal deletion primers carry an initiation codon ATG (*Nco* I site) followed by a string of nucleotide sequences downstream from nt 1082, 2518, 2798, 2960, 3098, or 3344, respectively (the start nt position for A₃₄₈, M₈₂₇, V₉₂₀, A₉₇₄, A₁₀₂₀ or G₁₁₀₂, respectively). In brief, to clone the construct encoding residues from A₃₄₈ to G₁₃₀₁, primer YL-11 was paired with JSY-16 in PCR and the resulting 675-bp product was used to replace the *Nco* I-*Not* I fragment (nt 39 to 1686) of pBR-150 to make pBR-A₃₄₈/G₁₃₀₁. To clone a construct encoding residues from M₈₂₇ to G₁₃₀₁, primer YL-30 was paired with JSY-7 in PCR and the resulting 1.1-kb fragment was used to replace the *Nco* I-*Sph* I fragment (nt 39 to 3391) of pBR-150 to generate pBR-M₈₂₇/G₁₃₀₁. To make the construct encoding sequences from V₉₂₀, A₉₇₄, A₁₀₂₀ or G₁₁₀₂ to G₁₃₀₁, a primer JSY-25, YL-25, YL-21 or YL-22 was respectively paired with JSY-12 in individual PCR and the resulting product was used to substitute the *Nco* I-*Nco* I fragment (nt 39 to 4023) of pBR-150 in the correct orientation. The constructed plasmids were named pBR-V₉₂₀/G₁₃₀₁, pBR-A₉₇₄/G₁₃₀₁, pBR-A₁₀₂₀/G₁₃₀₁ and pBR-G₁₁₀₂/G₁₃₀₁, respectively.

To make deletions from the C-terminus of p150, 5'- PCR primer JSY-25 was paired with each C-terminal deletion primer (YL-23, YL-24, YL-26, YL-27 or YL-28) in individual PCR (Table 1 and Fig. 6). The C-terminal deletion primers were complementary to nucleotide sequences consisted of sequences encoding the desired C-terminal amino acid (H₁₂₉₀, V₁₂₉₅, P₁₂₉₆, L₁₂₉₇, or R₁₂₉₉) plus its upstream residues, followed by stop codon TAA and the *Stu* I restriction site. Each of the five PCR fragments was subsequently used to replace the *Nco* I-*Stu* I fragment (nt 39 to 6965) of pBR-150 to generate plasmid: pBR-V₉₂₀/H₁₂₉₀, pBR-V₉₂₀/V₁₂₉₅, pBR-V₉₂₀/P₁₂₉₆, pBR-V₉₂₀/L₁₂₉₇ or pBR-V₉₂₀/R₁₂₉₉.

To make protease constructs encoding sequences from nested N-termini (V₉₂₀, A₉₇₄, A₁₀₂₀ and G₁₁₀₂) to I₁₇₇₃, amplifications using N-terminal deletion primers (JSY-25, YL-25, YL-21, and YL-22) and the subsequent cloning were described as above for making N-terminal deletions of p150, except that pBR-NSP (encoding RV wild-type NSP, without a stop codon between p150 and p90) rather than pBR-150 was used for both PCR template and cloning vector. The resultant plasmids were further modified to remove the C-terminal half of p90 sequence by *Bgl* II (nt 5355) / *Stu* I (nt 9336) digestion, end-gap-filling and religation. The derived ORFs, being terminated by a stop codon at nt 9466, encode protein products starting from residue V₉₂₀, A₉₇₄, A₁₀₂₀ or G₁₁₀₂ to I₁₇₇₃ of NSP sequence, followed by a 43-amino-acid sequence resulted from the shift in reading frame after deletion from nt 5355 to 9336. The plasmids were named pBR-V₉₂₀/I₁₇₇₃, pBR-A₉₇₄/I₁₇₇₃, pBR-A₁₀₂₀/I₁₇₇₃ and pBR-G₁₁₀₂/I₁₇₇₃. All protease constructs are schematically shown in Fig. 11.

Site-directed mutations C1152S, G1301S, R 1299A, G1300A, and G1301A

A panel of site-directed mutations was introduced into pBRM33 by PCR-mediated mutagenesis with primers containing the desired nucleotide changes (all of the primer sequences are given in Table 1).

To substitute S for catalytic C₁₁₅₂, to mutate G₁₃₀₁ to S, or to change R₁₂₉₉ to A, fusion PCR (Yao and Gillam, 1999) was employed with pBRM33 DNA as the template and two pairs of primers (schematically shown in Fig. 7). In brief, to make C1152S mutation, two pairs of primers, JSY-13 plus JSY-3 and JSY-2 plus JSY-12, were used in two PCRs to generate two products of 738-bp and 758-bp, respectively; the two partially overlapping PCR products were

annealed to serve as the template for amplification of the 1.47-kb fragment using JSY-13 and JSY-12. To make G1301S mutation, two pairs of primers, JSY-13 plus JSY-5 and JSY-4 plus JSY-12, were used in two PCRs to generate products of 1.19-kb and 311-bp, respectively; the two partially overlapping PCR products were annealed to serve as the template for amplification of the 1.47-kb fragment containing the G1301S mutation using JSY-13 and JSY-12. To construct the R1299A mutation, two pairs of primers, JSY-13 plus YL-16 and YL-15 plus JSY-12, were used in two PCRs to produce 1.19-kb and 311-bp, which were annealed for amplification of the 1.47-kb containing the R1299A mutation using JSY-13 and JSY-12. In the end, the resulting 1.47-kb PCR products containing desired mutations (C1152S, G1301S, and R1299A) were cut with *Nhe* I and *EcoR* V and inserted into pBRM33 (minus the *Nhe* I/*EcoR* V fragment) (Fig. 7) to generate pBRM33(C1152S), pBRM33(G1301S) and pBRM33(R1299A), respectively.

To facilitate mutagenesis, a silent mutation was introduced into pBRM33 to create a new *Xba* I site by changing CGG to AGA at nt 3935 to 3937. Fusion PCR was employed using pBRM33 DNA as the template and two paired primers, JSY-13 plus YL-14 and YL-13 plus JSY-12. The PCR product was used to replace the *Nhe* I-*EcoR* V fragment (nt 2803 to 4213) of pBRM33, and the resultant construct was named pBRM33-X. To construct the G1300A and G1301A mutations, PCR amplifications were performed using pBRM33-X as the template and mutagenic primers containing the desired mutations: YL-17 for mutation G1300A and YL-18 for mutation G1301A. The PCR products were used to replace the corresponding *Xba* I-*EcoR* V (nt 3933 to 4213) fragment of pBRM33-X. The constructs were named pBRM33(G1300A) and pBRM33(G1301A), respectively.

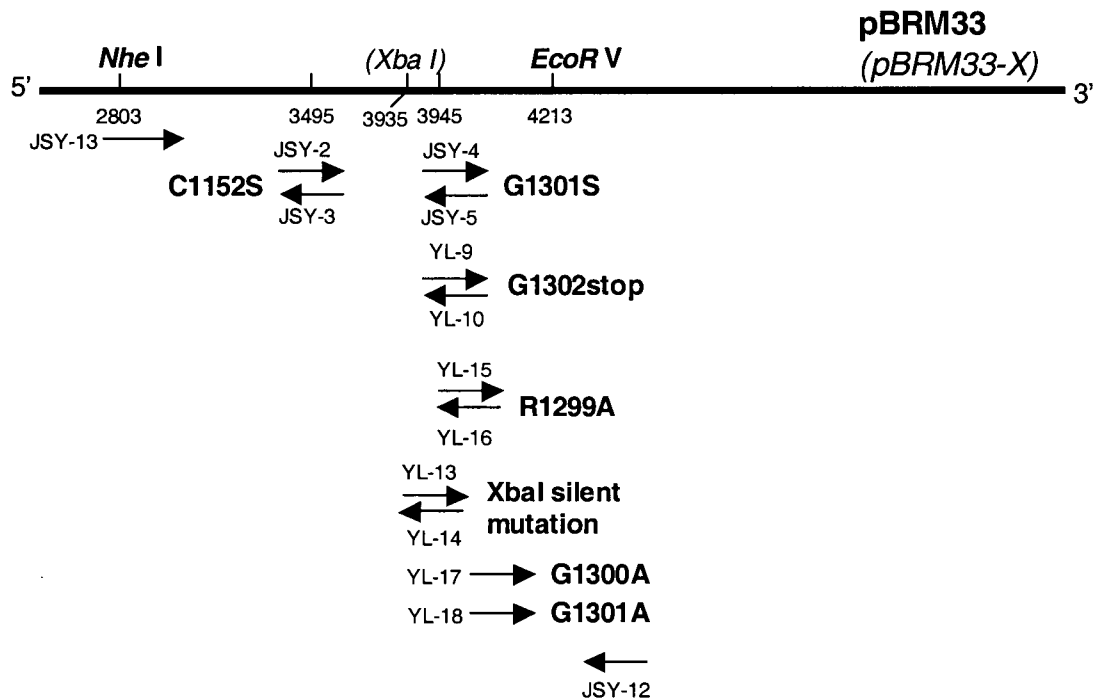


Figure 7. Locations of PCR primers for site-directed mutagenesis on RV genome.

Fusion PCR employed pBRM33 DNA as the template and two pairs of primers. For the C1152S mutation, paired primers, JSY-13 plus JSY-3 and JSY-2 plus JSY-12, were employed. For the G1301S mutation, paired primers, JSY-13 plus JSY-5 and JSY-4 plus JSY-12, were used. For the G1302stop mutation, paired primers, JSY-13 plus YL-10 and YL-9 plus JSY-12, were used. For the R1299A mutation, paired primers, JSY-13 plus YL-16 and YL-15 plus JSY-12, were used. To create a new *Xba* I site at nt 3935, paired primers, JSY-13 plus YL-14 and YL-13 plus JSY-12, were used. The amplified 1.47-kb fragments containing desired mutations were replaced back into the pBR-NSP using *Nhe* I and *EcoR* V sites indicated above the genome. To make the G1300A and G1301A mutations, pBRM33-X (containing a new *Xba* I site at nt 3935) was used as the template in PCRs, with mutagenic primers YL-17 and YL-18 paired respectively with JSY-12. All primers are shown as arrows indicating their polarities and nucleotide positions on RV genome RNA (numbered from the 5' end of M33 genome). Primer sequences are given in Table 1.

Plasmid pBR-150

To change the G1302 codon to stop codon TAA, fusion PCR was employed using pBRM33 DNA as the template and two paired primers, JSY-13 plus YL-10 and YL-9 plus JSY-12 with the products of 1.19-kb and 311-bp, respectively. The two partially overlapping PCR products were annealed to serve as the template for amplification of the 1.47-kb fragment containing the G1302stop mutation using JSY-13 and JSY-12. The resulting 1.47-kb PCR product containing the G1302stop mutation was cut with *Nhe* I and *EcoR* V and inserted into pBRM33 (minus the *Nhe* I/*EcoR* V fragment) (Fig. 7) to produce pBR-150.

pBRM33 Δ SS, pBRM33 Δ MM, and pBRM33(C1152S) Δ SS

Plasmid pBRM33 Δ SS was generated from pBRM33 by removing most of the structural protein ORF with the deletion from nt 6966 to 9336 after *Stu*I digestion and religation. Its derived RNA, M33 Δ SS, was a structural-protein-deleted RV RNA replicon. Construct pBRM33 Δ MM, encoding a NSP-deleted RV RNA, was generated by the deletion of fragment between nt 1081 and 5106 from pBRM33 using *Mlu*I sites. pBRM33(C1152S) Δ SS, encoding the M33(C1152S) Δ SS RNA, was constructed by deleting fragment between nt 6966 and 9336 from pBRM33(C1152S) using *Stu*I sites.

3.2.8. *In vitro* transcription.

The cDNA clones were linearized at the unique *Hind* III site and transcribed with SP6 RNA polymerase (Promega) in 40mM Tris-HCl (pH 7.9), 6mM MgCl₂, 10mM DTT, 10mM NaCl, 2mM spermidine, 0.05% Tween-20, 0.5mM each of NTPs, 1 mM cap analog 7mG_{5'}ppp_{5'}G, and 1 U RNasin Ribonuclease Inhibitor. The reaction mixture was incubated at 37 °C for 2 h. RNA

transcripts were extracted once with phenol/chloroform, precipitated with ethanol and resuspended in H₂O.

3.2.9. *In vitro* translation

In vitro translation was performed according to the manufacture's (Promega) protocol in 50- μ l reaction mixtures containing 35 μ l of nuclease-treated rabbit reticulocyte lysates, 20 mM amino acid mixture minus methionine, 0.4 U RNasin (ribonuclease inhibitor) and *in vitro* RNA transcripts, in the presence of either 400 μ Ci/ml of [³⁵S]methionine (NEN) or 20 μ g/ml of cold methionine. Translation reactions were carried out at 30 °C for desired times and terminated by the addition of SDS-PAGE loading buffer (62.5 mM Tris-HCl, pH7.4; 2% SDS; 5% β -mercaptoethanol; 0.2% bromophenol Blue Dye; 500 mM sucrose). Radiolabeled proteins were visualized by fluorescence autoradiography after SDS-polyacrylamide gel electrophoresis (PAGE) analysis.

In vitro translation using TNT Quick coupled transcription-translation system (Promega) was performed in 50 μ l of reaction mixtures containing 40- μ l TNT Quick Master Mix, 400 μ Ci/ml of [³⁵S]methionine (NEN), 0.4 U RNasin (ribonuclease inhibitor), and 1 μ g of plasmid DNA. Reactions were carried out at 30 °C for desired times.

3.2.10. Vero cells transfected by RNA transcripts using Lipofectin.

About 20 μ g of *in vitro* transcribed RNA (in 20- μ l transcription reaction) and 10 μ g of Lipofectin (Gibco BRL) were suspended in 0.5 ml of FCS-free MEM and incubated for 20 min at RT. The formed Lipofectin-RNA mixtures were applied to a 35-mm-diameter dish of Vero

cell monolayer, which had been washed with FCS-free MEM twice. After incubation for 2 to 3 h at 37°C, the mixtures were removed and replaced with the culture medium. At day 6 posttransfection, culture fluids were harvested and the virus released into the culture medium was quantitated by plaque assay on Vero cells.

3.2.11. BHK-21 cells transfected by RNA transcripts using electroporation

BHK-21 cells were harvested by trypsin treatment and washed twice with cold PBS (145 mM NaCl; 7 mM Na₂HPO₄; 3 mM NaH₂PO₄, pH7.0) and resuspended at a concentration of 10⁷ cells/ml. 0.5 ml of cell suspension was mixed with about 20 µg of *in vitro* transcribed RNA (in 20-µl transcription reaction), and transferred to a 2-mm-diameter cuvette. Electroporation utilized two consecutive 1.5-kV, 250 µF pulses with a Gene-Pulser (Bio-Rad). The cells were diluted with the culture medium, and distributed into 4 × 35-mm-diameter dishes. Culture fluids were collected at 48 h postelectroporation and the released virus particles were quantitated by plaque assay on Vero cells.

3.2.12. Plaque assay and virus growth analysis.

For viral plaque assay, Vero cells infected by a serially diluted virus stock were overlaid with 0.5% agarose in MEM containing 5% FCS, incubated at 35°C for 6 or 8 days, and stained with 5% neutral red diluted in MEM supplemented with 5% FCS. For virus growth rate analysis, Vero cell monolayers (35-mm-diameter dish) were transfected with the WT or mutant RNAs mediated by Lipofectin as described above. After removing the RNA-Lipofectin mixtures, the cells were washed with PBS, overlaid with fresh medium and incubated at 37 °C. The culture

medium was harvested and replaced with fresh medium every 24 h. The released virus was quantitated by plaque assay.

3.2.13. Metabolic labeling

Labeling of Vero cells transfected with RNA was performed according to Hobman and Gillam (1989). 6 days posttransfection, RNA-transfected Vero cells (in 35-mm-diameter dishes) were washed twice with PBS, incubated with methionine-deficient DMEM for 30 min, and labeled for 2 h with 0.5 ml of methionine-deficient DMEM containing 100 μ Ci [35 S]methionine and 5% FCS dialyzed against PBS. Cells were washed with cold Tris-saline and lysed with 500 μ l of lysate buffer (1% Triton X-100; 1 mM EDTA; 50 mM Tris-HCl, pH7.5; 0.15 M NaCl). After incubating on ice for 5 min, lysates were scraped off the plates and centrifuged at 4 °C for 5 min at 13000 rpm to remove the nuclei and debris. The supernatants were subjected to immunoprecipitation.

3.2.14. Immunoprecipitation

Cell lysates diluted with lysate buffer (1% Triton X-100; 1 mM EDTA; 50 mM Tris-HCl, pH7.5; 0.15 M NaCl) were mixed with Human polyclonal anti-rubella serum for at least 2 h at RT with constant rotation. Protein A-Sepharose beads (Pharmacia) were washed three times with lysate buffer, and mixed with the serum-lysates overnight at 4 °C with constant rotation. The beads were washed three times with lysate buffer. Antigen-antibody complexes were dissociated from the Protein A-Sepharose by boiling in 1 \times SDS dissociation buffer (62.5 mM Tris-HCl, pH6.8; 10% glycerol; 2% SDS; 2% β -mercaptoethanol) for 5 min, and the supernatants were used in SDS-PAGE analysis.

3.2.15. Total RNA preparation

Total cytoplasmic RNA was prepared from cell cultures using TRIzol reagent (GIBCO BRL). Cells cultured in 35-mm-diameter dish were lysed by 0.8 ml of TRIzol reagent and the lysates were passed through a pipette several times and transferred to a 1.5-ml microtube. The samples were incubated at RT for 5 min before 160 µl of chloroform were added and mixed well by vigorous shaking for 15 s. The samples were incubated at RT for another 3 min and centrifuged at 14000 rpm for 15 min at 4 °C. The aqueous phase was transferred to 0.4 ml of isopropanol. RNA was precipitated by incubating at RT for 10 min and collected by centrifuging at 14000 rpm for 10 min at 4 °C. The pelleted RNA was washed with 1 ml of 75% ethanol and briefly dried before dissolving with formamide. RNA was quantitated by measuring A_{260} (one A_{260} unit equals 40 µg/ml RNA).

3.2.16. RNase protection assay (RPA).

RPA was employed to analyze the synthesis of viral-specific RNAs during virus replication. For synthesis of plus- or minus-polarity RNA probe *in vitro*, a DNA fragment (nt 6323 to 6623) of pBRM33, representing the region covering the subgenomic RNA initiation site (nt 6436), was separately cloned into vector pSPT18 or pSPT19 (Pharmacia Biotech) at the *EcoR* I and *Xba* I sites to make construct pSPT-pb18 or pSPT-pb19. A 328-bp minus-polarity RNA probe (pb18), synthesized with SP6 RNA polymerase from *EcoR* I-linearized pSPT-pb18, can protect 301-nt positive-strand genomic RNA and the 188-nt subgenomic RNA. A 328-nt plus-polarity RNA probe (pb19), synthesized with SP6 RNA polymerase from *Hind* III-linearized pSPT-pb19, can protect 301-nt RV negative-strand genomic RNA.

For synthesis of another pair of plus- and minus-polarity RNA probes *in vitro*, a DNA fragment (nt 9175 to 9336) of pBRM33, in the E1 coding region, was cloned into vectors pSPT19 and

pSPT18 respectively at the *Hind* III and *Sma* I sites to make constructs pSPT-pb20 and pSPT-pb21. A 187-nt minus-polarity RNA probe (pb20), synthesized with SP6 RNA polymerase from *Hind* III-linearized pSPT-pb20, can protect 162-nt positive-strand RNA (including both genomic and subgenomic RNA). A 187-nt plus-polarity RNA probe (pb21), synthesized with SP6 RNA polymerase from *Eco*R I-linearized pSPT-pb21, can protect 162-nt negative-strand RNA.

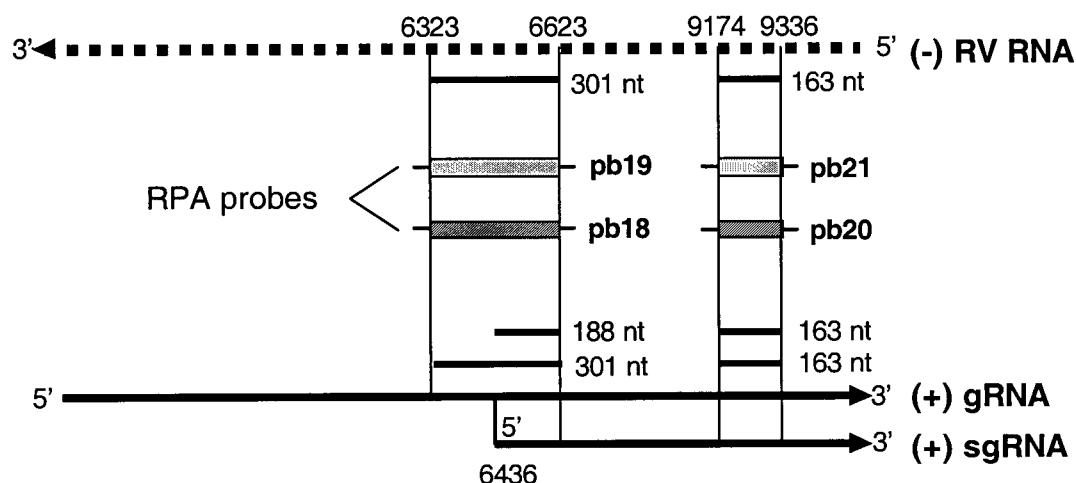


Figure 8. Probes used in RNase protection assay (RPA) and the relative positions and lengths of the protected regions.

The plus-polarity probe pb19 protects a 301-nt region from nt 6323 to nt 6623 of negative-strand RV RNA. The minus-polarity probe pb18, complementary to pb19, protects a 301-nt region of positive-strand genomic RNA and a 188-nt region from nt 6436 to nt 6623 of subgenomic RNA. The plus-polarity probe pb21 protects a 162-nt region from nt 9175 to nt 9336 of negative-strand RV RNA, and its counterpart minus-polarity probe pb20 protects a 162-nt region of both genomic and subgenomic RNAs.

The ^{35}S -labeled RNA probe was synthesized with SP6 polymerase in a 20- μl *in vitro* transcription reaction mixture containing buffer (40mM Tris-HCl, pH 7.9; 6mM MgCl_2 ; 10mM

DTT; 10mM NaCl; 2mM spermidine; 0.05% Tween-20), RNasin, 0.5 mM each of ATP, GTP and UTP, 12.5 μ M of CTP and 2.5 mCi/ml of [α -³⁵S]CTP (NEN). After incubation for 90 min at 37 °C, 2- μ l DNase I (7500 U/ml, Pharmacia Biotech) was added to the reaction mixture and incubated for a further 15 min. The probe was precipitated with ethanol after phenol/chloroform extraction and resuspended in H₂O.

For RNA analysis, total cytoplasmic RNAs were extracted with TRIzol reagent (GIBCO BRL) at indicated times posttransfection. Negative-strand RNA was analyzed by a two-cycle RPA essentially as described by Novak and Kirkegaard (1991). Approximately 20 μ g of cytoplasmic RNA was incubated with 20 ng of unlabeled probe pb19 (or pb21) (approximately 10¹¹ molecules) in 30 μ l of hybridization buffer (40 mM PIPES; 400 mM NaCl; 1 mM EDTA; 80% deionized formamide, pH6.4) overnight at 55 °C. RNase digestion was for 60 min at 30 °C in RNase mixture (300 mM sodium acetate; 10 mM Tris-HCl, pH 7.5; 5 mM EDTA; 10 μ g/ml of RNase A; 70 U/ml of RNase T1). The reaction mixture was treated with SDS-proteinase K for 15 min at 37 °C, extracted with phenol-chloroform, and ethanol precipitated with 5 μ g/ml of tRNA. Samples were resuspended in 30 μ l of hybridization buffer, and 1 \times 10⁶ cpm of ³⁵S-labeled RNA probe (pb19 or pb21) was added. The samples were denatured at 95 °C for 5 min, hybridized overnight at 55 °C, and subjected to RNase treatment as described above. The digestion products were resuspended in loading buffer (80% (v/v) formamide; 0.1% (v/v) xylene cyanol; 0.1% (v/v) bromophenol blue; and 2 mM EDTA) and analyzed on a 5% polyacrylamide-urea gel, which was fixed in 10% acetic acid, infiltrated with Enhancer (DuPont), dried and exposed to X-ray film.

Positive-strand genomic and subgenomic RNAs were analyzed by a single round of RPA. 2 μ g of total cytoplasmic RNAs were hybridized with 1×10^6 cpm of ^{35}S - labeled RNA probe (pb18 or pb20) overnight at 55°C. The samples were treated as described above.

3.2.17. Electrophoresis

3.2.15.1. Separation of DNA fragments by agarose gel electrophoresis

The buffer used in agarose gel electrophoresis was $1 \times$ TAE (40 mM Tri-acetate, pH8.0; 1 mM EDTA). The gel with concentration varied from 0.8 to 1% agarose was prepared using $1 \times$ TAE buffer with 1 μ g/ml ethidium bromide for visualization. DNA samples were mixed with loading buffer (8% sucrose, 20 mM EDTA, pH8.0; 0.05% bromophenol blue; 0.05% xylene cyanol) and separated by electrophoresis on 10 cm horizontal agarose gels at 100 volt.

3.2.15.2. Separation of short RNA fragments by urea-PAGE

Short RNA fragments (100 to 500 nt) in RPA were separated by 7M urea-5% polyacrylamide gel electrophoresis (PAGE). The gel contained 5% polyacrylamide (acrylamide:N,N'-methylenebisacrylamide = 19:1) and 7M urea in the presence of TBE buffer (89 mM Tris; 89 mM boric acid; 2 mM EDTA; pH8.0). Samples were dissolved in the loading buffer (80% formamide; 0.1% xylene cyanol; 0.1% bromophenol blue; 2 mM EDTA) and boiled for 5 min before loading. Gels were run in $1 \times$ TBE buffer at constant voltage of 200 volts until the markers moved to the desired positions. Gels were fixed in 10% acetic acid for 15 min, immersed in the fluorographic reagent Enhancer (DuPont) for 45 min, vacuum dried, and exposed to X-ray film at -70 °C.

3.2.15.3. Separation of proteins by SDS-PAGE

Proteins were separated using a discontinuous gel system described by Laemmli (1970). Stacking gels contained 4% polyacrylamide (acrylamide:N,N'-methylenebisacrylamide = 30:0.8) in the stacking buffer (0.125 M Tris-HCl, pH6.8; 0.1% SDS). Separating gels contained either 8 or 10% polyacrylamide (19:1) in the separating buffer (0.375 M Tris-HCl, pH8.8; 0.1% SDS). Protein samples were dissolved in 1 × SDS-PAGE loading buffer (62.5 mM Tris-HCl, pH6.8; 10% glycerol; 2% SDS; 2% β-mercaptoethanol) and boiled for 3 min before loading. Gels were running in the buffer (0.025 M Tris-HCl, pH8.3; 0.192 M glycine; 0.1% SDS) at constant voltage of 100 volts until the markers have run to the desired positions. The separating gel was fixed in 10% acetic acid, immersed in the fluorographic reagent Enhancer (Dupont) or Amplify (Amersham) for 30 min, vacuum dried, and exposed to X-ray film at -70 °C.

3.2.18. Image analysis and cleavage efficiency comparison.

Image analysis was performed on a PC computer using the Scion Image program for Windows (Beta 3b) (http://www.scioncorp.com/frames/fr_download_now.htm), the PC version of the public domain NIH Image program (developed at the U.S. National Institutes of Health and available on the Internet at <http://rsb.info.nih.gov/nih-image/>). The cleavage ratio at certain incubation times for each protease construct was calculated as the percentage of the quantity of the cleaved products over the total of remaining substrate and cleaved products. The cleavage ratio was plotted against the incubation time for each construct.

3.2.19. Sequence analysis.

Initial alignment of primary sequences between papain (SWISS-PROT access number P00784) and catalytic region of RV NS-pro (M33 strain GenBank access number S38480 with corrections by Pugachev *et al.*, 1997), Therien strain GenBank access number P13889 with corrections by Pugachev *et al.*, 1997) was done by ALIGN program (Myers and Miller, 1988) and modified manually. Secondary structure predictions were performed using the EMBL protein structure prediction service (<http://www.emblheidelberg.de/predictprotein/predictprotein.html>). The service was described by Rost *et al.* (1993a, 1993b, 1994a, 1994b).

4. RESULTS AND DISCUSSIONS

4.1. Characterization of domains involved in *cis*- and *trans*-cleavage activities of RV NS-pro

4.1.1. Processing of RV NSP by *in vitro* translation.

The RV NS-pro is a papain-like cysteine protease (PCP) encoded in the NSP ORF that cleaves the NSP ORF translation product (p200) at a single site to produce p150 and p90. Many viral PCPs were found to be active following *in vitro* translation using rabbit reticulocyte lysates (Bonilla *et al.*, 1997; Choi *et al.*, 1991a; Den Boon *et al.*, 1995; Hardy and Strauss, 1989). I therefore monitored the activity of RV-pro after translating RV NSP *in vitro* using the genomic-length RNA transcripts synthesized from an RV infectious cDNA clone derived from RV strain M33 (pBRM33) (Yao and Gillam, 1999). pBRM33 was linearized with *Hind* III and full-length RNA transcripts were synthesized using SP6 RNA polymerase in the presence of cap analog. *In vitro* translation and processing of NSP were programmed using rabbit reticulocyte lysates with synthesized RNA transcripts. A time course experiment was performed to monitor the kinetics of p200 processing. Translation of p200 was completed after 40 min (Fig. 9A, lane 2); cleavage was observed at 60 min (Fig. 9A, lane 3) and continued efficiently (Fig. 9A, lanes 4 to 6). Liu *et al.* (1998) suggested that activity of RV NS-pro *in vitro* depended on the addition of Zn^{2+} . However, in my *in vitro* translation system, addition of Zn^{2+} was not found to be required for NS-pro activity, nor did it increase the processing efficiency of RV NSP (Fig. 9A, comparing lanes 1 to 6 to lanes 7 to 12). The presence of Zn^{2+} even seemed to have a certain inhibition on the NSP processing efficiency, which, however, may come from experimental variation without statistic significance. Furthermore, using the TNT Quick coupled transcription-translation system (Promega), I also observed efficient

processing of RV NSP without the addition of Zn^{2+} (Fig. 9B, lanes 1 to 3), in contrast to the findings of Liu *et al.* (1998) that addition of Zn^{2+} was essential for RV NS-pro activity in the same translation system. In addition, I observed the efficient processing of NSP from strain Therien *in vitro* without the addition of Zn^{2+} , using infectious cDNA clone Robo302 (Pugachev *et al.*, 1997) or its derived RNA in either TNT transcription-translation system (Fig. 9B, lanes 4 to 6) or rabbit reticulocyte lysate (Fig. 9B, lanes 7 to 9). Liu *et al.* (1998) used a different Therien strain cDNA construct, Robo102, and its derived subclones in their studies. However, Robo102 has a substantially lower infectivity than Robo302 (Pugachev *et al.*, 1997b), which might account for the observed discrepancy. Nevertheless, the exact reasons behind these contradictions need further investigation.

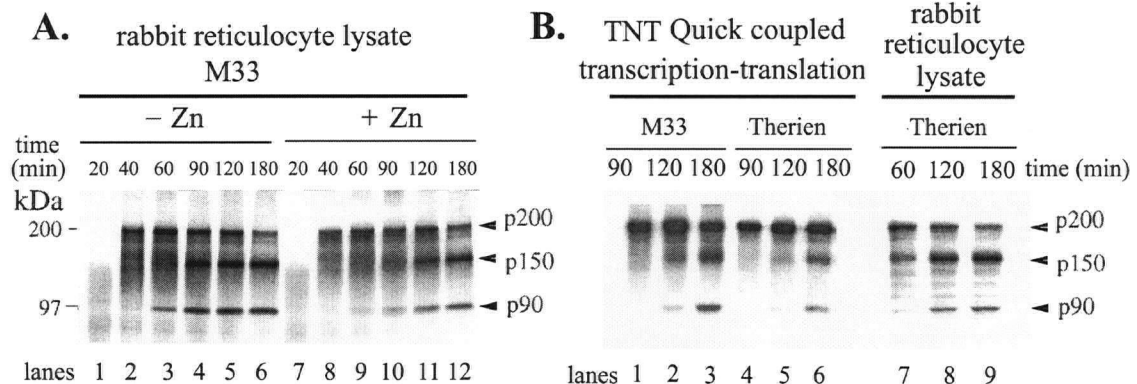


Figure 9. RV NSP processing in *in vitro* translation systems with or without addition of Zn^{2+} .

(A) *In vitro* translation reactions using rabbit reticulocyte lysates were programmed with genome-length RV RNA of M33 strain (transcribed *in vitro* from pBRM33) in the absence (lanes 1 to 6) or presence (lanes 7 to 12) of 200 μ M Zn^{2+} . Aliquots were removed at indicated times during incubation and subjected to SDS-8% polyacrylamide gel electrophoresis (PAGE) analysis. (B) *In vitro* translation reactions using TNT Quick coupled transcription-translation system were programmed with RV full-length infectious cDNA clones based on M33 strain (pBRM33, lanes 1 to 3) or Therien strain (Robo302, lanes 4 to 6). Genome-length RV RNA of Therien strain (transcribed *in vitro* from Robo302) was also translated *in vitro* using rabbit reticulocyte lysates (lanes 7 to 9). All Reactions were carried out without the addition of Zn^{2+} . Aliquots were removed at indicated times and subjected to SDS-8% PAGE analysis. Protein products were visualized by fluorescence autoradiography. Positions of molecular mass markers and cleavage products are indicated. Images were scanned using a UMAX Astra 1220U scanner with Adobe Photoshop 5.0 software.

It has been shown previously (Yao *et al.*, 1998) that NS-pro can function in *trans in vivo* by coexpression within BHK-21 cells of a construct p200(G1301S) that contains a cleavage site mutation (to serve as a protease) together with a construct p200(C1152S) that contains a protease mutation (to serve as a substrate). To demonstrate the NS-pro *trans*-cleavage activity *in vitro*, three full-length mutants with alterations in the NSP ORF were constructed. pBR-200(G1301S) is a cleavage site mutant carrying a G-to-S mutation at residue 1301; pBR-200(C1152S), a protease-inactive mutant carrying a C-to-S mutation at its catalytic C₁₁₅₂ residue; and pBR-150 is a mutant carrying a stop codon corresponding to residue 1302.

To assay for *trans*-cleavage activity of NS-pro, two separate translation reactions were carried out. Radiolabeled p200(C1152S) was synthesized *in vitro* in the presence of [³⁵S]methionine to serve as a source of substrate for protease, and p200(G1301S) or p150 was synthesized in the absence of [³⁵S]methionine to serve as a source of protease. After a 1-h incubation at 30°C, both *in vitro* translation reactions were terminated by the addition of RNase A and cycloheximide. When the radiolabeled p200(C1152S) was added to the unlabeled p200(G1301S) or p150 translation reaction mixture, the cleavage products of p150 and p90 were detected after a 1-h incubation (Fig. 10A and B), indicating that *trans* cleavage of p200(C1152S) catalyzed by p200(G1301S) or p150 protease had occurred. No cleavage product was observed when p200(C1152S) was incubated alone for 5 h (Fig. 10C). For a control, p200(G1301S) or p150 was synthesized in the presence of [³⁵S]methionine at 30°C and incubated alone for 5 h (Fig. 10A and B, lane 1).

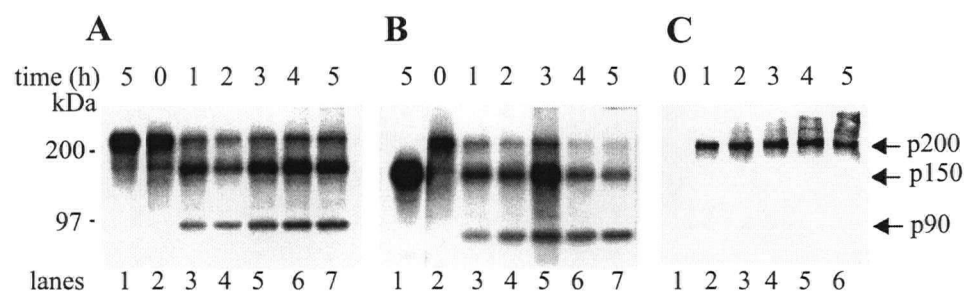


Figure 10. RV p200(G1301S) and p150 cleave substrate protein in *trans*.

Protein products were labeled by synthesis in the presence of [^{35}S]methionine or were unlabeled. After incubation at 30 °C for 1 h, translation was terminated by the addition of RNase A and cycloheximide to final concentrations of 1 and 0.6 mg/ml, respectively. Protein product p200(G1301S) or p150 (synthesized in the absence of [^{35}S]methionine) were mixed with radiolabeled substrate p200(C1152S) and incubated at 30 °C for up to 5 h. Samples removed at various times were subjected to SDS-PAGE analysis. (A) RV p200(C1152S) was labeled in the presence of [^{35}S]methionine and incubated alone for 5 h (lane 1). After translation reactions were terminated, unlabeled p200(G1301S) was mixed with ^{35}S -labeled substrate p200(C1152S) and incubated at 30 °C. Aliquots were removed from 0 to 5 h and subjected to SDS-PAGE analysis (lanes 2 to 7). (B) RV p150 was labeled in the presence of [^{35}S]methionine and incubated alone for 5 h (lane 1). After translation reactions were terminated, unlabeled p150 was mixed with ^{35}S labeled substrate p200(C1152S) and further incubated at 30 °C. Aliquots were removed from 0 to 5 h (lanes 2 to 7) and subjected to SDS-PAGE analysis. (C) *In vitro* transcription and translation of p200(C1152S) were carried out as described. Samples were taken at the indicated times and subjected to SDS-PAGE analysis. Positions of molecular mass markers and cleavage products are indicated. Images were scanned using a UMAX Astra 1220U scanner with Adobe Photoshop 5.0 software.

4.1.2. Construction of truncated NS-pro cDNA clones.

In order to identify the minimal domains required for functional protease activities, a panel of protease constructs was generated and expressed *in vitro* for protease activity analysis. The cDNA fragments encoding NS protease constructs were generated by PCR as described in section 3.2.7. The constructed plasmids were inserted downstream of the SP6 RNA polymerase promoter and RV 5' untranslated region (5'-UTR). The poly(A) addition site of the RV full-length cDNA clone (pBRM33) was preserved. The plasmids, protease products and their relative positions on the RV NSP ORF are shown in Fig. 11.



















Plasmids	Protease constructs	Schematics of protease ORFs	cleavage ratio (%)
pBR-NSP	p200	1  2116	70
pBR-p200(G1301S)	pBR-p200(G1301S)	1  2116	70
pBR-p150	p150	1  1301	83
pBR-A ₃₄₈ /G ₁₃₀₁	A ₃₄₈ /G ₁₃₀₁	348  1301	73
pBR-M ₈₂₇ /G ₁₃₀₁	M ₈₂₇ /G ₁₃₀₁	827  1301	77
pBR-V ₉₂₀ /G ₁₃₀₁	V ₉₂₀ /G ₁₃₀₁	920  1301	15
pBR-A ₉₇₄ /G ₁₃₀₁	A ₉₇₄ /G ₁₃₀₁	974  1301	0
pBR-A ₁₀₂₀ /G ₁₃₀₁	A ₁₀₂₀ /G ₁₃₀₁	1020  1301	0
pBR-G ₁₁₀₂ /G ₁₃₀₁	G ₁₁₀₂ /G ₁₃₀₁	1102  1301	0
pBR-V ₉₂₀ /H ₁₂₉₀	V ₉₂₀ /H ₁₂₉₀	920  1290	0
pBR-V ₉₂₀ /V ₁₂₉₅	V ₉₂₀ /V ₁₂₉₅	920  1295	0
pBR-V ₉₂₀ /P ₁₂₉₆	V ₉₂₀ /P ₁₂₉₆	920  1296	8
pBR-V ₉₂₀ /L ₁₂₉₇	V ₉₂₀ /L ₁₂₉₇	920  1297	10
pBR-V ₉₂₀ /R ₁₂₉₉	V ₉₂₀ /R ₁₂₉₉	920  1299	5
pBR-V ₉₂₀ /I ₁₇₇₃	V ₉₂₀ /I ₁₇₇₃	920  1773	52
pBR-A ₉₇₄ /I ₁₇₇₃	A ₉₇₄ /I ₁₇₇₃	974  1773	53
pBR-A ₁₀₂₀ /I ₁₇₇₃	A ₁₀₂₀ /I ₁₇₇₃	1020  1773	23
pBR-G ₁₁₀₂ /I ₁₇₇₃	G ₁₁₀₂ /I ₁₇₇₃	1102  1773	0

Figure 11. Plasmids and protease-encoding constructs.

All protease constructs were given a two-letter name; their lengths and relative positions on the RV NSP ORF are schematically shown, labeled with starting and ending protein residues (numbered according to NSP residues). The respective cleavage ratio of each construct, calculated by quantitating the cleavage products over total proteins, is given in percentage. Positions of the catalytic sites C₁₁₅₂ and H₁₂₇₃ on p200 are indicated by vertical solid lines.

All of the protease constructs are designated by a two-letter name indicating starting and ending amino acid positions. A₃₄₈/G₁₃₀₁, M₈₂₇/G₁₃₀₁, V₉₂₀/G₁₃₀₁, A₉₇₄/G₁₃₀₁, A₁₀₂₀/G₁₃₀₁ and G₁₁₀₂/G₁₃₀₁ are protein fragments starting from A₃₄₈, M₈₂₇, V₉₂₀, A₉₇₄, A₁₀₂₀, and G₁₁₀₂, respectively, and extending to G₁₃₀₁, the end of p150. Fragments V₉₂₀/H₁₂₉₀, V₉₂₀/V₁₂₉₅, V₉₂₀/P₁₂₉₆, V₉₂₀/L₁₂₉₇, and V₉₂₀/R₁₂₉₉ extend from V₉₂₀ to positions H₁₂₉₀, V₁₂₉₅, P₁₂₉₆, L₁₂₉₇, and R₁₂₉₉, respectively. These fragments did not contain a cleavage site and were examined for their *trans*-cleavage capacity. Fragments V₉₂₀/I₁₇₇₃, A₉₇₄/I₁₇₇₃, A₁₀₂₀/I₁₇₇₃, and G₁₁₀₂/I₁₇₇₃ extend from A₃₄₈, V₉₂₀, A₉₇₄, A₁₀₂₀, and G₁₁₀₂, respectively, to I₁₇₇₃ of the NSP sequence. They contain cleavage sites and C-terminal tails to be used for *cis*-cleavage analysis.

4.1.3. Defining the NS-pro domain required for *trans* cleavage.

To determine the *trans*-cleavage activity of the generated protease constructs, six protease constructs with nested N-terminal deletions (A₃₄₈/G₁₃₀₁, M₈₂₇/G₁₃₀₁, V₉₂₀/G₁₃₀₁, A₉₇₄/G₁₃₀₁, A₁₀₂₀/G₁₃₀₁, and G₁₁₀₂/G₁₃₀₁) were translated *in vitro* separately, producing protein products with apparent molecular masses of 102, 50, 41, 35, 30, and 21 kDa, respectively (Fig. 12A, B, C, D, E and F, lane 1). Each was examined for *trans* protease activity analysis against substrate by cotranslation with p200(C1152S). In the cases of A₃₄₈/G₁₃₀₁, M₈₂₇/G₁₃₀₁, and V₉₂₀/G₁₃₀₁, cleavage products p150 and p90 were detected after a 1-h incubation and increased with incubation time, suggesting that these constructs possess *trans* cleavage activity (Fig. 12A, B and C, lanes 2 to 6). No detectable cleavage products (p150 or p90) could be observed in the reactions of A₉₇₄/G₁₃₀₁, A₁₀₂₀/G₁₃₀₁, and G₁₁₀₂/G₁₃₀₁ (Fig. 12D, E and F, lanes 2 to 6), suggesting that they could not form active protease to cleave in *trans*. My data suggested that the domain containing active *trans* protease starts at V₉₂₀ or after, but at least upstream of A₉₇₄.

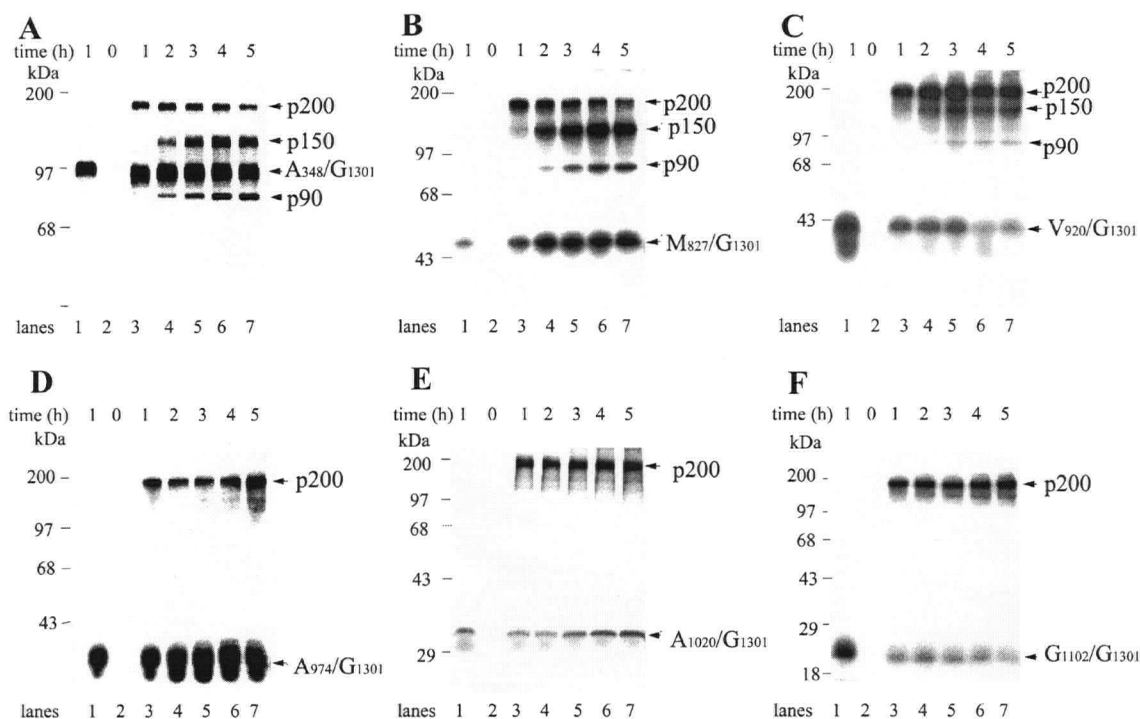


Figure 12. *In vitro* translation of protease constructs (*A*₃₄₈/*G*₁₃₀₁, *M*₈₂₇/*G*₁₃₀₁, *V*₉₂₀/*G*₁₃₀₁, *A*₉₇₄/*G*₁₃₀₁, *A*₁₀₂₀/*G*₁₃₀₁, and *G*₁₁₀₂/*G*₁₃₀₁) and examination of their *trans*-cleavage activities.

*A*₃₄₈/*G*₁₃₀₁ (A), *M*₈₂₇/*G*₁₃₀₁ (B), *V*₉₂₀/*G*₁₃₀₁ (C), *A*₉₇₄/*G*₁₃₀₁ (D), *A*₁₀₂₀/*G*₁₃₀₁ (E), and *G*₁₁₀₂/*G*₁₃₀₁ (F) were translated individually to give 102-, 50-, 41-, 35-, 30-, and 21-kDa products (lanes 1). Cotranslation of each construct with substrate p200(C1152S) was carried out at 30 °C for 0 to 5 h. Samples were removed at each time point and subjected to SDS-PAGE analysis. (lanes 2 to 7). Positions of molecular mass markers and cleavage products are indicated. Images were scanned using a UMAX Astra 1220U scanner with Adobe Photoshop 5.0 software.

Five protease constructs (*V*₉₂₀/*H*₁₂₉₀, *V*₉₂₀/*V*₁₂₉₅, *V*₉₂₀/*P*₁₂₉₆, *V*₉₂₀/*L*₁₂₉₇, and *V*₉₂₀/*R*₁₂₉₉) extending from *V*₉₂₀ to different C termini, were of the same molecular mass, 41 kDa, when expressed *in vitro* (Fig. 13, lanes 1). As described above, each of them was examined for potential *trans*-cleavage activity by cotranslation with p200(C1152S) for up to 5 h (Fig. 13). The appearance of cleavage products (p150 and p90) in the reactions of *V*₉₂₀/*P*₁₂₉₆, *V*₉₂₀/*L*₁₂₉₇, and *V*₉₂₀/*R*₁₂₉₉ demonstrated that they preserve protease activity (Fig. 13C, D and E, lanes 2 to

6). In contrast, neither V_{920}/H_{1290} nor V_{920}/V_{1295} was able to cleave substrate p200 (Fig. 13A and B, lanes 2 to 6). I therefore mapped the C terminus of the active RV NS-pro domain exactly to P_{1296} . The weak *trans*-cleavage activity observed in V_{920}/P_{1296} , V_{920}/L_{1297} , and V_{920}/R_{1299} could be due to the absence of the X domain in these constructs (see section 4.1.5. below).

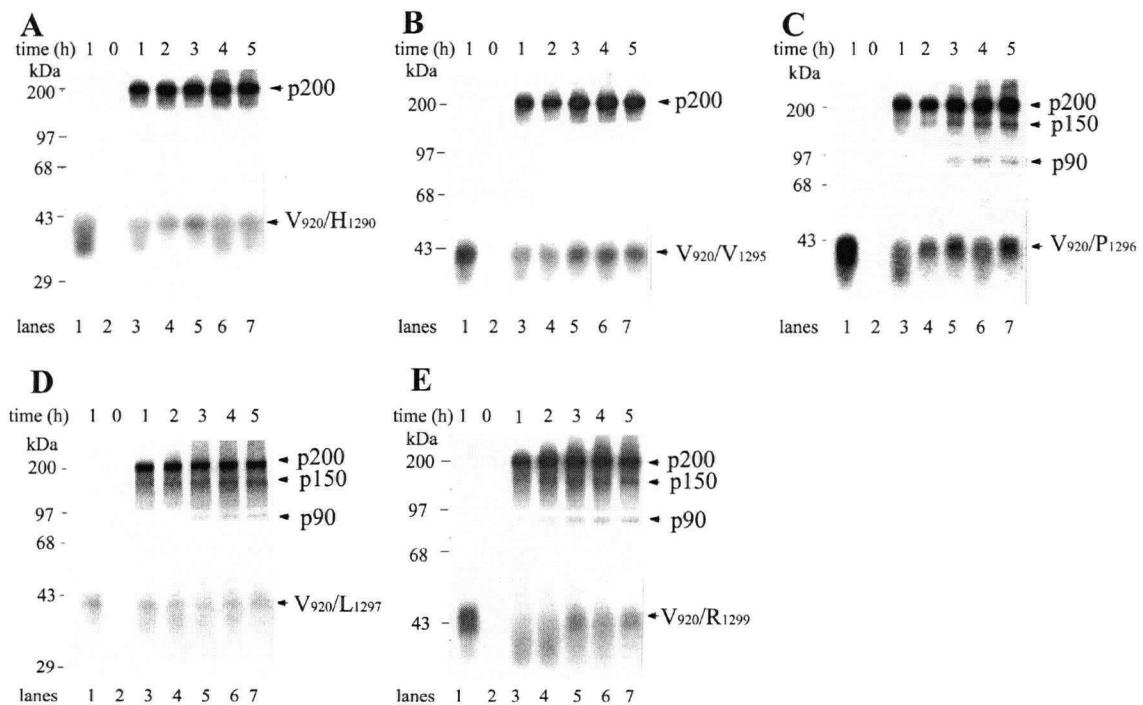


Figure 13. *In vitro* translation of protease constructs (V_{920}/H_{1290} , V_{920}/V_{1295} , V_{920}/P_{1296} , V_{920}/L_{1297} , and V_{920}/R_{1299}) and examination of their *trans*-cleavage activities.

V_{920}/H_{1290} (A), V_{920}/V_{1295} (B), V_{920}/P_{1296} (C), V_{920}/L_{1297} (D), and V_{920}/R_{1299} (E) were translated *in vitro* separately to yield a 40-kDa product (lanes 1). Cotranslation with substrate p200(C1152S) was carried out for 0 to 5 h (lanes 2 to 7), and samples were subjected to SDS-PAGE analysis. Positions of molecular mass markers and cleavage products are indicated. Images were scanned using a UMAX Astra 1220U scanner with Adobe Photoshop 5.0 software.

4.1.4. Domains required for *cis* cleavage.

RV NS-pro is known to possess both *trans*- and *cis*-cleavage activities (Yao *et al.*, 1998). The cotranslation experiments described above identified the NS-pro domain required for *trans* cleavage within the fragment from V₉₂₀ to P₁₂₉₆. This domain may or may not be the exact domain required for *cis* cleavage. Since the C terminus of the *cis* protease construct must extend beyond the cleavage site, I therefore examined the N-terminal domain requirement for *cis* cleavage by analysis of *in vitro* translation of the protease constructs V₉₂₀/I₁₇₇₃, A₉₇₄/I₁₇₇₃, A₁₀₂₀/I₁₇₇₃, and G₁₁₀₂/I₁₇₇₃. Processing of these protein constructs would accumulate a cleavage product with an apparent molecular mass of 58 kDa (p58, the C-terminal fragment extending from residue 1302 to 1773) throughout the incubation time. I found that V₉₂₀/I₁₇₇₃ and A₉₇₄/I₁₇₇₃ underwent efficient processing. V₉₂₀/I₁₇₇₃ was translated as a 98-kDa polyprotein, which was then cleaved into 58- and 41-kDa products within a 1-h incubation (Fig. 14A). A₉₇₄/I₁₇₇₃ was translated as a 92-kDa product and cleaved into 58-kDa and 35-kDa products efficiently (Fig. 14B). Self-cleavage of A₁₀₂₀/I₁₇₇₃ (87 kDa) into 58-kDa and 29-kDa products was less efficient (Fig. 14C). The band above p29 seems to be a translation by-product rather than a cleavage product since its amount did not increase with time as the p29 band did. No cleavage could be observed in the case of G₁₁₀₂/I₁₇₇₃ (78 kDa) (Fig. 14D). Of these constructs, only V₉₂₀/I₁₇₇₃ contains a protease domain (V₉₂₀ to G₁₃₀₁) that can cleave in *trans* at low efficiency (Fig. 12C). Therefore, the highly efficient processing of V₉₂₀/I₁₇₇₃ represents *cis*-cleavage activity rather than *trans*-cleavage activity. The other two constructs, A₉₇₄/I₁₇₇₃ and A₁₀₂₀/I₁₇₇₃, do not contain the necessary domain (V₉₂₀ to R₉₇₃) for *trans* cleavage and can function only in *cis*. To confirm that constructs V₉₂₀/I₁₇₇₃, A₉₇₄/I₁₇₇₃, and A₁₀₂₀/I₁₇₇₃ function in *cis*, a dilution experiment was performed (Fig. 14E). Translation reactions with V₉₂₀/I₁₇₇₃ (Fig. 14E, lanes 1 to 5), A₉₇₄/I₁₇₇₃ (Fig. 14E, lanes 6 to 10), and A₁₀₂₀/I₁₇₇₃ (Fig. 14E, lanes 11 to 15) were carried out using serial

dilutions (0, 1:20, 1:100, 1:200, and 1:500) of each RNA transcript. For each of them, the total translation products decreased correspondingly when more-diluted RNA was added. However, cleavage products were clearly demonstrated, and the cleavage ratio (determined as in section 3.2.15.) remained roughly unchanged from that for nondiluted samples, suggesting that these cleavages occur in *cis*.

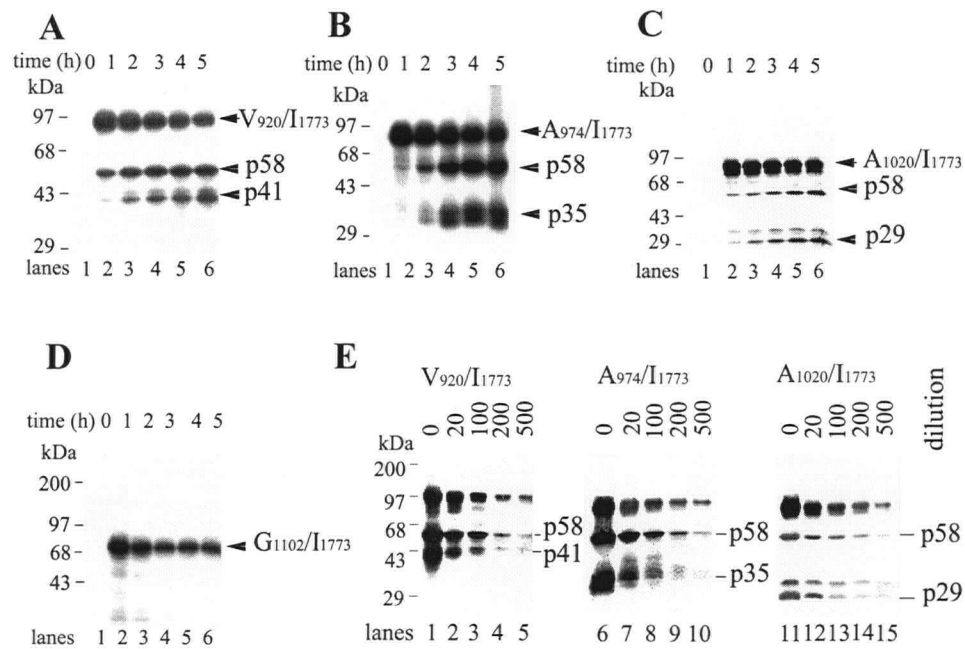


Figure 14. Autolytic processing of protease constructs V_{920}/I_{1773} , A_{974}/I_{1773} , A_{1020}/I_{1773} , and G_{1102}/I_{1773} .

V_{920}/I_{1773} (A), A_{974}/I_{1773} (B), A_{1020}/I_{1773} (C), and G_{1102}/I_{1773} (D) were transcribed and translated as described above for 5 h in the presence of [35 S]methionine. Samples were removed at the indicated times and subjected to SDS-PAGE analysis. (A) V_{920}/I_{1773} was translated as a 98-kDa protein and subsequently processed into 58- and 41-kDa fragments. Positions of V_{920}/I_{1773} , p58, and p41 are indicated by arrows. (B) A_{974}/I_{1773} gave a 92-kDa product, which was autocleaved into p58 and p35, as indicated by arrows. (C) A_{1020}/I_{1773} was translated into an 87-kDa product, whose processing generated p58 and p29 as indicated. (D) G_{1102}/I_{1773} gave a 78-kDa protein, whose autolytic processing was undetectable. (E) Translation reactions of V_{920}/I_{1773} , A_{974}/I_{1773} , and A_{1020}/I_{1773} were each programmed with input RNA at 0, 1:20, 1:100, 1:200, and 1:500 dilutions, and mixtures were incubated for 4 h. Positions of molecular mass markers and cleavage products are indicated. Images were scanned using a UMAX Astra 1220U scanner with Adobe Photoshop 5.0 software.

My results suggest that a construct starting from A₁₀₂₀ to a residue after the cleavage site such as to include the N terminus of p90 is sufficient for *cis* processing. Comparison between domains required for *cis*- and *trans*-cleavage activities of NS-pro indicated that the domains involved in *cis*- and *trans*-cleavage activities are different. Obviously, the *cis* protease domain must contain a cleavage site and C-terminal tail for *cis* cleavage to occur. This is not the case for the *trans* protease domain. However, it is interesting that the N-terminal domains are different between *cis* and *trans* cleavage for RV NS-pro. The domain from V₉₂₀ to A₁₀₂₀ is required for *trans* cleavage but is dispensable for *cis* cleavage. It will be of interest to examine the functions of the domain from V₉₂₀ to A₁₀₂₀ in *trans* cleavage.

4.1.5. Effect of N-terminal regions on cleavage efficiency.

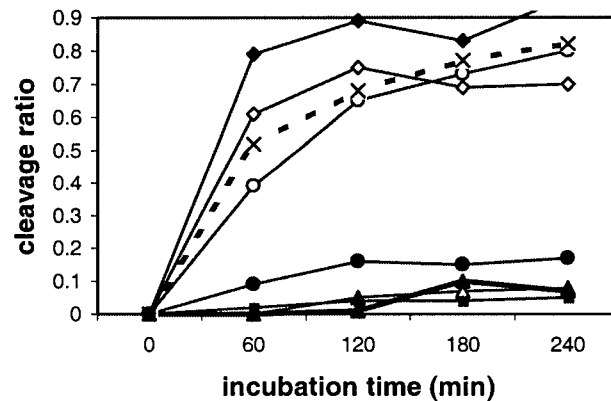
The protease constructs examined in this study were found to have variable cleavage efficiencies, depending on the region and length deleted. Cleavage efficiency was compared among different protease constructs by using the percentage of cleaved products with respect to total proteins, expressed as a cleavage ratio. The cleavage ratio for each protease construct at certain incubation time was calculated as described in section 3.2.15, and plotted against time.

Fig. 15A Compares the *trans*-cleavage efficiency among positive controls [p200(G1301S) and p150], A₃₄₈/G₁₃₀₁, M₈₂₇/G₁₃₀₁, V₉₂₀/G₁₃₀₁, V₉₂₀/P₁₂₉₆, V₉₂₀/L₁₂₉₇, and V₉₂₀/R₁₂₉₉. For p200(G1301S) and p150, the function time began when the protease and substrate were mixed. However, for each of A₃₄₈/G₁₃₀₁, M₈₂₇/G₁₃₀₁, V₉₂₀/G₁₃₀₁, V₉₂₀/P₁₂₉₆, V₉₂₀/L₁₂₉₇ and V₉₂₀/R₁₂₉₉, the protease functioned only after it had been translated, which took about 40 to 60 min. Therefore, the effective function time was taken as the real incubation time minus 60 min. The eight protease constructs could be separated into two groups according to their proteolytic

activity: one group with high cleavage ratio (70 to 90%), including p200(G1301S), p150, A₃₄₈/G₁₃₀₁, and M₈₂₇/G₁₃₀₁, and the other group with low cleavage ratio (5 to 17%), including V₉₂₀/G₁₃₀₁, V₉₂₀/P₁₂₉₆, V₉₂₀/L₁₂₉₇, and V₉₂₀/R₁₂₉₉. A₃₄₈/G₁₃₀₁ and M₈₂₇/G₁₃₀₁ had cleavage efficiencies comparable to those of p200(G1301S) and p150, the positive controls for *trans*-cleavage activity, whereas V₉₂₀/G₁₃₀₁, differing from M₈₂₇/G₁₃₀₁ in lacking an X domain, had a substantially lower cleavage ratio (17%) than M₈₂₇/G₁₃₀₁ (82%). These results suggest an important role of the X domain in *trans* cleavage.

As discussed above, the processing of V₉₂₀/I₁₇₇₃ is largely by *cis* cleavage, and the processing of A₉₇₄/I₁₇₇₃ or A₁₀₂₀/I₁₇₇₃ is the consequence of *cis* cleavage only. Therefore, the processing efficiencies of V₉₂₀/I₁₇₇₃, A₉₇₄/I₁₇₇₃, and A₁₀₂₀/I₁₇₇₃ (Fig. 15B) reflected their respective *cis*-cleavage abilities. The constructs compared in Fig. 15B can be classified into two groups: one with high processing ratios (60-70%) including WT NSP, V₉₂₀/I₁₇₇₃, and A₉₇₄/I₁₇₇₃, the other (A₁₀₂₀/I₁₇₇₃) with a processing ratio as low as 35%. The fact that V₉₂₀/I₁₇₇₃ and A₉₇₄/I₁₇₇₃ had as efficient *cis* cleavage as WT NSP suggested that the lack of an X domain in V₉₂₀/I₁₇₇₃ and A₉₇₄/I₁₇₇₃ had no significant influence on their self-processing. However, the domain from residue 974 to 1020, though not required absolutely, had a substantial effect on *cis* cleavage.

A. *trans* cleavage



B. *cis* processing

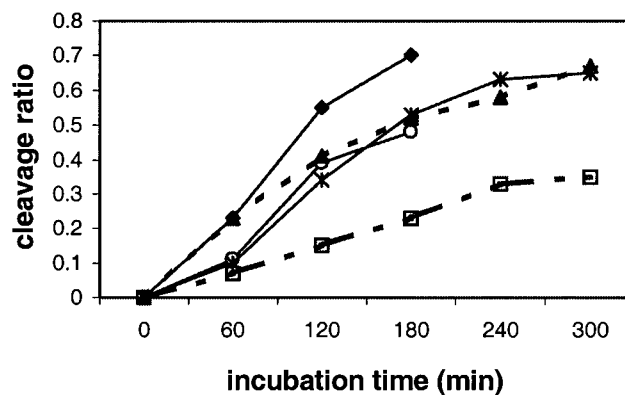


Figure 15. Cleavage efficiencies of protease constructs.

Protein bands of substrate and cleavage products on SDS-PAGE gel were quantitated using the Scion image program. The cleavage ratio for each protease construct was calculated, and plotted against incubation time. (A) *trans*-cleavage efficiency comparisons. ◇, p200(G1301S); ◆, p150; ○, A₃₄₈/G₁₃₀₁; ×, M₈₂₇/G₁₃₀₁; ●, V₉₂₀/G₁₃₀₁; △, V₉₂₀/P₁₂₉₆; ▲, V₉₂₀/L₁₂₉₇; ■, V₉₂₀/R₁₂₉₉. (B) *cis*-cleavage efficiency comparisons. ◆ and ○, WT NSP in the absence and presence, respectively, of Zn²⁺; ▲, V₉₂₀/I₁₇₇₃; *, A₉₇₄/I₁₇₇₃; □, A₁₀₂₀/I₁₇₇₃.

4.1.6. Secondary structure prediction for RV NS-pro.

Gorbalenya *et al.* (1991) reported sequence similarity between papain, a cellular cysteine protease, and RV NS-pro in the vicinity of catalytic C and H residues through local alignment. The catalytic C and H residues are separated by 133 residues in papain and 120 residues in RV NS-pro (Gorbalenya *et al.*, 1991). There are 24 residues upstream of the catalytic C residue in papain. The active RV NS-pro domain identified in this work was larger than papain, with about 230 residues upstream of the catalytic C₁₁₅₂ that are required for *trans* cleavage or about 130 residues upstream of C₁₁₅₂ that are required for *cis* cleavage. It has been reported that through sequence alignment and secondary structure comparison to known protein structures, topologic prediction of uncharacterized proteins is possible (Skern *et al.*, 1998). Skern *et al.* (1998) proposed a papain-like fold for the FMDV Lpro, a viral PCP, from the analysis of predicted secondary structure. This prediction was confirmed by a recent crystallographic analysis of FMDV Lpro showing a globular papain-like catalytic domain with adaptation for the specific requirements of the virus (Guarne *et al.*, 1998). In the hope of obtaining initial structural information on RV NS-pro, I compared the primary and secondary structures of RV NS-pro to those of papain. The analyses were performed with strains M33 and Therien, both of which are WT isolates of RV and differ from each other by two residues (A1140V and R1201W, M33 versus Therien) within the examined NS-pro catalytic region (from residue 1128 to 1301), with identical results. Only the result for RV strain M33 is presented here (Fig. 16).

To determine the global similarity between papain and RV NS-pro with respect to their catalytic sites, sequence alignment between papain and the RV NS-pro catalytic region (residues 1128 to 1296) was made using the ALIGN program (Myers and Miller, 1988) with

manual modification (Fig. 16). The alignment gave an identity of 18.1%, and, as expected, the two sequences exhibited most similarity around C and H, the catalytic sites. The derived alignment was further supported by the analysis of the predicted secondary structure of RV NS-pro (illustrated in Fig. 16). RV NS-pro was predicted to have the α - β structural organization found in cellular PCPs. This prediction has three α -helices (α L1, α L2/3, and α R1) and six β -sheets (A-F) in RV NS-pro. Most of these were present in the papain structure at corresponding positions including β A, α L1, α R1, β C, β D, β E, and β F (Kamphuis *et al.*, 1984, 1985). The match was highest in the catalytic C and H regions, with differences occurring in the linker regions and the C end. In NS-pro, an α -helix, α L2/3, took the place where two helices, α L2 and α L3, occurred in papain. β B1 and β B2 for NS-pro did not match the position of β B for papain well. Furthermore, the α R2 in the linker region and β G at the C end were missing in the NS-pro prediction. RV NS-pro had a shorter linker region (120 residues) between catalytic C and H residues than papain (133 residues) and a shorter tail after the catalytic H residue (23 residues) than papain (53 residues), which explained the discrepancies. It was proposed (Skern *et al.*, 1998) that loops between the secondary elements that define the papain topology can be modified, by insertions or deletions, without interfering with the overall folding of the molecule. Therefore, the global similarity of their secondary structures suggested that RV NS-pro might maintain a papain-like topology for its catalytic region, whereas those differences may come from the adaptive changes for the viral specificity. Crystallographic data are necessary for precise structure determination for RV NS-pro.

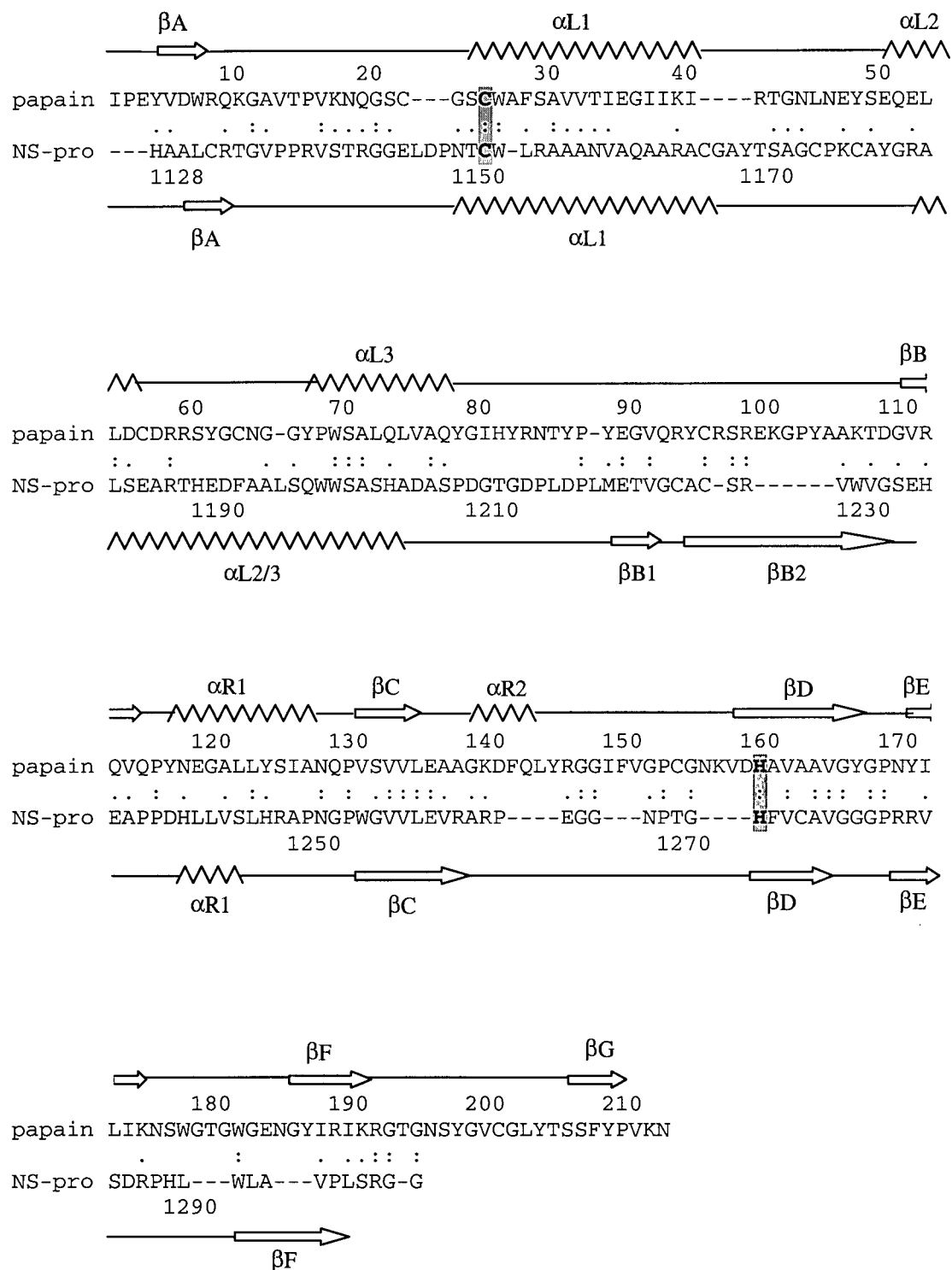


Figure 16. Comparison of primary and secondary structures between RV NS-pro and papain.

Figure 16. Comparison of primary and secondary structures between RV NS-pro and papain. The protein sequence of papain (SWISS-PROT accession number P00784) was aligned to that of NS-pro (strain M33; GenBank accession number S38480 with corrections by Pugachev *et al.*, 1997) using ALIGN software, with manual adjustment. The papain sequence is numbered as for mature protease, and RV-NS-pro sequence is numbered as for the NSP ORF. Identical residues are marked ":", conserved amino acids with ".". Cys and His at the catalytic sites are in boldface and shaded. Features of the secondary structure of papain (Kamphuis *et al.*, 1984) are illustrated above the sequence. Secondary structure for RV NS-pro was calculated by the EMBL protein prediction server (Rost *et al.*, 1993, 1994) and is illustrated below the NS-pro sequence. α -helices are shown as curves, and β -sheets are shown as arrows. α -helices are named according to the nomenclature of Kamphuis *et al.* (1984); β -sheets are named as described by Skern *et al.* (1998).

4.1.7. Discussion I

I have used an *in vitro* translation system to identify domains important for *cis*- and *trans*-cleavage activities of RV NS-pro. The results are summarized in Fig. 17. Through analysis of protease activity using RNA transcripts from cloned material with serial deletions from either end of p150, I have demonstrated that RV NS-pro requires a region from residue 920 to 1296 to perform functional *trans* cleavage (Figs. 12 and 13). The N-terminal region of NS-pro was roughly determined to reside between residues 920 and 974 (Fig. 12C and D). The C end was precisely determined to be P₁₂₉₆ (Fig. 13B and C). However, the minimal NS-pro domain (residues 920 to 1296) for *trans* cleavage processed only 5 to 17% of substrate after 4 h of incubation, compared to the 70 to 96% for the positive controls, p200(G1301S) and p150 (Fig. 15A). The NS-pro domain that maintains as high *trans*-cleavage ability as the positive controls is found in the construct M₈₂₇/G₁₃₀₁ (80% cleavage at 4 h), starting from around residue M₈₂₇ (Fig. 15A).

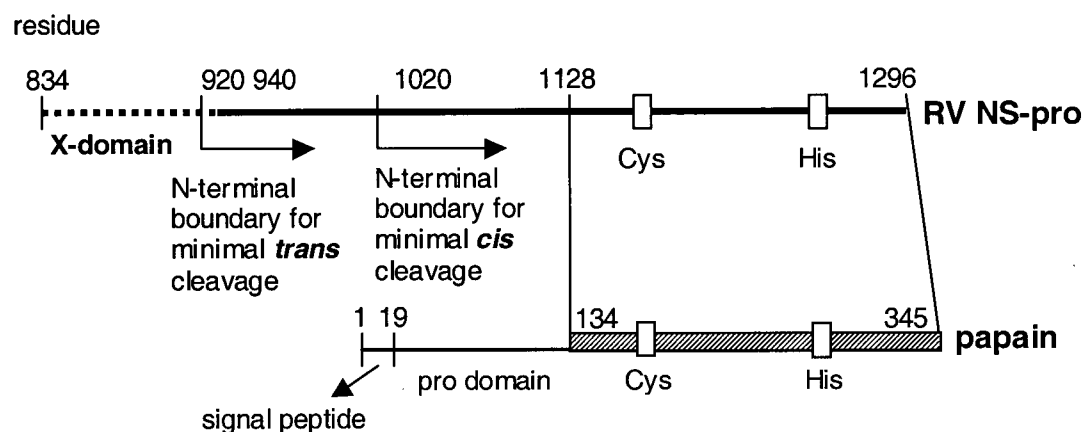


Figure 17. Functional domains of RV NS-pro and comparison with complete papain sequence.

Residues of RV NS-pro are numbered as for the RV NSP ORF. The X domain (residues 834 to 940) is shown by the dotted line, positioned outside the essential protease domains of NS-pro shown as a solid heavy line. The N-terminal boundary for the minimal domain of either *trans*- or *cis*-cleavage activity is indicated by the arrow starting from residue 920 or 1020, respectively. The region from residue 1128 to 1301 is compared to the mature papain protease in this work, and the boundary is indicated by vertical dotted lines. The predicted catalytic residues Cys and His of RV NS-pro and catalytic residues Cys and His of papain are represented by open squares. For a complete papain sequence, residues 1 to 18 encode the signal peptide shown as a heavy line, residues 19 to 133 are the pro region, and residues 134 to 345 contain the mature papain sequence.

RV NS-pro possesses both *cis* and *trans* activities (Yao *et al.*, 1998). Both use the same cysteine protease cleavage mechanism and thus should employ the same core catalytic structure (Kamphuis *et al.*, 1985). They may vary in other external domain requirements. In addition to the protease domain, the *cis* protease must include intact cleavage site and substrate regions. The most significant difference between *cis* and *trans* cleavage for RV NS-pro lies at the N-terminal domains. When a panel of protease constructs with nested N-terminal deletions (V₉₂₀/I₁₇₇₃, A₉₇₄/I₁₇₇₃, A₁₀₂₀/I₁₇₇₃, and G₁₁₀₂/I₁₇₇₃), with weak or no *trans*-cleavage activity, was examined for autoprocessing, V₉₂₀/I₁₇₇₃, A₉₇₄/I₁₇₇₃, and A₁₀₂₀/I₁₇₇₃ were active in *cis*, while

G₁₁₀₂/I₁₇₇₃ was not (Fig. 14). Thus, protease active in *trans* starts after residue 920 but before 974, while that in *cis* begins after residue 1020. These results suggested that the core protease domain (required for both *cis* and *trans* activity) ranges from around residue 1020 to residue 1296, and that the fragment from residue 920 to 1020 is required only for *trans* cleavage while being dispensable for *cis* processing (Fig. 17). My data are the first to show that RV NS-pro uses different domains for *cis* and *trans* cleavage. Since *trans* cleavage is a bimolecular interaction, it is likely that the domain of residues 920 to 1020 is involved in protein-protein interaction, required to position substrate protein into the *trans* protease catalytic site. For *cis* cleavage, this protein-protein interaction is not necessary in order to hold substrate and enzyme together. Identification of the *trans*-specific domain facilitates the future studies on the biological significance of *trans*-cleavage activity.

Sequence analysis on M-group PCPs of several virus families (such as alphavirus and coronavirus, etc.) had identified a conserved X domain near the protease domain (Gorbalenya *et al.*, 1991; Strauss and Strauss, 1994). In RV, this X domain lies N-terminal to the protease domain, ranging from residue 834 to 940 (Fig. 17) (Gorbalenya *et al.*, 1991). Functions of the X domain remain to be characterized. Association of X domain with M-group PCPs (possessing both *cis* and *trans* activity) rather than L-group PCPs (containing only *cis* activity) encouraged the speculation that the X domain might be involved in the regulation of polyprotein processing (Gorbalenya *et al.*, 1991). Elimination of the X domain from PLP-1 of MHV reduced cleavage by 22 to 63% (Bonilla *et al.*, 1995; Teng *et al.*, 1999). In my experiments, RV NS-pro remained enzymatically active after all or most of the X domain had been removed. V₉₂₀/G₁₃₀₁ cleaved substrate in *trans*, and A₉₇₄/I₁₇₇₃ processed itself efficiently (Figs. 12C and 14B). However, cleavage efficiencies differed considerably. In *trans* cleavage, the absence of the X domain in V₉₂₀/G₁₃₀₁ caused a substantially decreased cleavage ratio

(17%) compared to that for M₈₂₇/G₁₃₀₁ (82%), which contains the X domain (Fig. 15A). In contrast, *cis* cleavage was not affected significantly by the presence of the X domain, since V₉₂₀/I₁₇₇₃ and A₉₇₄/I₁₇₇₃ (both missing the X domain) processed themselves almost as efficiently as the positive control, WT-NSP (Fig. 15B). My results demonstrate the importance of the X domain in *trans* cleavage. Although it is unclear at present what function it could play in RV NS-pro *trans* cleavage, I speculate that this proline-rich region might provide a protein-protein interaction domain that enhances the opportunity for protease to meet its *trans* cleavage substrate and thus decreases the *K_m* of protease. Further studies of the biologic significance and functional mechanism of the X domain in NSP processing and virus replication are indicated.

The PCP family include a group of cellular and viral proteases which employ the catalytic C and H dyad. The distant relationship between viral and cellular PCPs was suggested from many primary sequence comparisons (Berti and Storer, 1995; Gorbalenya *et al.*, 1991) and from the crystal structure of FMDV Lpro, the only structure determined on a viral PCP (Guarne *et al.*, 1998). Sequence alignment showed that the catalytic region of RV NS-pro (from residue 1128 to 1296) has global sequence similarity with papain (Fig. 16). Secondary structure comparison also supported their topologic relationship (Fig. 16). It is possible that the catalytic region of RV NS-pro exhibits a papain-like folding with adapted modifications. To obtain the full tertiary structural information of RV NS-pro will require crystallographic analysis.

The additional N-terminal region of the RV NS-pro core domain (from A₁₀₂₀ to A₁₁₂₇) has no corresponding sequence in papain and was excluded from alignment with it. It is likely that this N domain may not contain sequences directly required for protease activity. Rather, it may serve other subsidiary functions, such as folding assistance, conformational stability, and/or protein-protein interactions. Papain, as well as other proteases, is translated as a pro-protease

with an additional N-terminal region (115 residues of pro region for papain) (SWISS-PROT accession number P00784) (Fig. 17). In many proteases, the pro region plays an active role in protein folding. Subtilisin (Bryan *et al.*, 1995), α -lytic protease (Baker *et al.*, 1992), carboxypeptidase A1 (Phillips and Rutter, 1996), and carboxypeptidase Y (Ramos *et al.*, 1994) do not fold into active conformations in the absence of their pro regions. The pro region is essential for folding of at least one PCP (cathepsin L) (Tao *et al.*, 1994). The pro regions of PCPs can also perform other biological roles, such as stabilization (Mach *et al.*, 1994; Tao *et al.*, 1994) and subcellular targeting (Mao *et al.*, 1998; McIntyre and Erickson, 1993). It would be interesting to determine whether the region from A₁₀₂₀ to A₁₁₂₇ of RV NS-pro serves subsidiary roles similar to those of the pro regions for many other proteases.

4.2. *Effects of NSP cleavage on virus replication and RNA synthesis*

4.2.1. Construction of mutants.

In order to study the effects of RV NSP processing on virus replication, the RV genome was altered by mutations that affect only NSP processing while avoiding any other possible structural or functional alterations in the NSP or in the viral genome. A panel of site-directed mutations was generated by PCR mutagenesis. These included catalytic-site mutation C1152S and cleavage-site mutations G1301S, R1299A, G1300A, and G1301A. Most of the introduced mutations are conservative alterations, such as C to S and G to A, and thus are unlikely to affect the overall structure of the protein or functions of NSP other than proteolytic processing. To facilitate the process of mutagenesis for construction of the G1300A and G1301A mutations, a silent mutation was introduced into the RV infectious cDNA clone pBRM33 (Yao and Gillam, 1999) to create a new *Xba* I site at nt 3935. The resultant cDNA clone was named pBRM33-X.

In terms of virus growth, plaque size, and specific infectivity, pBRM33-X was indistinguishable from pBRM33 (Table 3, Fig. 20, and Fig. 21). Amplified PCR fragments containing the desired mutations were reintroduced into pBRM33 or pBRM33-X, and the respective cDNA clones were named after their mutations: pBRM33(C1152S), pBRM33(G1301S), pBRM33(R1299A), pBRM33(G1300A), and pBRM33(G1301A). The plasmid constructs encoding these mutations are listed in Table 2.

Table 2. Mutations created at the catalytic site and around the cleavage site.

Mutation	Catalytic site	Around cleavage site ^a
None (WT)	C ₁₁₅₂	R ₁₂₉₉ -G ₁₃₀₀ -G ₁₃₀₁ ↓G ₁₃₀₂
C1152S	S	
R1299A		A
G1300A		A
G1301A		A
G1301S		S

^a Cleavage occurs after G₁₃₀₁, as indicated by the vertical arrow.

4.2.2. Effects of mutations on NSP processing.

To determine whether the p200 polyprotein itself can function in RNA replication, I constructed a panel of cleavage-defective mutations. The effect of mutations on NSP processing was determined using time course analysis of *in vitro* translation reactions programmed with full-length RNA transcripts from cDNA clones as described in section 4.1. The extent of NSP processing differed greatly among the WT and mutant RNAs (Fig. 18). To compare their cleavage efficiencies more precisely, the processing ratio, calculated as the percentage of the cleavage products in the total proteins, was assessed for each mutant and plotted against the incubation time (Fig. 19). From both gel analysis and the calculated processing ratio, WT NSP processing (Fig. 18A) was almost complete at 3 h of incubation (Fig.

19). The NSP processing of the G1300A mutant was slightly delayed and decreased (Fig. 18B and 19); its processing ratio at 3 h was 75% of the WT level (Fig. 19). Mutation R1299A substantially impaired NSP processing, since the cleavage products were detected only after 3 h of incubation (Fig. 18C) and the cleavage ratio at 3 h was approximately 20% of the WT level (Fig. 19). Mutation G1301A resulted in minimally detectable cleavage of p200, with a minute amount of p90 detected after a 3-h incubation time (Fig. 18D). Mutations C1152S and G1301S abolished NSP processing completely (Fig. 18E and F). Thus, my generated mutations either abolished (C1152S and G1301S) or blocked (R1299A, G1300A and G1301A) NSP processing to various degrees.

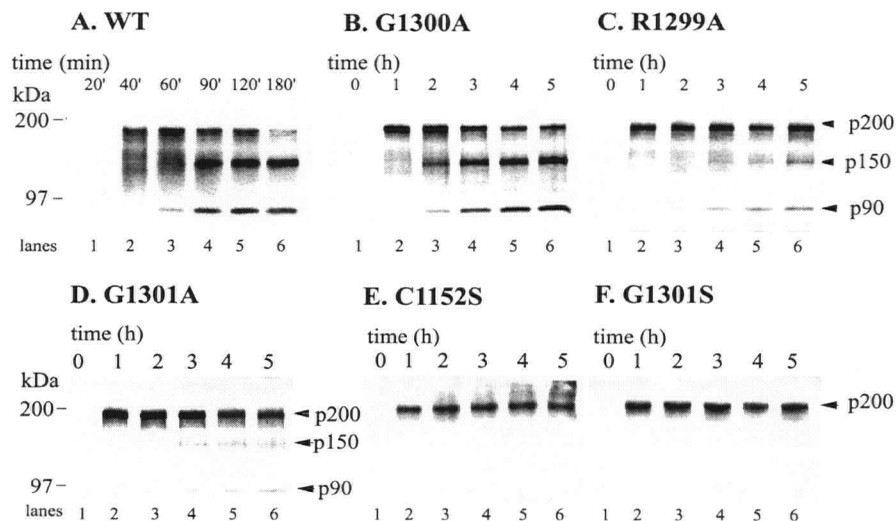


Figure 18. Effects of mutations on NSP processing in an *in vitro* translation system.

Full-length RV RNAs containing site-directed mutations were generated from corresponding *Hind* III-linearized cDNA templates with SP6 RNA polymerase. *In vitro* translation reaction mixtures containing rabbit reticulocyte lysates were prepared at 30°C. Aliquots were removed at the indicated times, and the protein products were resolved by sodium dodecyl sulfate-polyacrylamide gel electrophoresis (SDS-PAGE). Panels: A, WT NSP; B, G1300A mutant NSP; C, R1299A mutant NSP; D, G1301A mutant NSP; E, C1152S mutant NSP; F, G1301S mutant NSP. Positions of molecular mass markers and protein products are indicated. Images were scanned using a UMAX Astra 1220U scanner with Adobe Photoshop 5.0 software.

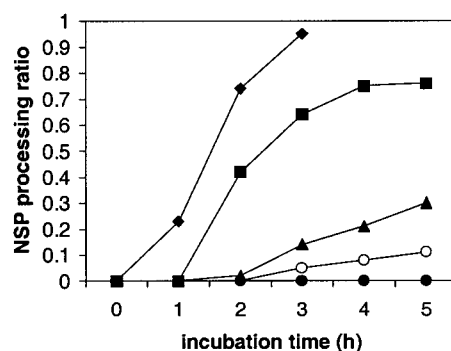


Figure 19. Comparison of processing ratios between the WT and mutant NSPs.

Protein bands of p200 and cleavage products, p150 and p90, were each quantitated at indicated times using SCImage software as described in Materials and Methods. The cleavage ratio was calculated as the percentage of the cleaved products over the total proteins, and plotted against incubation time. ◆, WT NSP; ■, NSP(G1300A); ▲, NSP(R1299A); ○, NSP(G1301A); ●, NSP(C1152S) and NSP(G1301S).

4.2.3. Effects of mutations on virus growth.

In order to examine the effects of mutations on RV replication, WT or mutant RNA, transcribed from respective full-length cDNA clones, was used to transfect either Vero or BHK-21 cells. The transfected Vero cells were incubated for 5 days and assayed for infectious virus released into the culture medium (Table 3). Infectious virus particles could be harvested from Vero cells transfected by the WT RNA and those with the G1300A and R1299A mutations, yielding virus titers of 3.4×10^6 , 1.2×10^6 , and 1.0×10^3 PFU/ml, respectively. In contrast, no plaques were detected in the medium containing RNAs with the mutations G1301A, G1301S and C1152S, indicating that they are noninfectious (Table 3). Transfected Vero cells were also analyzed for the production of RV-specific SPs by immunoprecipitation with human anti-RV serum. RV SPs were readily detectable for the WT and the G1300A mutant but in a substantially lower quantity for the R1299A mutant. No RV SPs could be

detected from cells transfected by the G1301A, G1301S and C1152S RNAs (Fig. 20), indicating that they are defective in replication. To confirm that the different amounts of virus produced by the WT and mutant RNAs are not dependent on the host cells used, I also transfected BHK-21 cells with RNA transcripts by electroporation. At 48 h postelectroporation, the culture medium was collected and the released virus particles were quantitated. Consistent with the results obtained with Vero cells, infectious virus particles were only detected from BHK-21 cells transfected with the WT, G1300A and R1299A RNAs. The virus titers were 1.5×10^7 , 6×10^6 , and 5×10^3 PFU/ml, respectively. Again, no infectious virus could be harvested from BHK-21 cells transfected with transcripts of G1301A, C1152S, or G1301S mutant RNA (Table 3). RNA transfection of BHK-21 cells by electroporation resulted in higher virus titers than that of Vero cells using Lipofectin, most likely due to the higher transfection efficiency of electroporation.

Table 3. Effects of RV NSP cleavage mutants on virus replication.

RV	Virus titer ^a (PFU/ml) at:		Plaque phenotype on Vero cells ^c
	Day 5 posttransfection of Vero cells	48 h posttransfection of BHK-21 cells	
WT	3.4×10^6	1.5×10^7	Big, clear, 6 dpi
WT M33-X	2.6×10^6	N/A	Big, clear, 6 dpi
G1300A mutant	1.2×10^6	6.0×10^6	Big, clear, 6 dpi
R1299A mutant	1.0×10^3	5.0×10^3	Tiny, unclear, 8 dpi
G1301A mutant	0 ^b	0 ^b	None
G1301S mutant	0 ^b	0 ^b	None
C1152S mutant	0 ^b	0 ^b	None

^aThe virus titers, determined by plaque assay on Vero cells, are the means of at least two independent experiments. N/A, data not available.

^bThe culture medium was tested without dilution and at 1:10 and 1:100 dilutions for the plaque assay. 0, no plaque formation was observed.

^cVero cells infected by the WT or mutant virus initiated by RNA transfection were overlaid with agarose medium and incubated for 6 days (for the WT and G1300A mutant) or 8 days (for the R1299A) before being stained with neutral red. dpi, days postinfection.

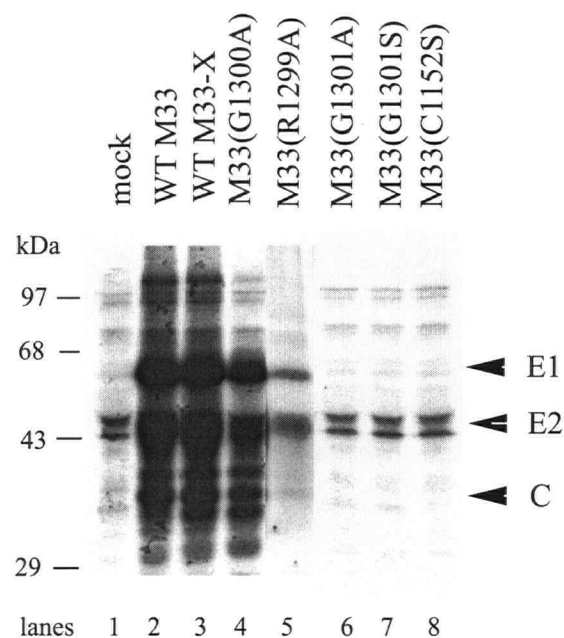


Figure 20. Immunoprecipitation of RV-specific SPs from cells transfected by WT and mutant RNAs.

Vero cells in 35-mm-diameter dishes were transfected with WT or mutant RV RNAs mediated by Lipofectin for 2 h at 37 °C and incubated with fresh medium for 6 days. Transfected cells were labeled with [³⁵S]-methionine for 2 h and lysed with lysate buffer. RV specific proteins were immunoprecipitated using human anti-RV serum and separated by 10% SDS-PAGE. Lane 1, mock transfection. Lane 2, WT M33 RNA. Lane 3, WT M33-X RNA. Lane 4, M33(G1300A) RNA. Lane 5, M33(R1299A) RNA. Lane 6, M33(G1301A) RNA. Lane 7, M33(G1301S) RNA. Lane 8, M33(C1152S) RNA. The positions of molecular mass marker and RV structural proteins were indicated. Images were scanned using a UMAX Astra 1220U scanner with Adobe Photoshop 5.0 software.

The results obtained with the two cell types are comparable. The amount of virus produced from each infectious RNA (WT, G1300A, or R1299A) varies with its NSP processing efficiency. In both cases, WT RNA, having the most efficient NSP processing, produced the highest virus titer. The G1300A mutant RNA, with 75% of the WT level of NSP processing, produced viruses at 30 to 40% of the WT level. The R1299A mutant RNA, with NSP

processing at 20% of the WT, released viruses at a level 2×10^3 to 3×10^3 -fold lower than that of the WT. The G1301A mutant RNA, with minimally detectable NSP processing *in vitro* (processing ratio of less than 10% at 5 h of incubation), and the C1152S and G1301S mutant RNAs, abolishing NSP processing completely, released no infectious virus particles in either Vero or BHK-21 cells and thus are effectively lethal. In addition to the differences in virus titer, the WT and mutants also have different plaque phenotypes. The WT and the G1300A mutant produced large, clear plaques at day 6 postinfection while the R1299A mutant resulted in tiny, unclear plaques only after day 8 postinfection.

To further analyze the influences of NSP cleavage on virus replication, growth rates were determined for the WT and infectious mutant (R1299A and G1300A) RNAs. Vero cells were transfected with the respective full-length RNAs mediated by Lipofectin. Culture medium was harvested every 24 h and replaced with fresh medium. Virus titers in the culture medium were quantitated by plaque assay on Vero cells and are shown in Fig. 21. For the WT, the amount of virus produced was about 3×10^3 PFU/ml at day 1 and reached a peak of 5×10^6 PFU/ml at day 4. The G1300A mutant had growth kinetics similar to those of the WT but yielded a 10-fold lower amount of released virus (2×10^2 PFU/ml) at day 1 and a 3-fold lower amount (1.6×10^6 PFU/ml) at day 4. The R1299A mutant virus was not detectable until after day 3, and its titer at day 5 was 2×10^3 -fold lower than that of the WT. The failure to detect R1299A virus plaques before day 3 posttransfection may be due to their small size at early stages of infection. My results demonstrate that NSP cleavage plays an important role in virus replication.

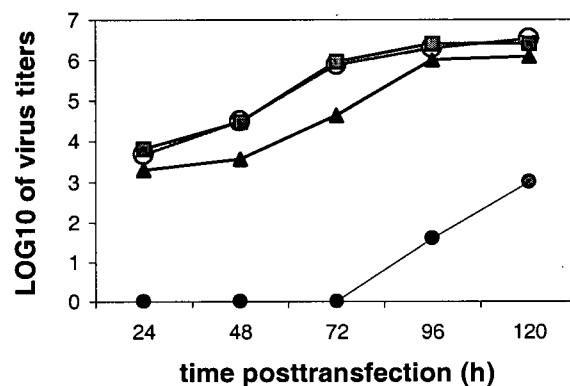


Figure 21. Growth curves of the WT, G1300A, and R1299A mutant viruses.

Vero cells in 35-mm-diameter dishes were transfected with WT or mutant RNAs mediated by Lipofectin for 2 h at 37 °C. The cells were overlaid with culture medium after removal of the Lipofectin-RNA mixtures. The culture medium was changed every 24 h, and the virus particles released into the medium were quantitated by plaque assay. The results shown are the means of at least two independent experiments. Symbols: ○, WT M33 RNA; ■, WT M33-X RNA; ▲, G1300A mutant; ●, R1299A mutant.

4.2.4. Effects of mutations on viral RNA synthesis.

The reduction in virus yield due to defects in NSP cleavage presumably occurred at the level of viral RNA synthesis. To determine at which step(s) RNA synthesis is impaired in the mutant viruses, I examined the synthesis of three viral RNA species in the WT and NSP cleavage mutant viruses at the early stage of virus replication using an RNase protection assay (RPA).

To evaluate the sensitivity of the RPA for detection of positive-strand RV RNA, various amounts of positive-strand RV RNA, transcribed *in vitro* from pBRM33, were subjected to an

RPA using 10^6 cpm of ^{35}S -labeled probe pb18, which contains 301 nt of the RV sequence and 27 nt of the vector sequence. The negative-polarity RV RNA, transcribed from a cDNA clone encoding an RV genome of reverse polarity, was also used as a negative control. As shown in Fig. 22A, a protected band of 301 nt was present in reaction mixtures containing 100 pg (lane 3), 1 ng (lane 4), 10 ng (lane 5), and 20 ng (lane 6) of positive-strand RNA, but was absent in reaction mixtures containing 10 pg of positive-strand RNA (lane 2) and 20 ng of negative-strand genomic RNA (lane 7). These data indicate that this assay is strand specific and sensitive enough to detect at least 100 pg of positive-strand RV RNA (approximately 10^7 molecules). Furthermore, quantitative analysis of the protected probe suggested that the signal was proportional to the amount of positive-strand RNA used.

In virus-infected cells, RV negative-strand genomic RNA exists mostly as a double-stranded intermediate form with positive-strand RNA present in large molar excess. To prevent interference between the probe and negative-strand RNA by the large molar excess of positive-strand RNA, a two-cycle RPA was employed to detect negative-strand genomic RNA (Novak and Kirkegaard, 1991). To determine the sensitivity of the two-cycle RPA for negative-strand RNA, various amounts of negative-strand genomic RNA, transcribed *in vitro* from a cDNA clone encoding an RV genome of reverse polarity, were hybridized with 20 ng of unlabeled RNA probe pb19 (the complementary sequence of pb18) in the first-cycle RPA. The products were subsequently hybridized with 10^6 cpm of ^{35}S -labeled pb19 and subjected to a second cycle (Fig. 22B). The probe pb19 is negative-strand specific, since no signal band was observed in the reaction mixture containing 10 ng of positive-strand genomic RNA (lane 7). The 301-nt signal band was apparent in a reaction mixture containing 1 ng (lane 4), 10 ng (lane 5), or 20 ng (lane 6) of negative-strand genomic RNA. A longer exposure (3 days) also detected the existence of this band in a reaction mixture containing 100 pg of negative RNA (lane 3).

Therefore, this two-cycle RPA is sensitive enough to detect more than 100 pg of negative-strand genomic RNA (approximately 10^7 RNA molecules). The signal intensity was proportional to the amount of negative-strand RNA.

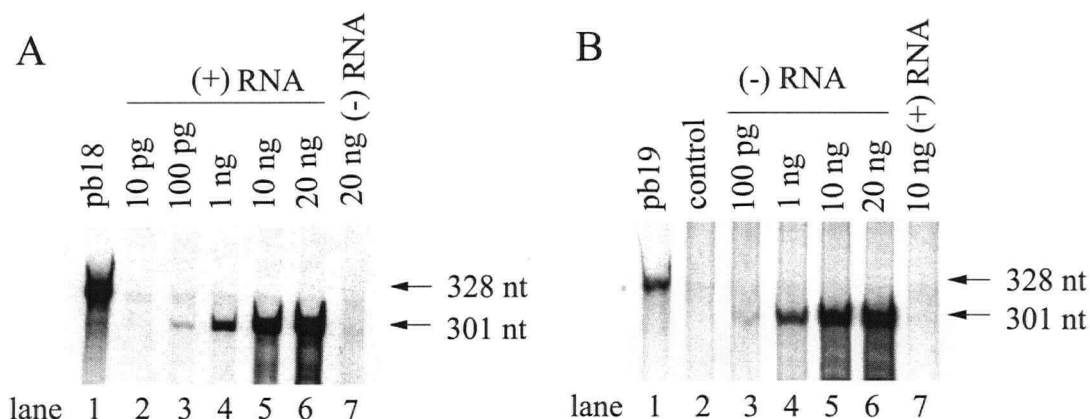


Figure 22. Sensitivity of RPA for detection of both positive- and negative-strand RV RNAs.

RPA reactions were carried out as described in section 3.2.14. The full-length RV RNAs of either positive or negative polarity used in this experiment were transcribed *in vitro* from the respective RV cDNA clone, pBRM33 or pBRNM33, encoding a full-length RV genome downstream of the SP6 RNA polymerase promoter in either the forward or the backward orientation. (A) Standard RPA reactions were performed on 10 pg, 100 pg, 1 ng, 10 ng, and 20 ng (lanes 2 to 6) of positive-strand RV RNAs in the presence of 1×10^6 cpm of ^{35}S -labeled probe pb18. A reaction mixture containing 20 ng of negative-strand RV RNA (lane 7) was also included as a negative control (lane 7). The products of RPA reactions along with 2×10^3 cpm of pb18 (lane 1) were resolved on a 5% polyacrylamide-7 M urea gel, which was treated with Enhancer (DuPont), dried, and exposed to X-ray film. (B) Two-cycle RPA reactions were performed with various amounts of negative-strand RV RNA. Negative-strand RV RNA was hybridized with 10 ng of transcribed unlabeled pb19 and subjected to the first-cycle RPA reaction. The products of the first-cycle RPA reaction were hybridized with 1×10^6 cpm of ^{35}S -labeled pb19 and subjected to the second-round RPA reaction. To examine the strand specificity of probe pb19, 10 ng of positive-strand RV RNA (lane 7) was analyzed in parallel. The control reaction mixture contained no RV RNA (lane 2). Lanes 3 to 6 represent reaction mixtures containing 100 pg, 1 ng, 10 ng and 20 ng of negative-strand RV RNA, respectively. Lane 1, pb19. The autoradiographs were exposed for 1 day. The positions of the 328-nt and the 301-nt bands are indicated. Images were scanned using UMAX Astra 1220U scanner with Adobe Photoshop 5.0 software.

I then examined viral RNA synthesis in BHK-21 cells transfected by electroporation with WT or mutant RNA transcripts. I consider virus-infected cells a less ideal system for the analysis of viral RNA synthesis because (1) revertants or second-site mutations may exist in virus stocks, (2) the system might be affected by the early steps of virus entry prior to viral RNA synthesis (e.g., virus entry and nucleocapsid uncoating), (3) the percentage of cells initially infected by RV is quite low (10 to 20%) (Frey, 1994; Hemphill *et al.*, 1988), and (4) studies of noninfectious mutants are impossible. In contrast, electroporation of viral RNA transcripts into BHK-21 cells provides an advantageous system for the analysis of RNA synthesis at an early stage of virus replication. This system bypasses the steps of virus entry and nucleocapsid disassembly; has a high efficiency of transfection, allowing detection of low levels of negative-strand RNA; and allows studies of noninfectious mutants.

To determine RNA synthesis of WT and mutant viruses, the respective viral RNAs transcribed *in vitro* were used to transfect BHK-21 cells by electroporation. At the indicated times, total cellular RNA was extracted and subjected to an RPA. A 2- μ g sample of RNA was used for positive-strand RNA detection, and 20 μ g was used for negative-strand RNA detection. At 0 h postelectroporation, the 301-nt protected fragment representing the positive-strand genomic RNA was apparent for all constructs (Fig. 23A, lanes 3, 6, 9, 12, 15, 18), representing the input genomic RNA transfected into cells. By 8 h postelectroporation, the intensity of the 301-nt band decreased to a low level (Fig. 23A, lanes 4, 7, 10, 13, 16, 19), suggesting that the input genomic RNA had mostly been degraded at that time. At 24 h postelectroporation, accumulation of both the protected 301-nt fragment and the 188-nt fragments (representing subgenomic RNA) was apparent for the WT and mutant G1300A (Fig. 23A, lanes 5 and 8). Much less of these bands was found with the R1299A mutant RNA (Fig. 23A, lane 11). The

G1301S and C1152S mutant RNAs exhibited decreased levels of the 301-nt band (compared with the amounts detected at 8 h; Fig. 23A, lanes 17 and 20). Subgenomic RNA represented by the 188-nt fragment was scarcely detectable for the two mutants. Thus, they show no evidence of production of positive-strand RNA. The G1301A mutant showed the presence of low levels of the 301-nt band with little increase at 24 h over the level found at 8 h. By 24 h, a trace of the 188-nt fragment was detected (Fig. 23A, lane 14), indicating some slight synthesis of positive-strand RNA. These results confirm that the more-infectious constructs produce more positive-strand RNAs and the noninfectious ones produce little (G1301A) or no (G1301S and C1152S) positive strands. Detailed quantitation of the amount of positive-strand RNA is presented below.

Fig. 23B shows the levels of negative-strand RNA produced by the constructs. At 0 h postelectroporation, no protected negative-strand RNA fragment (301 nt) was observed for any construct (Fig. 23B, lanes 3, 7, 11, 15, 19, and 23). By 4 h postelectroporation, all constructs had produced detectable negative-strand RNA (Fig. 23B, lanes 4, 8, 12, 16, 20, 24), with the WT showing the lowest level. Negative-strand RNA continued to accumulate at 8 h in all constructs (Fig. 23B, lanes 5, 9, 13, 17, 21, 25). At 24 h, the amount of negative-strand RNA had further increased in the WT and the G1300A and R1299A mutants (Fig. 23B, lanes 6, 10, and 14), but had not increased (or even decreased) in the G1301A, G1301S and C1152S mutants (Fig. 23B, lanes 18, 22, 26). The last three mutants are those that showed little or no positive-strand RNA synthesis (see above), suggesting that the absence of positive-strand RNA accumulation prevents continued synthesis of negative-strand RNA or allows its degradation. The increased amount of negative-strand RNA in the WT, G1300A and R1299A at 24 h may mean that the presence of newly synthesized positive-strand RNA allows negative-strand RNA to accumulate further. Whether this occurs in new cells from reinfection or in the same cells is

unclear. In general, all of the constructs, including those without synthesis of positive-strand RNA, produced negative-strand RNA at early stages of infection.

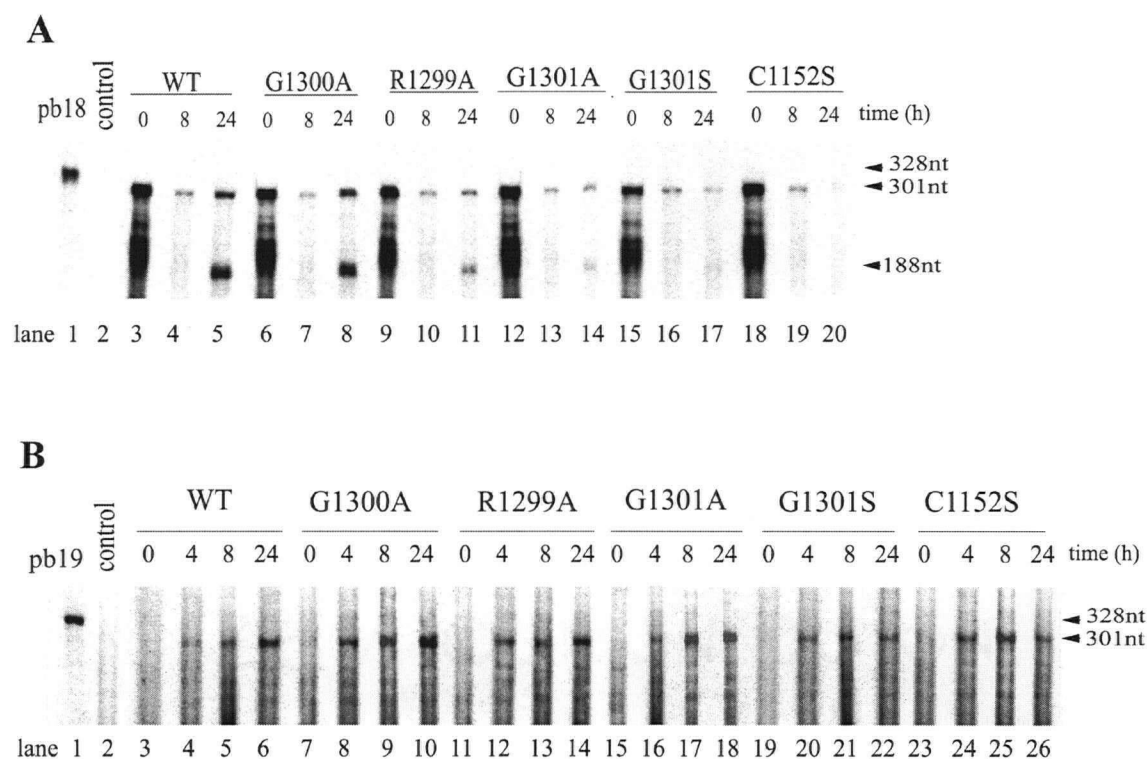


Figure 23. RNA analysis of the WT and mutant constructs.

(A) Positive-strand RNA analysis. BHK-21 cells were electroporated with RNAs transcribed *in vitro* from cDNA clone containing the WT (lanes 3 to 5), mutant G1300A (lanes 6 to 8), R1299A (lanes 9 to 11), G1301A (lanes 12 to 14), G1301S (lanes 15 to 17), or C1152S (lanes 18 to 20). At indicated time of postelectroporation (0, 8, and 24 h), total cytoplasmic RNAs were extracted using TRIzol reagent and subjected to RPA using ^{35}S -labeled probe pb18, which was loaded in lane 1. BHK-21 cells electroporated with no RV RNA served as control (lane 2). The autoradiograph was exposed for 1 day. (B) Negative-strand genomic RNA analysis. Total cytoplasmic RNAs extracted at 0, 4, 8 and 24 h postelectroporation of BHK-21 cells transfected respectively with the WT (lanes 3 to 6), G13000A (lanes 7 to 10), R1299A (lanes 11 to 14), G1301A (lanes 15 to 18), G1301S (lanes 19 to 22), or C1152S (lanes 23 to 26), were subjected to the two-cycle RPA, as described in Materials and Methods. The ^{35}S -labeled probe pb19 was loaded in lane 1. BHK-21 cells electroporated with no RV RNA served as control (lane 2). The autoradiograph was exposed for two days. The positions of the 328, 301, and 188-nt were indicated by arrowheads. Images were scanned using UMAX Astra 1220U scanner with Adobe Photoshop 5.0 software.

To compare the efficiencies of RNA production between the WT and mutants more precisely, I assessed the amount of negative-strand RNA, positive-strand genomic RNA, and subgenomic RNA for all the constructs and normalized the results for mutants against that for the WT. The molar ratio of subgenomic RNA to positive-strand genomic RNA was also calculated for the WT, G1300A, and R1299A. Results are summarized in Table 4.

Table 4. Comparison of the relative amounts of RNAs produced in the WT and mutants.

Construct	Negative-strand RNA ^b		Positive-strand RNA ^c		SG/G molar ratio ^d
	4 h	8 h	Genomic	Subgenomic	
WT	1	1	1	1	4.70 ± 1.00
G1300A	2.54 ± 0.37	1.13 ± 0.40	0.88 ± 0.13	0.82 ± 0.08	4.45 ± 1.20
R1299A	2.05 ± 0.50	1.41 ± 0.35	0.19 ± 0.13	0.24 ± 0.10	5.15 ± 1.06
G1301A	2.21 ± 1.11	1.39 ± 0.37	N/A ^e	N/A	N/A
G1301S	2.36 ± 0.52	0.97 ± 0.11	N/A	N/A	N/A
C1152S	1.90 ± 0.57	1.43 ± 0.33	N/A	N/A	N/A

^a The values shown are the results of at least two independent experiments.

^b The amount of negative-strand RNA at the respective time point (4 or 8 h postelectroporation) was assessed as described in Materials and Methods and normalized against that of the WT (value of 1.0).

^c Positive-strand RNA, either genomic or subgenomic, produced at 24 h postelectroporation was assessed and normalized against that of the WT (value of 1.0).

^d The SG/G molar ratio is the calculated molar ratio of subgenomic RNA to genomic RNA.

^e N/A, data not available.

Negative-strand RNA was compared at 4 and 8 h, because these were the points when synthesis of negative-strand RNA was not complicated by new synthesis of positive-strand RNA or by reinfection. In general, the mutants produced significantly more negative-strand RNA than did the WT at 4 h, and almost equally with the WT at 8 h. I also compared the amount of negative-strand RNA between the WT and mutant G1301S every 2 h after electroporation (Fig. 24). Mutant G1301S produced substantially more negative-strand RNA at early stage from 2 to 6 h

than WT (Fig. 24, comparing lanes 3 to 5 to lanes 8 to 10), whereas both reached nearly the same level at 8 h (Fig. 24, lanes 6 and 11). In what way the WT differs from the mutants at early stages is unclear. One explanation might be that more efficient processing of the WT-NSP decreases the available negative-strand RNA replication complex. However, the widely varied NSP cleavage among the mutants (from 0% to 75% cleavage ratio) did not result in correlated production of negative-strand RNA at 4 h. A likely reason is that a limiting host factor(s) might define the number of replication complexes formed, so further increased amounts of p200 had no effect on levels of replication complexes available. I propose that, at 4 h, the WT p200 has not saturated the limited host factor(s) in the formation of negative-strand RNA replication complex. Increased amounts of p200 in G1300A, due to delayed and less efficient NSP cleavage, result in higher production of negative-strands. Yet further increased amounts of p200 in other mutants would not further increase negative-strand RNA synthesis because such host factor(s) are limited. At 8 h, all the constructs produced similar amount of negative-strands, suggesting that they contained comparable negative-strand RNA replication complexes, possibly limited by host factor(s).

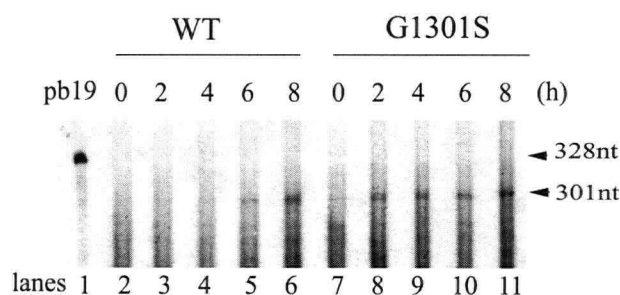


Figure 24. Comparison of WT and mutant G1301S on the levels of negative-strand RNA synthesis.

BHK-21 cells were electroporated with either WT RNA (lanes 2 to 6) or mutant G1301S RNA (lanes 7 to 11). Total cellular RNAs were prepared every 2 h postelectroporation and subjected to the detection of negative-strand RNA using two-cycle RPA with pb19 (lane 1).

It was assumed that mutants G1301S and C1152S synthesized no positive-strand RNA. The average density of the 301-nt band for the two at 24 h was taken to represent the level of input genomic RNA present in other mutants and was subtracted from their measured values. Although G1301A produced a low level of subgenomic RNA and possibly some genomic RNA as well (Fig. 5A), these were not subjected to quantitation or molar ratio calculation because of the likely presence of background genomic RNA. It is evident that all the mutants produced less positive-strand RNA than did the WT (Table 4). Positive-strand RNA levels in mutants are in accord with their respective NSP processing efficiencies and virus yields. The more the NSP cleavage is impaired, the less positive-strand RNA is produced. The slightly impaired mutant G1300A produced 88% of the level of genomic RNA and 82% of the subgenomic RNA produced by the WT. The substantially impaired mutant R1299A transcribed levels of 19% of genomic RNA and 24% of subgenomic RNA produced by the WT. Production of the genomic and subgenomic positive-strand RNAs were almost equally lowered. The molar ratio of subgenomic/genomic RNA, ranging from 4.5-5.2 for the mutants did not vary dramatically from the WT. These results indicate that NSP cleavage may not be the cause for the differential production of subgenomic and genomic RNA in virus-infected cells.

4.2.5. Discussion II

The cleavage of p200 is essential for virus replication. In RNA viruses, processing of nonstructural polyprotein is temporally regulated such that the ratio of polyprotein and cleavage products changes over the course of infection. Nonstructural polyprotein processing has been demonstrated to be essential for virus replication in alphavirus (Shirako and Strauss, 1994), Flavivirus yellow fever virus (YFV) (Chambers *et al.*, 1993, 1995; Nestorowicz *et al.*, 1994) and Bovine viral diarrhea virus (BVDV) (Xu *et al.*, 1997) by examining the effects of

mutations that inactivate the protease function or block the cleavage site with the use of infectious cDNA clones. In this study, I generated a panel of cleavage mutants and demonstrated that the cleavage of nonstructural polyprotein p200 is essential for RV replication. The effects on RV replication were found to correlate with the efficiency of p200 polyprotein processing. Mutations that completely abolished (G1301S and C1152S) or nearly abolished (G1301A) p200 cleavage shut down virus replication (Table 3). A mutation with a minor influence on NSP processing (mutant G1300A) produced infectious virus with a growth rate decreased by 3 - 10 fold. A mutation with a profound effect on NSP cleavage (mutant R1299A) was viable but with a growth rate lowered by 2000 - 3000 fold. Examination of RNA synthesis suggested that defective production of positive-strand RNA in the mutants, including both positive-strand genomic RNA and subgenomic RNA, may be the cause for reduced virus production (Table 4). More infectious constructs produced more positive-strand RNAs than less infectious ones, with noninfectious constructs producing little or none. However, given its 20% of p200 processing level and 20% of positive-strand genomic RNA, R1299A produced an unexpectedly lower level of virus yield (10^3 -fold lower than the WT). Although alternative explanations may exist, a likely reason is reinfection. The positive-strand RNA level was compared at 24 h postelectroporation, whereas virus yields were compared at 48 h (BHK-21 cells) or 5 days (Vero cells) posttransfection. It also seems that productive release of infectious virus particles may require a threshold level of positive-strand RNA synthesis. For example, mutant G1301A is noninfectious by plaque-assay, although a minimal level of positive-strand RNA could be detected from RPA. I believe that these mutations act by impairing p200 cleavage rather than by directly affecting the activity of the RNA replicase. First, the introduced mutations, except for R1299A, are conserved substitutions. Second, the mutations at cleavage sites are unlikely to be important for the replicase activity. Third, for all the mutants,

there is a good correlation between p200 cleavage efficiency, virus production, and viral RNA synthesis.

Uncleaved polyprotein p200 can produce negative-strand RNA, whereas cleavage products from p200 are required for efficient positive-strand RNA synthesis. I have shown that all the mutants, including the noninfectious cleavage-defective mutants G1301S and C1152S, accumulated negative-strand RNA as efficiently as the WT at 8 h (Fig. 23B and Table 4), suggesting that uncleaved p200 is sufficient to produce negative-strand RNA from the input genomic RNA. Interestingly, mutants even produced more negative-strand RNA at 4 h than the WT, providing further evidence for the role of p200 in negative-strand RNA synthesis. However, the amount of negative-strand RNA did not increase proportionally to the amount of p200 among mutants, suggesting that limiting host factor(s) may also play a role in regulating the number of replication complexes for negative-strand RNA synthesis.

The capacity to synthesize positive-strand RNA differed greatly between the WT and mutants. All mutants produced lower levels of positive-strand RNA, both genomic and subgenomic RNA, than the WT. Mutants more defective in cleaving p200 produced less positive-strand RNA (Fig 21A and Table 4). The cleavage-defective mutants G1301S and C1152S showed accumulation of positive-strand RNA barely detected by RPA (Fig. 23A, lane 8). This suggests that cleavage products from p200 (i.e., p150 and p90) are responsible for efficient synthesis of both positive-strand genomic RNA and subgenomic RNA. In view of the limited sensitivity of RPA used in the study, the possibility of an inefficient synthesis of positive-strand RNA by uncleaved p200 cannot be ruled out. For the two infectious mutants (G1300A and R1299A), the molar ratios of subgenomic RNA to positive-strand genomic RNA were not significantly

different from the WT, indicating that p200 cleavage does not contribute to the differential synthesis of positive-strand genomic and subgenomic RNA.

My studies suggest a strong similarity between RV and alphavirus (for a review, see Strauss and Strauss, 1994), a well-characterized positive-strand RNA virus genus, in NSP processing and viral RNA synthesis. Alphavirus NSP contains three cleavage sites generating four cleavage products (nsP1 to nsP4) and a number of intermediates. A model for the composition of replication complexes and the temporal regulation of negative- and positive-strand RNAs has been proposed from several lines of studies (Lemm and Rice, 1993a, 1993b; Lemm *et al.*, 1994, 1998; Shirako and Strauss, 1994). Three forms of replication complexes are involved in alphavirus replication: the uncleaved P123 and nsP4 generates only negative-strand RNA; the complex composed of nsP1, P23, and nsP4 is active in both negative-strand RNA and 49S positive-strand genomic RNA syntheses; the complex consisting of the final cleavage products nsP1, nsP2, nsP3, and nsP4 produces only 49S positive-strand genomic RNA and subgenomic RNA. Cleavage at the 1/2 and 2/3 sites respectively switches the product preference of the replication complex from negative- to positive-strand RNA, and also inactivates its capacity for negative-strand RNA synthesis, which explains the shutoff of negative-strand RNA synthesis after 4 to 6 hours post infection. In RV, p200 is cleaved into p150 and p90, giving a much simpler NSP composition. This work demonstrates that the replication complex composed of polyprotein p200 is active in negative-strand RNA synthesis but incapable of efficient positive-strand RNA synthesis, while cleavage of p200 is required for efficient positive-strand RNA synthesis. For both alphavirus and RV, cleavage of polyprotein or intermediates causes the switching of negative-strand to more efficient positive-strand RNA synthesis. However, it has yet to be determined that synthesis of negative-strand RNA ceases after an early stage of RV replication. My RNase protection assay results are complicated by reinfection as well as the

fast growth rate of BHK-21 cells. Studies using virus-infected Vero cells are under way. It also remains to be examined whether or not the cleaved products of RV NSP, p150 and p90, transcribe negative-strand RNA.

My work provides the first experimental data demonstrating the relationships between RV NSP cleavage and virus replication, and particularly, between NSP cleavage and viral RNA synthesis. From my results and the studies of alphavirus replication, I hypothesize that uncleaved p200 forms the replication complex for negative-strand RNA synthesis and that cleavage of p200 into p150 and p90 converts the complex into one with the capacity for efficient positive-strand RNA synthesis. Whether p150 and p90 also produce negative-strand RNA remains to be investigated. It is of interest that p200 is capable of negative-strand RNA synthesis but incapable of positive-strand RNA synthesis. One possibility is that recognition of positive-strand RNA promoters or initiation of positive-strand RNA synthesis needs a specific component or conformation not present in p200 but generated by its cleavage. Positive-strand RNA viruses replicate through negative-strand intermediates, the regulatory mechanism of which is worthy of study. Previous studies on alphavirus and the present one on RV may indicate a possible mechanism of RNA replication for a group of viruses, namely that the change from synthesis of negative-strand RNA to positive-strand RNA is mediated by NSP cleavage.

4.3. Molecular characterization of RV RNA synthesis

4.3.1. RV RNA replication is *cis*-preferential.

In order to study the roles of NSPs in synthesizing distinct viral RNAs, I employed complementation experiments, in which engineered RNA transcripts were coelectroporated into BHK-21 cells. Resulting production of viral RNAs was monitored by RPA. M33 Δ SS is a modified RV RNA transcript with most of the SP region deleted, from nt 6966 to 9334 (Fig. 25A). M33 Δ MM is a replication-defective RNA transcript with a frame-shift deletion in the NSP ORF from nt 1081 to 5106 (Fig. 25A). RNA molecules were introduced by electroporation, separately or together, into BHK-21 cells. At different times postelectroporation, total RNAs were isolated and subjected to RPA using either probes specific to both molecules (pb18 and pb19), or probes specific to M33 Δ MM only (pb20 and pb21) (Fig. 25A). pb18 is positive-strand specific and differentiates genomic from subgenomic RNA by the size of protected bands, 301 nt for genomic and 188 nt for subgenomic RNA. pb20 is also positive-strand specific but fails to differentiate genomic from subgenomic RNA, as both generate 162-nt protected bands. pb19 and pb21, complementary to pb18 and pb20 respectively, are negative-strand specific giving protected bands of 301 nt and 162 nt, respectively. When the M33 Δ SS RNA was electroporated into BHK cells alone, the 301-nt band, representing negative-strand RNA, was detected by pb19 at 4, 7, and 24 h (Fig. 25B, lanes 13 to 15). The 301-nt product, representing genomic RNA, and the 188-nt band, representing subgenomic RNA, were detected by pb18 at 24 h (Fig. 25B, lane 4). The results demonstrated that the M33 Δ SS RNA replicates itself in essentially the same way as does the WT M33 RNA (Fig. 23). When the M33 Δ MM RNA was introduced alone, no signal band representing negative-strand RNA was detected by either pb19 (Fig. 25B, lanes 17 to 19) or by

pb21 (Fig. 25C, lane 12), nor was the band specific to positive-strand RNAs detected by pb18 (Fig. 25B, lane 7) or by pb20 (Fig. 25C, lane 5) at 24 h. This demonstrated that the M33 Δ MM RNA was defective in both negative- and positive-strand RNA syntheses. When both RNAs were coelectroporated, no signal band specific to negative-strand RNA was detected at 7 and 24 h using pb21 (Fig. 25C, lanes 15 and 16), nor were bands specific to positive-strand RNAs detected by pb20 at 24 h (Fig. 25C, lane 8), indicating that replication of the M33 Δ MM RNA was not rescued by the M33 Δ SS RNA. The positive-strand RNAs detected by pb18 (Fig. 25B, lane 10) and the negative-strand RNA detected by pb19 (Fig. 25B, lanes 21 to 23) were therefore generated solely by the self-replication of the M33 Δ SS RNA.

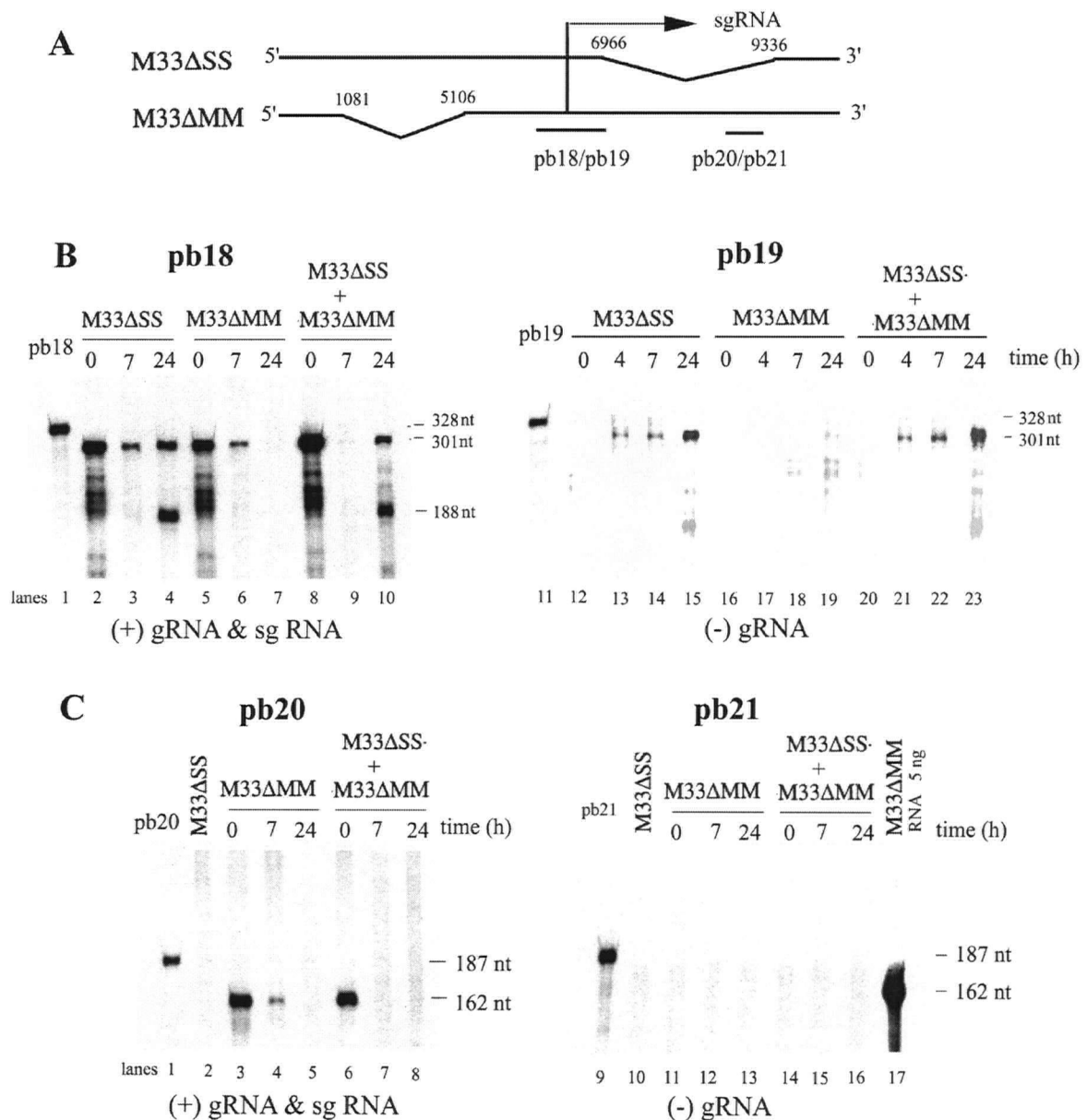


Figure 25. *Trans* complementation of RV replication.

(A) Schematic diagram of the replication-defective RNA M33ΔMM and the helper RNA M33ΔSS, with the relative positions of RPA probes (pb18/pb19, pb20/pb21). The start of the subgenomic RNA is indicated by the arrow. (B) RPAs using pb18 (lane 1) and pb19 (lane 11), specific to both M33ΔMM and M33ΔSS RNA. The two RNAs were introduced by electroporation either singly or in combination into BHK-21 cells. 4 μg of total RNA prepared at 0, 7, and 24 h postelectroporation was used for positive-strand RNA detection by pb18 (lanes 2 to 10), and 20 μg of those at 0, 4, 7, and 24 h was used for negative-strand RNA detection by pb19 (lanes 12 to 23). The autograph was exposed for 1 day. (C) RPAs using pb20 (lane 1) and pb21 (lane 9), specific to the M33ΔMM RNA only. The M33ΔSS RNA produced no specific band using either pb20 (lane 2) or pb21 (lane 10). After the M33ΔMM RNA was electroporated alone or in combination with the M33ΔSS RNA, 4 μg of total RNA prepared at 0, 7, and 24 h was used for positive-strand RNA detection by pb20 (lanes 3 to 8), and 20 μg of those was used

for negative-strand RNA detection by pb21 (lanes 11 to 16). A reaction mixture containing 5 ng of full-length negative-strand RNA transcript produced *in vitro* was included as a positive control for RPA by pb21 (lane 17). The autograph was exposed for 1 day. Positions of specific protected bands are indicated. Images were scanned using an UMAX Astra 1220U scanner with Adobe Photoshop 5.0 software.

The failure of *trans*-complementation of the M33 Δ MM RNA does not appear to be due to the absence or disruption of critical *cis*-RNA elements. I created several replication-defective constructs with either frame-shift addition, deletions, or a stop codon in different NSP regions (Fig. 26). None of these could be rescued by the helper RNA. I therefore suggest that replication of RV RNA, or at least the negative-strand RNA, is *cis*-preferential. I then examined whether the failure of positive-strand RNA replication is caused by its *cis*-preferred replication or by the absence of prerequisite negative-strand RNA synthesis.

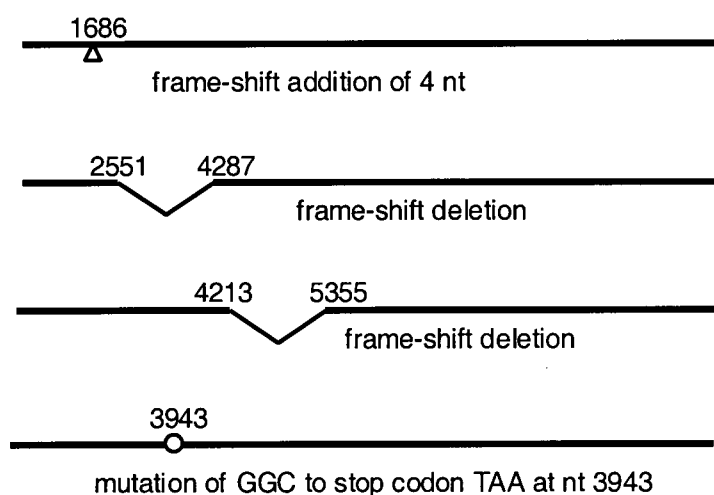


Figure 26. Schematic diagrams of constructed replication-defective mutants.

Mutants were constructed on pBRM33 with frameshift addition, deletions, and a stop codon within NSP ORF (nt 41 to 6388).

As described in section 4.2.4, both the C1152S mutant (containing mutated NS-pro catalytic site) and the G1301S mutant (containing mutated NSP cleavage site) are functional in negative-strand RNA synthesis but defective in positive-strand RNA synthesis, because they are unable to process the NS polyprotein p200. The two mutants differ in that p200(C1152S) can be processed by a functional protease, such as p200(G1301S), provided in *trans*, whereas p200(G1301S) cannot be cleaved due to its mutated NSP cleavage site. I designed complementation experiments to examine the *trans* or *cis* function of p150/p90 in synthesizing positive-strand RNAs. M33(C1152S) RNA was further modified with a deletion in the SP region from nt 6966 to 9334 to yield M33(C1152S) Δ SS RNA (Fig. 27A). Its replication can be separated from that of the M33(G1301S) RNA by RPA using different probes: pb18/pb19 is specific to both RNAs and pb20/pb21 is specific to M33(G1301S) only (Fig. 27A). When the M33(C1152S) Δ SS and M33(G1301S) RNAs were introduced in cells separately or together, the 301-nt signal band specific to negative-strand RNA was detected by pb19 at 4 and 7 h (Fig. 27C), demonstrating the successful synthesis of negative-strand RNA. In contrast, when the M33(C1152S) Δ SS and M33(G1301S) RNAs were electroporated separately, no accumulation of the 301-nt product specific to genomic RNA or the 188-nt band specific to subgenomic RNA was observed at 24 h using pb18 (Fig. 27B, lanes 4 and 7) or pb20 (Fig. 27B, lane 15), suggesting that synthesis of positive-strand RNAs was defective in both constructs. However, when the RNAs were introduced together, accumulations of both 301- and 188-nt products, representing genomic and subgenomic RNAs, were clearly detected by pb18 at 24 h (Fig. 27B, lane 10), indicating the efficient rescue of synthesis of positive-strand RNAs. However, a very low level of the 162-nt band was detected by pb20 at 24 h (Fig. 27B, lane 18). This probe is specific only to the M33(G1301S) RNA, suggesting that synthesis of positive-strand RNAs of the M33(G1301S) RNA was not functionally rescued. Therefore, the large amount of the

positive-strand RNAs generated (Fig. 27B, lane 10) derived mostly from the M33(C1152S) Δ SS RNA. A straightforward explanation is that p200(C1152S) was cleaved by p200(G1301S) into p150 and p90. These functioned preferentially in *cis* to produce positive-strand RNAs efficiently from their own negative-strand template on the M33(C1152S) Δ SS RNA, but functioned inefficiently in *trans* using the negative-strand template of the M33(G1301S) RNA. These results strongly support the hypothesis that synthesis of the positive-strand RNAs is carried out preferentially in *cis* by replication complexes composed of p150/p90. In conclusion, I have shown for the first time that both negative- and positive-strand RV RNAs are replicated preferentially in *cis*.

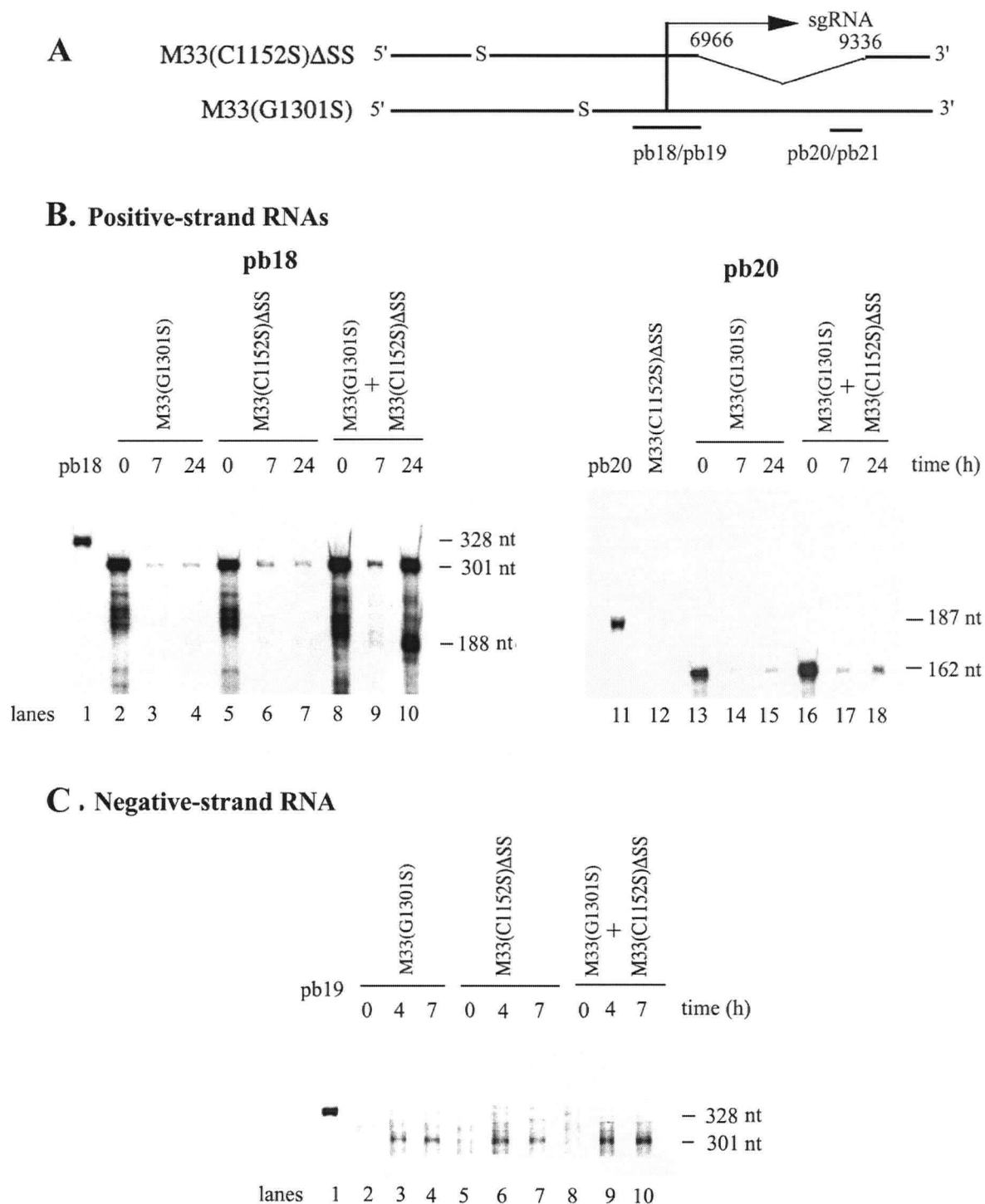


Figure 27. Synthesis of positive-strand RNA is *cis*-preferential.

(A) Schematic diagram of M33(C1152S)ΔSS and M33(G1301S) RNAs with the relative positions of pb18/pb19 and pb20/pb21. The NS polyprotein p200(C1152S) translated from M33(C1152S)ΔSS RNA can be processed by p200(G1301S) translated from M33(G1301S) RNA. The start of the subgenomic RNA (sgRNA) is indicated. (B) Positive-strand RNAs detected by pb18 (lane 1), specific to both M33(C1152S)ΔSS and M33(G1301S) RNAs, or by pb20 (lane 11), specific to M33(G1301S) RNA only. After the two RNAs were electroporated

separately or together, 4 µg of total RNA prepared at 0, 7, and 24 h were used in RPA with pb18 (lanes 2 to 10). RPA reactions using pb20 were also conducted on samples prepared from M33(G1301S) electroporated alone (lanes 13 to 15) and from coelectroporation (lanes 16 to 18). pb20 was not specific to the M33(C1152S)ΔSS transcript (lane 12). The autograph was exposed for 1 day. (C) Negative-strand RNA detected by pb19 (lane 1). The two RNAs were electroporated separately or together into BHK-21 cells. 20 µg of total RNA samples prepared at 0, 4, and 7 h postelectroporation were used for negative-strand RNA detection by pb19 (lanes 2 to 10). The autograph was exposed for 1 day. Positions of specific protected bands are indicated. Images were scanned using an UMAX Astra 1220U scanner with Adobe Photoshop 5.0 software.

4.3.2. Time course of RV RNA synthesis.

Incorporation of [³H]uridine into infected cells is not a sensitive assay for detection of RV RNA synthesis (Hemphill *et al.*, 1988), because of the very low level of RV RNA replication against the high background of cellular RNA synthesis. By analyzing [³H]uridine-labeled, actinomycin D-resistant total RNA on glyoxal-agarose gel electrophoresis, Hemphill *et al.* (1988) were able to detect genomic and subgenomic viral RNAs and quantitated their respective amounts at each time point. RNA synthesis was found to increase dramatically from 6 through 19 hpi, with maximal RNA synthesis at 24 hpi (Hemphill *et al.*, 1988). However, this study did not differentiate negative-strand from positive-strand RNA and was not sensitive enough to detect RNA synthesis at very early stages of virus infection. To determine whether RV negative-strand RNA synthesis stops after a certain time (as does that of alphavirus), a more sensitive assay is needed. In the above experiments, I employed RPA to quantitate three RV RNA species at early stages of replication. I then used the same technique to determine the amounts of three viral RNAs at each time point postinfection.

Vero cell monolayers on 35-mm-diameter dishes were infected with RV (M33 strain) at m.o.i. of 0.1 PFU/cell for 1 h. Total RNA was extracted every 2 h and subjected to RPA. Negative-strand RNA was detected using pb19 in a two-cycle reaction and positive-strand RNAs were determined using probe18 in a one-cycle reaction. The total RNA at each time point was suitably diluted so that the probe used was not saturating. Intensities of the signal bands specific to the three viral RNAs were quantitated, standardized against the amount of total RNA, and plotted against infection time (Fig. 28). Note that the scale for negative-strand RNA (on the right) is much lower than that for positive-strand RNAs (on the left).

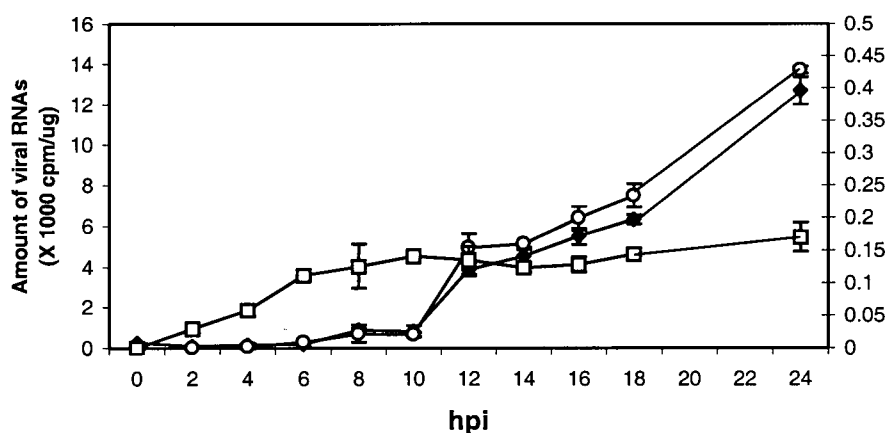


Figure 28. Accumulated amounts of viral RNAs during virus infection.

Vero cell monolayers on 35-mm-diameter dishes were infected with RV (M33 strain) at m.o.i. of 0.1 PFU/cell for 1 h at 37 °C. At 2-h intervals, total RNAs were prepared, and subjected to detection of positive- and negative-strand RNAs using pb18 and pb19, respectively. Samples were diluted differently in order not to saturate the probe. The negative-strand RNA, positive-strand genomic and subgenomic RNAs were analyzed by RNase protection assay (RPA) as described below. Intensity of RPA band was quantitated by image analysis and converted to the amount of probe (cpm) loaded at the same time. The amount of viral RNA was calculated from the intensity of its corresponding signal band (cpm) to allow for dilution and standardized against the amount of total RNA (mg). Amounts of each viral RNA were plotted against infection times (hpi). □, negative-strand RNA; ◆, positive-strand genomic RNA; ○, subgenomic RNA. Note positive- (left) and negative-strand RNA (right) use different y scales. Values presented are the results of two independent experiments.

Negative-strand RNA was first detected at 2 hpi and increased continuously until 10 hpi, remaining almost constant thereafter. This result suggests that synthesis of negative-strand RNA ceases after 10 hpi. In contrast, positive-strand RNAs (both genomic and subgenomic RNAs) appeared at low level after 4 to 6 hpi, and increased dramatically after 10 hpi. Syntheses of genomic and subgenomic RNAs seem to be synchronized and the ratio of subgenomic to genomic RNA (SG/G) remained fairly level between 2.3 and 3.7. It is of interest to note that the dramatic increase of positive-strand RNAs started after 10 hpi, when synthesis of negative-strand RNA had stopped.

4.3.4. Discussion III

RV RNA replication is *cis*-preferential. For a number of positive-strand RNA viruses, RNA replication was found to require the translation of part or all of the NSP coding region (de Groot *et al.*, 1992; Mahajan *et al.*, 1996; Neeleman and Bol, 1999; Novak and Kirkegaard, 1994; Schaad *et al.*, 1996; Scholthof and Jackson, 1997; van Bokhoven *et al.*, 1993; Weiland and Dreher, 1993; White *et al.*, 1992; Zhou and Jackson, 1996). Using complementation experiments, I demonstrated that neither negative- nor positive-strand RNAs of RV can be functionally rescued by *trans*-provided NSPs translated from another helper RNA molecule, suggesting that replication of RV RNAs depends on the translation of RV NSPs in *cis*. Although other explanations are possible, this requirement for translation in *cis* appears to be the result of the preferential *cis* action of p200 in synthesizing RV negative-strand RNA and the preferential *cis* action of p150/p90 in synthesizing positive-strand RNAs. Mechanisms for the *cis* requirement of a protein remain obscure but several possibilities have been proposed (Novak and Kirkegaard, 1994). One explanation is the establishment of a template. The newly

synthesized p200 might interact with the positive-strand genomic RNA from which it is being translated to enable that RNA molecule to become the functional template for negative-strand RNA synthesis. The negative-strand RNA might interact with the replication complex by which it was produced to become a functional template for positive-strand RNA synthesis. More likely is the restriction of diffusion of NSPs, which could be limited by subcellular localization or protein stability. RV replication complexes, consisting of NSPs, host factors, and viral RNAs, are localized to membrane-bound virus-modified lysosomes (Lee *et al.*, 1992; 1994; Magliano *et al.*, 1998). Binding to membrane might restrict the diffusion of p200 and its cleavage products p150/p90. As a negative-strand RNA replicase, p200 is probably present at high concentration only near the RNA from which it is translated, because of efficient self-processing. Therefore, both subcellular localization and protein stability could restrict p200 from using other RNA templates. After the cleavage of p200 into p150/p90, the replication complex may still remain associated with the newly-synthesized negative-strand RNA, serving as its preferential template. The mechanisms for the *cis*-preferential replication of RV need further investigation.

Synthesis of RV negative- and positive-strand RNAs is regulated by NSP cleavage. In a precise determination of the time courses of three RV RNAs, I have shown that negative-strand RNA accumulates until 10 hpi and remains nearly constant thereafter. In contrast, positive-strand RNAs (both genomic and subgenomic) do not increase much before 10 hpi and accumulate rapidly thereafter. Synthesis of negative-strand RV RNA seems to stop after 10 hpi with a switch to efficient synthesis of positive-strand RNAs. This replication pattern of RV resembles that of alphavirus, in which negative-strand RNA synthesis ceases after 4 to 6 hpi and switches to the positive-strand RNA synthesis (Sawicki *et al.*, 1981).

The switch from the negative-strand RV RNA synthesis to the production of positive-strand RNAs is regulated by the cleavage of NSP, converting p200 into p150/p90. In studies described in section 4.2.4, I have shown that polyprotein p200 is functional in negative-strand RNA synthesis and the cleavage of p200 into p150/p90 is required for efficient synthesis of positive-strand RNA (Fig. 23 and Table 4). One question to be answered is whether p150/p90 produces negative-strand RNA as well. A straightforward approach to study the roles of p150 and p90 in negative-strand RNA synthesis is to conduct reconstitution or complementation experiments, in which p150 and p90 are provided separately from either expression vectors or from two RNA molecules cotransfected and examined for their capacity to replicate a template RNA. However, this approach is unsuitable for RV because its RNA replication is *cis*-preferential (Fig. 25 and Fig. 27). Furthermore, no mutation has been identified in RV comparable to N614D in alphavirus, which enhances the protease activity so much that no polyprotein can be detected (Strauss *et al.*, 1992; Strauss and Strauss, 1994). My results suggest that p150/p90 is not an effective replicase for negative-strand RNA synthesis, because (1) synthesis of negative-strand RNA increases only in the early stages of infection and stops later when the concentration of p150/p90 increases (Fig. 28); (2) at very early stages of infection, cleavage-defective mutants with lower NSP cleavage efficiencies and thus lower levels of p150/p90 produce higher levels of negative-strand RNA than WT (Fig. 23 and Table 4). It is likely that RV shares a similar mechanism for regulation of RNA synthesis with alphavirus, in which different viral RNA species are produced by distinct replication complexes containing different NSP components that result from NSP processing. In alphavirus, uncleaved P123 and nsP4 form the replicase for negative-strand RNA; nsP1, P23, and nsP4 form the replicase for both negative-strand RNA and 49S positive-strand genomic RNA; the final cleavage products, nsP1, nsP2, nsP3, and nsP4, form the replicase only for 49S positive-strand genomic RNA and subgenomic RNA. The NSP of RV is cleaved only once and thus gives much simpler

components. p200 is the main negative-strand RNA replicase, whereas p150/p90 is the main positive-strand RNA replicase for both genomic and subgenomic RNAs. Therefore, the time-dependent transition from negative- to positive-strand RNA synthesis is controlled by the temporal regulation of the processing of p200 into p150/p90, which not only activates the efficient positive-strand RNA synthesis but also shuts off the negative-strand RNA synthesis. Early in infection, levels of p200 support the accumulation of negative-strand RNA while low levels of cleavage products p150/p90 produce limited positive-strand RNAs. After 10 hpi, the processing of much of the translated p200 and perhaps limited novel NSP translation significantly increase the level of p150/p90, causing a dramatic increase in production of positive-strand RNAs. At this stage, synthesis of negative-strand RNA is largely shut down due to lack of intact p200. My work contributes to understanding the mechanism of viral RNA synthesis. All positive-strand RNA viruses replicate through a negative-strand RNA intermediate and the regulatory mechanism of the transition from negative- to positive-strand RNA synthesis is of great interest. From previous studies on alphavirus (Lemm and Rice, 1993, 1994, Lemm *et al.*, 1994, 1998; Shirako and Strauss, 1994) and my work on RV, the temporal regulation of polyprotein cleavage may represent a common strategy for viral RNA regulation. In addition, the binding of host factors to the replication complexes may also play a critical role in this process (Pogue *et al.*, 1994).

Mechanism for RV NSP translation, processing, and RNA synthesis. From previous studies on other positive-strand RNA viruses, particularly alphavirus (Lemm and Strauss, 1993a, 1993b; Lemm *et al.*, 1994, 1998; Shirako and Strauss, 1994; Novak and Kirkegaard, 1994) and my work on RV, a mechanism of RV NSP translation, processing and RNA synthesis is proposed (Fig. 29). Upon infection, the input genomic RNA serves as the template for

translation of polyprotein p200. This, associated with host factors, binds to the 3' end of the RNA, from which it is being translated, and functions in *cis* to synthesize a full-length negative-strand RNA. The subsequent processing of p200 into p150/p90 converts the original replication complex into one with specificity for synthesis of positive-strand RNAs. This complex remains associated with the nascent negative-strand RNA template, recognizes the promoter for either genomic RNA or subgenomic RNA, and functions in *cis* to produce genomic or subgenomic RNA efficiently.

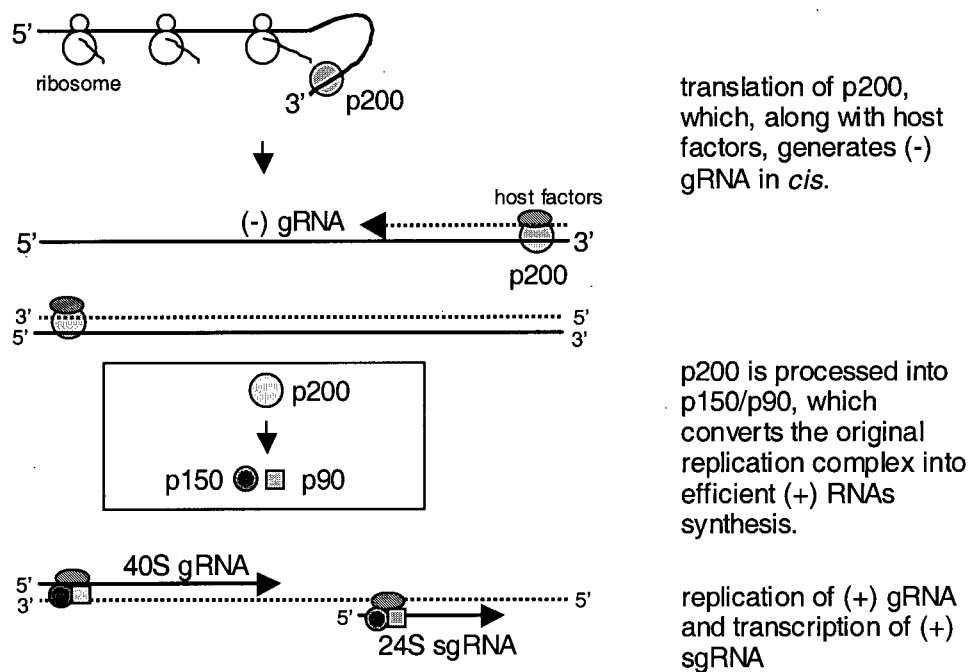


Figure 29. Proposed mechanism for RV NSP translation, processing, and viral RNA synthesis.

Upon infection, p200 is translated from the input genomic RNA (gRNA) and possibly binds to the 3' end of the template RV RNA. Along with host factors, p200 functions in *cis* to generate a full-length negative-strand RNA. The subsequent processing of p200 into p150/p90 not only disables the capacity for negative-strand RNA synthesis, but also permits efficient positive-strand RNA synthesis, including both 40S genomic RNA and 24S subgenomic RNA (sgRNA).

5. SUMMARY AND PERSPECTIVE

In summary, my work identified the domains required by RV NS-pro for cleavages in *trans* and *cis* (Fig. 17). Both cleavages require a core catalytic domain from A₁₀₂₀ to P₁₂₉₆, while containing different N and C ends. To cleave in *trans* protease needs an additional domain (V₉₂₀ to A₁₀₂₀) at the N end, while *cis* protease contains a four-residue linker, the cleavage site G₁₃₀₁ and the substrate region at the C end. I also demonstrated that the X domain is important in *trans* cleavage of RV NS-pro but has no significant influence on *cis* cleavage. Defining the regions and roles of protease-related domains of RV NS-pro clarifies our understanding of this specific viral PCP and provides a basis for comparison with other proteases. Primary sequence analysis and predicted secondary structure of RV NS-pro showed distant homology to papain. Crystallographic data are needed for more precise three-dimensional structure determination.

My work also characterized the features of RV RNA synthesis at a molecular level and its regulation by NSP cleavage. Both negative- and positive-strand RNAs are synthesized preferentially in *cis*. Synthesis of negative-strand RNA stops around 10 hpi and is switched to the efficient production of positive-strand RNAs. Polyprotein p200 is required for negative-strand RNA synthesis but not for positive strands, whereas its cleavage products p150/p90 are required for efficient positive-strand RNA synthesis. A molecular mechanism is proposed for RV NSP translation, processing and RNA synthesis. Upon infection, NSP is translated from input genomic RNA into p200, which remains bound to the 3' end of the translation-template RNA and functions to generate a full-length negative-strand RNA, with the help of host factors. The cleavage of p200 into p150/p90 leaves the replicase with little or no capacity for negative-strand RNA synthesis, but allows efficient activity for positive-strand RNA synthesis, resulting in the large amount of genomic RNA and subgenomic RNA produced thereafter.

Some questions still remain to be answered in future studies on RV NSPs and viral RNA replication. It will be interesting to define the protein-protein interaction domains among RV NSPs, including the proposed protein-protein interaction domains within NS-pro, and to characterize the effects of these interactions on viral RNA synthesis. The underlying reason for the differential synthesis of genomic and subgenomic RNA has not been characterized. Whether it is because of additional host factors, different promoter activities, or other reasons, is worthy of studying. Host factors identified so far as binding specifically to RV RNA are autoantigens (calreticulin, La autoantigen), whose functions for viral RNA synthesis remain elusive. Characterization of the complete components of replication complexes, including both NSPs and host factors, is needed for a clear understanding of RV RNA replication. Such knowledge may illuminate good targets for prevention of RV infection and combating this and other virus induced diseases.

REFERENCES

- Adkins, S., R. Siegel, J. H. Sun, and C. C. Kao.** 1997. Minimal templates directing accurate initiation of subgenomic RNA synthesis *in vitro* by the brome mosaic virus RNA-dependent RNA polymerase. *RNA* 3: 634—647.
- Ahlquist, P.** 1992. Bromovirus RNA replication and transcription. *Curr. Opin. Genet. Dev.* 2: 71-76.
- Ahola, T., and P. Ahlquist.** 1999. Putative RNA capping activities encoded by brome mosaic virus: methylation and covalent binding of guanylate by replicase protein 1a. *J. Virol.* 73(12): 10061-10069.
- Aliperti, G., and M. J. Schlesinger.** 1978. Evidence for an autoprotease activity of Sindbis virus capsid protein. *Virology* 90: 366-369.
- Allaire, M., M. M. Chernaia, B. A. Malcolm, and M. N. James.** 1994. Picornaviral 3C cysteine proteinases have a fold similar to chymotrypsin-like serine proteinases. *Nature* 369(6475): 72-6.
- Andino, R., G. E. Rieckhof, and D. Baltimore.** 1990. A functional ribonucleoprotein complex forms around the 5' end of poliovirus RNA. *Cell* 63(2): 369-380.
- Andino, R., G. E. Rieckhof, P. L. Achacoso, and D. Baltimore.** 1993. Poliovirus RNA synthesis utilizes an RNP complex formed around the 5'-end of viral RNA. *EMBO J.* 12:3587-3598.
- Anthony, R. P., and D. T. Brown.** 1991. Protein-protein interactions in an alphavirus membrane. *J. Virol.* 65: 1187-94.
- Baker, D., J. L. Sohl, and D. A. Agard.** 1992. A protein-folding reaction under kinetic control. *Nature* 356: 263-265.
- Baker, S. C., K. Yokomori, S. Fong, R. Carlisle, A. E. Gorbalenya, E. V. Koonin, and M. M. C. Lai.** 1993. Identification of the catalytic sites of a papain-like cysteine proteinase of murine coronavirus. *J. Virol.* 67: 6056-6063.
- Bardeletti, G., J. Tektoff, and D. Gautheron.** 1979. Rubella virus maturation and production in two host cell system. *Intervirology* 11: 97-103.
- Bardeletti, G., N. Kessler, N. Aymard-Henry.** 1975. Morphology, biochemical analysis and neuraminidase activity of rubella virus. *Arch Virol.* 49: 175-186.
- Baron, M. D., and K. Forsell.** 1991. Oligomerization of the structural proteins of rubella virus. *Virology* 185: 811-819.
- Baron, M. D., T. Ebel, and M. Suomalainen.** 1992. Intracellular transport of rubella virus structural proteins expressed from cloned cDNA. *J. Gen. Virol.* 73: 1073-1086.

- Barton, D. J., and J. B. Flanagan.** 1993. Coupled translation and replication of poliovirus RNA *in vitro*: synthesis of functional 3D polymerase and infectious virus. *J. Virol.* 67: 822-831.
- Barton, D. J., and J. B. Flanagan.** 1997. Synchronous replication of poliovirus RNA: initiation of negative-strand RNA synthesis requires the guanidine-inhibited activity of protein 2C. *J. Virol.* 71(11): 8482-8489
- Barton, D. J., B. J. Morasco, and J. B. Flanagan.** 1996. Assays for poliovirus polymerase, 3D(Pol), and authentic RNA replication in HeLa S10 extracts. *Methods Enzymol.* 275: 35-57.
- Barton, D. J., B. J. Morasco, and J. B. Flanagan.** 1999. Translating ribosomes inhibit poliovirus negative-strand RNA synthesis. *J. Virol.* 73(12): 10104-10112.
- Barton, D. J., E. P. Black, and J. B. Flanagan.** 1995. Complete replication of poliovirus *in vitro*: preinitiation RNA replication complexes require soluble cellular factors for the synthesis of VPg-linked RNA. *J. Virol.* 69: 5516-5527.
- Barton, D. J., S. G. Sawicki, and D. L. Sawicki.** 1991. Solubilization and immunoprecipitation of alphavirus replication complexes. *J. Virol.* 65:1496-1506.
- Bazan, J. F., and R. J. Fletterick.** 1988. Viral cysteine proteases are homologous to the trypsin-like family of serine proteases: structural and functional implications. *Proc. Natl. Aca. Sci. USA.* 85: 7872-7876.
- Berti, P. J and A. C. Storer.** 1995. Alignment/phylogeny of the papain superfamily of cysteine proteases. *J. Mol. Biol.* 246: 273-283.
- Bienz, K., D. Egger, M. Troxler, and L. Pasamontes.** 1990. Structural organization of poliovirus RNA replication is mediated by viral proteins of the P2 genomic region. *J. Virol.* 64: 1156-1163.
- Bisaillon, M., and G. Lemay.** 1997. Viral and cellular enzymes involved in synthesis of mRNA cap structure. *Virology* 236: 1-7.
- Blyn, L. B., R. Chen, B. L. Semler, and E. Ehrenfeld.** 1995. Host cell proteins binding to domain IV of the 5' noncoding region of poliovirus RNA. *J. Virol.* 69: 4381-4389.
- Bonilla, P. J., S. A. Hughes, and S. R. Weiss.** 1997. Characterization of a second cleavage site and demonstration of activity *in trans* by the papain-like protease of the murine coronavirus mouse hepatitis virus A59. *J. Virol.* 71: 900-909.
- Bonilla, P. J., S. A. Hughes, J. F. Pinon, and S. R. Weiss.** 1995. Characterization of the leader papain-like proteinase of MHV-A59: identification of a new *in vitro* cleavage site. *Virology* 209: 489-497.
- Bowden, D. S., and E. G. Westaway.** 1984. Rubella virus structural and nonstructural proteins. *J. Gen. Virol.* 65: 933-943.

- Bowden, D. S., and E. G. Westaway.** 1985. Changes in glycosylation of rubella virus envelope proteins during maturation. *J. Gen. Virol.* 66: 201-206.
- Buck, K. W.** 1996. Comparison of the replication of positive-stranded RNA viruses of plants and animals. *Adv. Virus Res.* 47: 159-251.
- Bruss, V., and D. Ganem.** 1991. The role of envelope proteins in hepatitis B virus assembly. *Proc. Natl. Acad. Sci. USA* 88: 1059-1063.
- Bryan, P., L. Wang, J. Hoskins, S. Ruvinov, S. Strausberg, P. Alexander, O. Almog, G. Gilliland, and T. Gallagher.** 1995. Catalysis of a protein reaction: mechanistic implications of the 2.0 Å structure of the subtilisin-prodomain complex. *Biochemistry* 34: 10310-10318.
- Calisher, C. H., and N. Karabatsos.** 1988. Arbovirus serogroups: definition and geographic distribution, p. 19-57. In T. P. Monath (ed.), *The arboviruses: epidemiology and ecology*. CRC Press, Inc., Boca Raton, Fla.
- Chambers, T. J., A. Nestorowicz, and C. M. Rice.** 1995. Mutagenesis of the yellow fever virus NS2B/3 cleavage site: determinants of cleavage site specificity and effects on polyprotein processing and viral replication. *J. Virol.* 69: 1600-1605.
- Chapman, M. R., and C. C. Kao.** 1999. A minimal RNA promoter for minus-strand RNA synthesis by the brome mosaic virus polymerase complex. *J Mol Biol.* 286(3): 709-720.
- Chaye, H., P. Chong, B. Tripet, B. Brush, and S. Gillam.** 1992. Localization of the virus neutralizing and hemagglutinin epitopes of E1 glycoprotein of rubella virus. *Virology* 189: 483-492.
- Chen, J., and P. Ahlquist.** 2000. Brome mosaic virus polymerase-like protein 2a is directed to the endoplasmic reticulum by helicase-like viral protein 1a. *J Virol.* 74(9): 4310-4318.
- Chen, J.-P., J. H. Strauss, E. G. Strauss, and T. K. Frey.** 1996. Characterization of the rubella virus nonstructural protease domain and its cleavage site. *J. Virol.* 70: 4707-4713.
- Chen, M. H., and T. K. Frey.** 1999. Mutagenic analysis of the 3' *cis*-acting elements of the rubella virus genome. *J. Virol.* 73(4): 3386-403.
- Cheng, R. H., R. J. Kuhn, N. H. Olson, M. G. Rossmann, H. K. Choi, T. J. Smith, T. S. Baker.** 1995. Nucleocapsid and glycoprotein organization in an enveloped virus. *Cell* 80(4): 621-30.
- Choi, G. H., D. M. Pawlyk, and D. L. Nuss.** 1991. The autocatalytic protease p29 encoded by hypovirulence-associated virus of the chestnut blight fungus resembles the potyvirus-encoded protease HC-Pro. *Virology* 183: 747-752.
- Choi, H. K., L. Tong, W. Minor, P. Dumas, U. Boege, M. G. Rossmann, G. Wengler.** 1991. Structure of Sindbis virus core protein reveals a chymotrypsin-like serine proteinase and the organization of the virion. *Nature* 354(6348): 37-43.

- Clarke, D. M., T. W. Loo, H. McDonald, and S. Gillam.** 1988. Expression of rubella virus cDNA coding for the structural proteins. *Gene* 65:23-30.
- Clarke, D. M., T. W. Loo, I. Hui, P. Chong, and S. Gillam.** 1987. Nucleotide sequence and *in vitro* expression of rubella virus 24S subgenomic mRNA encoding the structural proteins E1, E2, and C. *Nucleic Acid Res.* 15: 3041-3057.
- de Groot, R. J., R. G. van der Most, and W. J. M. Spann.** 1992. The fitness of defective interfering murine coronavirus DI-a and its derivatives is decreased by nonsense and frame-shift mutations. *J. Virol.* 66: 5898-5905.
- de Groot, R. J., W. R. Hardy, Y. Shirako, and J. H. Strauss.** 1990. Cleavage-site preferences of Sindbis virus polyproteins containing the nonstructural proteinase: evidence for temporal regulation of proteinase: evidence for temporal regulation of polyprotein processing *in vivo*. *EMBO J.* 9: 2631-2638.
- Delchambre, M., D. Gheysen, D. Thines, C. Thiriart, E. Jacobs, E. Verdin, M. Horth, A. Burny, and F. Bex.** 1989. The GAG precursor of simian immunodeficiency virus assembles into virus-like particles. *EMBO J.* 8: 2653-2660.
- Den Boon, J. A., K. S. Faaberg, J. J. M. Meulenberg, A. I. M. Wassenaar, P. G. W. Plagemann, A. E. Gornaleny, and E. J. Snijder.** 1995. Processing and evolution of the N-terminal region of the arterivirus replicase ORF1a protein: identification of two papain-like cysteine proteases. *J. Virol.* 69: 4500-4505.
- Diez, J., M. Ishikawa, M. Kaido, and P. Ahlquist.** 2000. Identification and characterization of a host protein required for efficient template selection in viral RNA replication. *Proc Natl Acad Sci U S A.* 97(8): 3913-3918.
- Dominguez, G., C. Y. Wang and T. K. Frey.** 1990. Sequence of the genome RNA of rubella virus: Evidence for genetic rearrangement during Togavirus evolution. *Virology* 177: 225-238.
- Dorsett, P. H., D. C. Miller, K. Y. Green, F. I. Byrd.** 1985. Structure and function of the rubella virus proteins. *Rev Infect Dis. Suppl* 1: S150-6.
- Doxsey, S. J., F. M. Brodsky, G. S. Blank, A. Helenius.** 1987. Inhibition of endocytosis by anti-clathrin antibodies. *Cell* 50(3): 453-63.
- Dreher, T. W., and T. C. Hall.** 1988a. Mutational analysis of the sequence and structural requirements in brome mosaic virus RNA for minus-strand promoter activity *J. Mol. Biol.* 201: 31-40.
- Dreher, T. W., and T. C. Hall.** 1988b. Mutational analysis of the tRNA mimicry of brome mosaic virus RNA *J. Mol. Biol.* 201: 41-55.
- Forng, R.-Y., and T. K. Frey.** 1995. Identification of the rubella virus nonstructural proteins. *Virology.* 206: 843-853.

Francki, R. I. B., C. M. Fauquet, D. L. Knudson, and F. Brown. (eds) 1991. Classification and nomenclature of viruses. Fifth report of the international committee on Taxonomy of Viruses. Archives of Virology, Suppl 2. Springer-Verlag, Vienna.

Frey, T. K. 1994. Molecular biology of rubella virus. Adv. in Virus Res. 44: 69-160.

Frey, T. K., and I. D. Marr. 1988. Sequence of the region coding virion proteins C and E2 and the carboxy terminus of the nonstructural proteins of rubella virus: comparison to alphavirus. Gene 62: 85-99.

Frolova, E., I. Frolov, S. Schlesinger. 1997. Packaging signals in alphaviruses. J. Virol. 71(1): 248-58.

Furuya, T., and M. M. C. Lai. 1993. Three different cellular proteins bind to complementary sites on the 5'- end-positive and 3'-end-negative strands of mouse hepatitis virus RNA. J. Virol. 67: 7215-7222.

Gallagher, P. J., J. M. Henneberry, J. F. Sambrook, and M. J. H. Gething. 1992. Glycosylation requirements for intracellular transport and function of the hemagglutinin of influenza virus. J. Virol. 66: 7136-7145.

Garoff, H., R. Hewson, and D. J. E. Opstelten. 1998. Virus maturation by budding. Microbiol Mol Biol Rev. 62(4): 1171-1190. Review.

Gerna, G., M. G. Revello, M. Dosis, E. Petruzzelli, G. Achilli, E. Percivall, M. Torsellini. 1987. Synergistic neutralization of rubella virus by monoclonal antibodies to viral haemagglutinin. J. Gen. Virol. 68: 2007-2012.

Gheysen, D., E. Jacobs, F. de Foresta, C. Thiriart, M. Francotte, D. Thines, and M. De Wilde. 1989. Assembly and release of HIV-1 precursor Pr55gag virus-like particles from recombinant baculovirus-infected cells. Cell 59: 103-112

Gorbalenya, A. E., A. P. Donchenko, V. M. Blinov, and E. V. Koonin. 1989a. Cysteine proteases of positive strand RNA viruses and chymotrypsin-like serine proteases. A distinct protein superfamily with a common structural fold. FEBS Lett. 243(2): 103-114.

Gorbalenya, A. E., E. V. Koonin, A. P. Donchenko, and V. M. Blinov. 1989b. Coronavirus genome: prediction of putative functional domains in the non-structural polyprotein by comparative amino acid sequence analysis. Nucleic Acids Res. 17(12): 4847-4861.

Gorbalenya, A. E., E. V. Koonin, and M. M.-C. Lai. 1991. Putative papain-related thiol proteases of positive-strand RNA viruses. FEBS Lett. 288: 201-205.

Gorbalenya, A. E., E. V. Koonin, and Y. I. Wolf. 1990. A new superfamily of putative NTP-binding domains encoded by genomes of small DNA and RNA viruses. FEBS Lett. 262: 145-148.

- Gorbalenya, A. E., V. M. Blinov, A. P. Donchenko, and E. V. Koonin.** 1989. An NTP-binding motif is the most conserved sequence in a highly diverged monophyletic group of proteins involved in positive strand RNA virus replication. *J. Mol. Evol.* 28: 256-268.
- Green, K. Y., and P. H. Dorsett.** 1986. Rubella virus antigens: localization of epitopes involved in hemagglutination and neutralization by using monoclonal antibodies. *J. Virol.* 57(3): 893-898.
- Guarne, A., J. Tormo, R. Kirchweger, D. Pfistermueller, I. Fita, and T. Skern.** 1998. Structure of the foot-and-mouth disease virus leader protease: a papain-like fold adapted for self-processing and eIF4G recognition. *EMBO J.* 17: 7469-7479.
- Hardy, W. R., and J. H. Strauss.** 1989. Processing the nonstructural polyproteins of Sindbis virus: nonstructural proteinase is in the C-terminal half of nsP2 and functions both in *cis* and in *trans*. *J. Virol.* 63: 4653-4664.
- Hemphill, M. L., R.-Y. Forng, E. S. Abernathy, and T.K. Frey.** 1988. Time course of virus-specific macromolecular synthesis during rubella virus infection in Vero cells. *Virology* 162: 65-75.
- Hobman, T. C., and S. Gillam.** 1989. *In vitro* and *in vivo* expression of rubella virus E2 glycoprotein: the signal peptide is located in the C-terminal region of capsid protein. *Virology* 173: 241-250.
- Hobman, T. C., L. Woodward, and M. G. Farquhar.** 1992. The rubella virus E1 glycoprotein is arrested in a novel post-ER, pre-Golgi complex. *J. Cell Biol.* 118: 781-792.
- Hobman, T. C., L. Woodward, and M. G. Farquhar.** 1993. The rubella virus E2 and E1 spike glycoproteins are targeted to the Golgi complex. *J. Cell Biol.* 121: 269-281.
- Hobman, T. C., M. L. Lundstrom, and S. Gillam.** 1990. Processing and intracellular transport of rubella virus structural proteins in COS cells. *Virology* 178: 122-133.
- Hobman, T. C., N. O. Seto., and S. Gillam.** 1994. Expression of soluble forms of rubella virus glycoproteins in mammalian cells. *Virus Res.* 31: 277-289.
- Hobman, T. C., R. Shukin, and S. Gillam.** 1988. Translocation of rubella virus glycoprotein E1 into the endoplasmic reticulum. *J. Virol.* 62: 4259-4264.
- Hobman, T. C., Z. Qiu, H. Chaye, and S. Gillam.** 1991. Analysis of rubella virus E1 glycosylation mutants expressed in COS cells. *Virology* 181: 768-772.
- Ho-Terry, L., and A. Cohen.** 1984. The role of glycosylation on haemagglutination and immunological reactivity of rubella virus. *Arch Virol.* 79: 139-146.
- Ho-Terry, L., and A. Cohen.** 1985. Rubella virus hemagglutinin: association with a single virion glycoprotein. *Arch Virol.* 72: 47-54.

- Ishikawa, M., J. Diez, M. Restrepo-Hartwig, and P. Ahlquist.** 1997. Yeast mutations in multiple complementation groups inhibit brome mosaic virus RNA replication and transcription and perturb regulated expression of the viral polymerase-like gene. *Proc Natl Acad Sci U S A.* 94(25): 13810-13815.
- Ito, Y., and M. M. C. Lai.** 1997. Determination of the secondary structure and cellular protein binding to the 3'-untranslated region of the hepatitis C virus RNA genome. *J. Virol.* 71: 8698-8706.
- Janda, M., and P. Ahlquist.** 1993. RNA-dependent replication, transcription, and persistence of brome mosaic virus RNA replicons in *S. cerevisiae*. *Cell* 72(6): 961-970.
- Jin, H., G. P. Leser, and R. A. Lamb.** 1994. The influenza virus hemagglutinin cytoplasmic tail is not essential for virus assembly or infectivity. *EMBO J.* 13: 5504-5515.
- Justice, P. A., W. Sun, Y. Li, Z. Ye, P. R. Grigera, and R. R. Wagner.** 1995. Membrane vesiculation function and exocytosis of wild-type and mutant matrix proteins of vesicular stomatitis virus. *J. Virol.* 69: 3156-3160.
- Kadare, G., and A.-L. Haenni.** 1997. Virus-encoded RNA helicases. *J. Virol.* 71: 2583-2590. Review.
- Kamer, G., and P. Argos.** 1984. Primary structural comparison of RNA-dependent polymerase from plant, animal and bacterial viruses. *Nucleic Acid Res.* 12: 7269-7282.
- Kamphuis, I. G., J. Drenth and E. N. Baker.** 1985. Thiol proteases. Comparative studies based on the high-resolution structures of papain and actinidin, and on amino acid sequence information for cathepsins B and H, and stem bromelain. *J. Mol Biol.* 182(2): 317-329.
- Kamphuis, I. G., K. H. Kalk, M. B. A. Swarte and J. Drenth.** 1984. Structure of papain refined at 1.65 Å resolution. *J. Mol. Biol.* 179: 233-256.
- Kao, C. C., and J. H. Sun.** 1996. Initiation of minus-strand RNA synthesis by the brome mosaic virus RNA-dependent RNA polymerase: use of oligoribonucleotide primers. *J. Virol.* 70: 6826-6830.
- Katow, S., and A. Sugiura.** 1988a. Conformational change of rubella virus spike proteins induced by 2-mercaptoethanol. *Jpn J Med Sci Biol.* 41: 109-115.
- Katow, S., and A. Sugiura.** 1988b. Low pH-induced conformational change of rubella virus envelope proteins. *J. Gen. Virol.* 69: 2797-2807.
- Kong, F., K. Sivakumaran, and C. Kao.** 1999. The N-terminal half of the brome mosaic virus 1a protein has RNA capping-associated activities: specificity for GTP and S-adenosylmethionine. *Virology* 259(1): 200-210.
- Koonin, E. V., and V. V. Dolja.** 1993. Evolution and taxonomy of positive-strand RNA viruses: implications of comparative analysis of amino acid sequences. *Crit. Rev. Biochem. Mol. Biol.* 28: 375-430.

- Kowal, E. V., and V. Stollar.** 1981. Temperature-sensitive host-dependent mutants of Sindbis virus. *Virology* 114: 140-148.
- Krol, M. A., N. H. Olson, J. Tate, J. E. Johnson, T. S. Baker, and P. Ahlquist.** 1999. RNA-controlled polymorphism in the *in vivo* assembly of 180-subunit and 120-subunit virions from a single capsid protein. *Proc Natl Acad Sci U S A.* 96(24): 13650-13655.
- Kuhn, R. J., X. Hong, and J. H. Strauss.** 1990. Mutagenesis of the 3' nontranslated region of Sindbis virus RNA. *J. Virol.* 64: 1465-1476.
- Laemmli, U. K.** 1970. Cleavage of structural proteins during assemble of the head of bacteriophage T4. *Nature* 227: 680-685.
- Lee, J. Y., D. Hwang, and S. Gillam.** 1996. Dimerization of rubella virus capsid protein is not required for virus particle formation. *Virology* 216: 223-227.
- Lee, J.-Y., J. A. Marshall, and D. S. Bowden.** 1992. Replication complexes associated with the morphogenesis of rubella virus. *Arch. Virol.* 122: 95-106.
- Lee, J.-Y., J. A. Marshall, and D. S. Bowden.** 1994. Characterization of rubella virus replication complexes using antibodies to double-stranded RNA. *Virology* 200: 307-312.
- Lemm, J. A., and C. M. Rice.** 1993a. Assembly of functional Sindbis virus RNA replication complexes: requirement for coexpression of P123 and P34. *J. Virol.* 67: 1905-1915.
- Lemm, J. A., and C. M. Rice.** 1993b. Roles of nonstructural polyproteins and cleavage products in regulating Sindbis virus RNA replication and transcription. *J. Virol.* 67: 1916-1926.
- Lemm, J. A., A. Bergqvist, C. M. Read, and C. M. Rice.** 1998. Template-dependent initiation of sindbis virus RNA replication *in vitro*. *J. Virol.* 72: 6546-6553.
- Lemm, J. A., T. Rümenapf, R. G. Strauss, J. H. Strauss, and C. M. Rice.** 1994. Polypeptide requirements for assembly of functional Sindbis virus replication complexes: a model for the temporal regulation of minus-strand and plus-strand RNA-synthesis. *EMBO J.* 13: 2925-2934.
- Li, H. P., X. Zhang, R. Duncan, L. Comai, and M. M. Lai.** 1997. Heterogeneous nuclear ribonucleoprotein A1 binds to the transcription-regulatory region of mouse hepatitis virus RNA. *Proc. Natl. Acad. Sci. USA* 94: 9544-9549.
- Li, Y., L. Luo, M. Schubert, R. R. Wagner, and C. Y. Kang.** 1993. Viral liposomes released from insect cells infected with recombinant baculovirus expressing the matrix protein of vesicular stomatitis virus. *J. Virol.* 67: 4415-4420.
- Liu, C., and G. M. Air.** 1993. Selection and characterization of a neuraminidase-minus mutant of influenza virus and its rescue by cloned neuraminidase genes. *Virology* 194: 403-407.

- Liu, C., M. C. Eichelberger, R. W. Compans, and G. M. Air.** 1995. Influenza type A virus neuraminidase does not play a role in viral entry, replication, assembly, or budding. *J. Virol.* 69: 1099-1106.
- Liu, X., S. L. Ropp, R. J. Jackson, and T. K. Frey.** 1998. The rubella virus nonstructural protease requires divalent cations for activity and functions in *trans*. *J. Virol.* 72: 4463-4466.
- Liu, Z., D. Yang, Z. Qiu, K.-T. Lim, P. Chong, and S. Gillam.** 1996. Identification of domains in rubella virus genomic RNA and capsid protein necessary for specific interaction. *J. Virol.* 70: 2184-2190.
- Lundstrom, M. L., C. A. Mauracher, and A. J. Tingle.** 1991. Characterization of carbohydrates linked to rubella virus glycoprotein E1. *J. Gen. Virol.* 72: 843-850.
- Mach, L., J. S. Mort, and J. Glossl.** 1994. Noncovalent complexes between the lysosomal proteinase cathepsin B and its propeptide account for stable, extracellular, high molecular mass forms of the enzyme. *J. Biol. Chem.* 269: 13036-13040.
- Magliano, D., J. A. Marshall, D. S. Bowden, N. Vardaxis, J. Meanger, and J.-Y. Lee.** 1998. Rubella virus replication complexes are virus-modified lysosomes. *Virology* 240: 57-63.
- Mahajan, S., V. Dolja, and J. C. Carrington.** 1996. Roles of the sequence encoding tobacco etch virus capsid protein in genome amplification : requirements for the translation process and a *cis*-active element. *J. Virol.* 70: 4370-4379.
- Maniatis, T., E. F. Fritsch, and J. Sambrook.** 1992. Molecular cloning: a laboratory manual, 2nd ed. Cold Spring Harbor Laboratory, Cold Spring Harbor, New York, N.Y.
- Mao, P. L., Y. Jiang, B. Y. Wee and A. G. Porter.** 1998. Activation of caspase-1 in the nucleus requires nuclear translocation of pro-caspase-1 mediated by its prodomain. *J Biol Chem.* 273(37): 23621-23624.
- Marr, L. D., A. Sanchez, T. K. Frey.** 1991. Efficient *in vitro* translation and processing of the rubella virus structural proteins in the presence of microsomes. *Virology* 180: 400-5.
- Marr, L. D., C.-Y. Wang, and T. K. Frey.** 1994. Expression of the rubella virus nonstructural protein ORF and demonstration of proteolytic processing. *Virology.* 198: 1-7.
- Matthews, D. A., W. W. Smith, R. A. Ferre, B. Condon, G. Budahazi, W. Sisson, J. E. Villafranca, C. A. Janson, H. E. McElroy, C. L. Gribskov, and S. Worland.** 1994. Structure of human rhinovirus 3C protease reveals a trypsin-like polypeptide fold, RNA-binding site, and means for cleaving precursor polypeptide. *Cell* 77(5): 761-71.
- Mauracher, C. A., S. Gillam, R. Shukin, and A. J. Tingle.** 1991. pH-dependent solubility shift of rubella virus capsid protein. *Virology* 181: 773-777.
- McDonald, H., T. C. Hobman, and S. Gillam.** 1991. The influence of capsid protein cleavage on the processing of E2 and E1 glycoproteins of rubella virus. *Virology* 183: 52-60.

- McIntyre, G. F. and A. H. Erickson.** 1993. The lysosomal proenzyme receptor that binds procathepsin L to microsomal membranes at pH5 is a 43-kDa integral membrane protein. *Proc. Natl. Acad. Sci. USA* 90: 10588-10592.
- Mebatsion, T., M. König, and K.-K. Conzelmann.** 1996. Budding of rabies virus particles in the absence of the spike glycoprotein. *Cell* 84: 941-951
- Melancon, P., and H. Garoff.** 1987. Processing of the Semliki Forest virus structural polyprotein: role of the capsid protease. *J. Virol.* 61: 1301-1309.
- Miller, W. A., J. J. Bujarski, T. W. Dreher, and T. C. Hall.** 1986. Minus-strand initiation by brome mosaic virus replicase within the 3' tRNA-like structure of native and modified RNA templates. *J. Mol. Biol.* 187: 537-546.
- Mitnaul, L. J., M. R. Castrucci, K. G. Murti, and Y. Kawaoka.** 1996. The cytoplasmic tail of influenza A virus neuraminidase (NA) affects NA incorporation into virions, virion morphology, and virulence in mice but is not essential for virus replication. *J. Virol.* 70: 873-879
- Molla, A., A. V. Paul, and E. Wimmer.** 1991. Cell-free, de novo synthesis of poliovirus. *Science* 254: 1647-1651.
- Murphy, F. A.** 1980. Togavirus morphology and morphogenesis. p241-316. In R. W. Schlesinger (ed.). *The Togaviruses*. Academic Press, New York.
- Murphy, F. A., C. M. Fauquet, D. H. L. Bishop, S. A. Ghabrial, A. W. Jarvis, G. P. Martelli, M. A. Mayo, and M. D. Summers.** 1995. *Virus Taxonomy: The Classification and Nomenclature of Viruses. The Sixth Report of the International Committee on Taxonomy of Viruses* (book). Springer-Verlag, Vienna,
- Murphy, F. A., P. E. Halonen, A. K. Harrison.** 1968. Electronmicroscopy of the development of rubella virus. *J. Virol.* 2: 1223-1227.
- Myers, E., and W. Miller.** 1988. Optimal alignments in linear space. *CABIOS* 4:11-17.
- Naim, H. Y., and H. Koblet.** 1990. The cleavage of p62, the precursor of E2 and E3, is an early and continuous event in Semliki Forest virus-infected *Aedes albopictus* cells. *Arch. Virol.* 110: 221-237.
- Nakhasi, H. L., D. X. Zheng, I. K. Hewlett, and T. Y. Liu.** 1988. Rubella virus replication: effect of interferons and actinomycin D. *Virus Res.* 10(1): 1-15.
- Nakhasi, H. L., N. K. Singh, G. P. Pogue, X. Q. Cao, and T. A. Rouault.** 1994. Identification and characterization of host factor interactions with *cis*-acting elements of rubella virus RNA. *Arch Virol Suppl.* 9: 255-267.
- Nakhasi, H. L., T. A. Rouault, D. J. Haile, T.-Y. Liu, and R. D. Klausner.** 1990. Specific high-affinity binding of host cell proteins to the 3' region of rubella virus RNA. *New Biol.* 2: 255-264.

- Nakhasi, H. L., X. Q. Cao, T. A. Rouault, and T. Y. Liu.** 1991. Specific binding of host cell proteins to the 3'-terminal stem-loop structure of rubella virus negative-strand RNA. *J. Virol.* 65(11): 5961-5967.
- Neeleman, L., and J. F. Bol.** 1999. *Cis*-acting functions of alfalfa mosaic virus proteins involved in replication and encapsidation of viral RNA. *Virology* 254: 324-333.
- Nestorowicz, A., T. S. Chambers, and C. M. Rice.** 1994. Mutagenesis of the yellow fever virus NS2A/2B cleavage site: effects on proteolytic processing, viral replication and evidence for alternative processing of the NS2A protein. *Virology* 199: 114-123.
- Ng, D. P., S. W. Hiebert, and R. A. Lamb.** 1990. Different roles of individual N-linked oligosaccharide chains in folding, assembly, and transport of the simian virus 5 hemagglutinin neuraminidase. *Mol. Cell Biol.* 10: 1989-2001.
- Niesters, H. G. M., and J. H. Strauss.** 1990. Defined mutations in the 5' nontranslated sequence of Sindbis virus RNA. *J. Virol.* 64: 4162-4168.
- Novak, J. E. and K. Kirkegaard.** 1991. Improved method for detecting poliovirus negative strands used to demonstrate specificity of positive-strand encapsidation and the ratio of positive to negative strands in infected cells. *J. Virol.* 65: 3384-3387.
- Novak, J. E., and K. Kirkegaard.** 1994. Coupling between genome translation and replication in an RNA virus. *Genes Dev.* 8: 1726-1737.
- Oh, C. S., and J. C. Carrington.** 1989. Identification of essential residues in potyvirus proteinase HC-Pro by site-directed mutagenesis. *Virology* 173(2): 692-9.
- Oker-Blom, C.** 1984. The gene order for rubella virus structural proteins is NH₂-C-E2-E1-COOH. *J. Virol.* 51: 354-358.
- Oker-Blom, C., I. Ulmanen, L. Kaariainen, and R. F. Pettersson.** 1984. Rubella virus 40S genome RNA specifies a 24S subgenomic mRNA that codes for a precursor to structural proteins. *J. Virol.* 49: 403-408.
- Oker-Blom, C., N. Kalkkinen, L. Kaariainen, and R. F. Pettersson.** 1983. Rubella virus contains one capsid protein and three envelope glycoproteins, E1, E2a, and E2b. *J. Virol.* 46(3): 964-973.
- O'Reilly, E. K., and C. C. Kao.** 1998. Analysis of RNA-dependent RNA polymerase structure and function as guided by known polymerase structures and computer predictions of secondary structure. *Virology* 252: 287-303. Review.
- Owen, K. E., and R. J. Kuhn.** 1996. Identification of a region in the Sindbis virus nucleocapsid protein that is involved in specificity of RNA encapsidation. *J. Virol.* 70(5): 2757-2763.

- Pardigon, N., and J. H. Strauss.** 1992. Cellular proteins bind to the 3' end of Sindbis virus minus strand RNA. *J. Virol.* 66: 1007-1015.
- Pardigon, N., and J. H. Strauss.** 1996. Mosquito homolog of the La autoantigen binds to Sindbis virus RNA. *J. Virol.* 70(2): 1173-81.
- Pardigon, N., E. Lenches, and J. H. Strauss.** 1993. Multiple binding sites for cellular proteins in the 3' end of Sindbis alphavirus minus sense RNA. *J. Virol.* 67: 5003-5011.
- Paredes, A. M., M. N. Simon, D. T. Brown.** 1992. The mass of the Sindbis virus nucleocapsid suggests it has $T=4$ icosahedral symmetry. *Virology* 187(1): 329-332.
- Pattnaik, A. K., D. J. Brown, and D. P. Nayak.** 1986. Formation of influenza virus particles lacking hemagglutinin on the viral envelope. *J. Virol.* 60: 994-1001.
- Payment, R., D. Ajdukovic, V. Pavlanis.** 1975. Rubella virus. I. Morphology and structural proteins. *Can J Microbiol.* 21(5): 703-709. French.
- Phillips, M. A., and W. J. Rutter.** 1996. Role of the prodomain in folding and secretion of rat pancreatic carboxypeptidase A1. *Biochemistry* 35: 6771-6776.
- Piccone, M. E., M. Zellner, T. F. Kumosinski, P. W. Mason, and M. J. Grubman.** 1995. Identification of the active-site residues of the L proteinase of foot-and-mouth disease virus. *J. Virol.* 69: 4950-4956.
- Pogue, G. P., C. C. Huntley, and T. C. Hall.** 1994. Common replication strategies emerging from the study of diverse groups of positive-strand RNA viruses. *Arch Virol Suppl.* 9: 181-194. Review.
- Pogue, G. P., X.-Q. Cao, N. K. Singh, and H. L. Nakhasi.** 1993. 5' sequences of rubella virus RNA stimulate translation of chimeric RNAs and specifically interact with two host-encoded proteins. *J. Virol.* 67: 7106-7117.
- Pogue, G., P. Hofmann, R. Duncan, J. M. Best, J. Etherington, R. D. Sontheimer, and H. L. Nakhasi.** 1996. Autoantigens interact with *cis*-acting elements of rubella virus RNA. *J. Virol.* 70: 6269-6277.
- Pugachev, K. V., and T. K. Frey.** 1998. Effects of defined mutations in the 5' nontranslated region of rubella virus genomic RNA on virus viability and macromolecule synthesis. *J. Virol.* 72(1): 641-650.
- Pugachev, K. V., E. S. Abernathy, and T. K. Frey.** 1997a. Genomic sequence of the RA27/3 vaccine strain of rubella virus. *Arch Virol.* 142(6): 1165-1180.
- Pugachev, K. V., E. S. Abernathy, and T. K. Frey.** 1997b. Improvements of the specific infectivity of the rubella virus (RUB) infectious clone; determinants of cytopathogenicity induced by RUB map to the nonstructural proteins. *J. Virol.* 71: 562-568.

Qiu, Z., F. Tufaro, and S. Gillam. 1992a. The influence of N-linked glycosylation on the antigenicity and immunogenicity of rubella virus E1 glycoprotein. *Virology* 190: 876-881.

Qiu, Z., T. C. Hobman, H. McDonald, N. O. Seto, and S. Gillam. 1992b. Role of N-linked oligosaccharides in processing and intracellular transport of E2 glycoprotein of rubella virus. *J. Virol.* 66: 3514-3521.

Qiu, Z., D. Ou, H. Wu, T. C. Hobman, and S. Gillam. 1994a. Expression and characterization of virus-like particles containing rubella virus structural proteins. *J. Virol.* 68: 4086-4091.

Qiu, Z., H. McDonald, J. Chen, T. C. Hobman, and S. Gillam. 1994b. Mutational analysis of the arginine residues in the E2-E1 junction region on the proteolytic processing of the polyprotein precursor of rubella virus. *Virology* 100: 821-825.

Quadt, R., and E. M. Jaspars. 1990. Purification and characterization of brome mosaic virus RNA-dependent RNA polymerase. *Virology*. 178(1): 189-194.

Ramos, C., J. R. Winther, M. C. Kielland-Brandt. 1994. Requirement of the propeptide for *in vivo* formation of active yeast carboxypeptidase Y. *J. Biol.Chem.* 269: 7006-7012.

Rawlings, N. D., and A. J. Barrett. 1993. Evolutionary families of peptidases. *Biochem. J.* 290: 205-218.

Restrepo-Hartwig, M., and P. Ahlquist. 1996. Brome mosaic virus helicase- and polymerase-like proteins colocalize on the endoplasmic reticulum at sites of viral RNA synthesis. *J. Virol.* 70(12): 8908-8916.

Restrepo-Hartwig, M., and P. Ahlquist. 1999. Brome mosaic virus RNA replication proteins 1a and 2a colocalize and 1a independently localizes on the yeast endoplasmic reticulum. *J. Virol.* 73(12): 10303-10309.

Roehl, H. H., T. B. Parsley, T. V. Ho, and B. L. Semler. 1997. Processing of a cellular polypeptide by 3CD proteinase is required for poliovirus ribonucleoprotein complex formation. *J. Virol.* 71(1): 578-585.

Rost, B. and C. Sander. 1993a. Improved prediction of protein secondary structure by use of sequence profiles and neural networks. *Proc. Natl. Acad. Sci. U.S.A.* 90: 7558-7562.

Rost, B. and C. Sander. 1993b. Prediction of protein structure at better than 70% accuracy. *J. Mol. Biol.* 232: 584-599.

Rost, B. and C. Sander. 1994a. Combining evolutionary information and neural networks to predict protein secondary structure. *Proteins* 19: 55-72.

Rost, B., C. Sander and R. Schneider. 1994b. PHD - an automatic mail server for protein secondary structure prediction. *CABIOS* 10: 53-60.

- Rozanov, M. N., E. V. Koonin, and A. E. Gorbalenya.** 1992. Conservation of the putative methyltransferase domain: a hallmark of the "Sindbis-like" supergroup of positive-strand RNA virus. *J. Gen. Virol.* 73(8): 2129-2134.
- Sanchez, A., and T. K. Frey.** 1991. Vaccinia-vectored expression of rubella virus structural proteins and characterization of the E1 and E2 glycosidic linkages. *Virology* 183: 636-646.
- Sawicki, D. L., and S. G. Sawicki.** 1980. Short-lived minus-strand polymerase for Semliki Forest virus. *J. Virol.* 34: 108-118.
- Sawicki, S. G., D. L. Sawicki, L. Kääriäinen, and S. Keränen.** 1981. A Sindbis virus mutant temperature-sensitive in the regulation of minus-strand RNA synthesis. *Virology* 115: 161-172.
- Schaad, M. C., R. Haldeman-Cahill, S. Cronin, and J. C. Carrington.** 1996. Analysis of the VPg-proteinase (NIa) encoded by tobacco etch potyvirus: Effects of mutations on subcellular transport, proteolytic processing, and genome amplification. *J. Virol.* 70: 7039-7048.
- Schechter, I., and A. Berger.** 1967. On the size of the active site in proteases. *Biochem. Biophys. Res. Com.* 27: 157-162.
- Schmid, M., and E. Wimmer.** 1994. IRES-controlled protein synthesis and genome replication of poliovirus. *Arch Virol Suppl.* 9: 279-289. Review.
- Schnell, M. J., T. Mebatsion, and K.-K. Conzelmann.** 1994. Infectious rabies viruses from cloned cDNA. *EMBO J.* 13: 4195-4203.
- Scholthof, J. B., and A. O. Jackson.** 1997. The enigma of pX: A host-dependent *cis*-acting element with various effects on tombus-virus RNA accumulation. *Virology* 237: 56-65.
- Shapira, R., and D. L. Nuss.** 1991. Gene expression by a hypovirulence-associated virus of the chestnut blight fungus involves 2 papain-like proteinase activities: essential residues and cleavage site requirements for p48 autoproteolysis. *J. Biol. Chem.* 266: 19419-19425.
- Shirako, Y., and J. H. Strauss.** 1994. Regulation of Sindbis virus RNA replication: uncleaved P123 and nsP4 function in minus strand RNA synthesis whereas cleaved products from P123 are required for efficient plus strand RNA synthesis. *J. Virol.* 68: 1874-1885.
- Siegel, R. W., S. Adkins, and C. C. Kao.** 1997. Sequence-specific recognition of a subgenomic promoter by a viral RNA polymerase. *Proc. Natl Acad. Sci. USA* 94: 11238-11243.
- Simons, K., and H. Garoff.** 1980. The budding mechanism of enveloped animal viruses. *J. Gen. Virol.* 50: 1-21.
- Singer, S. J., P. A. maher, and M. P. Yaffe.** 1987. On the transfer of integral membrane protein into membranes. *Prot. Natl. Acad. Sci. USA.* 84: 1960-1964.
- Singh, N. K., C. D. Atreya, and H. L. Nakhasi.** 1994. Identification of calreticulin as a rubella virus RNA binding protein. *Proc. Natl. Acad. Sci. USA* 91: 12770-12774

- Sivakumaran, K. and C.C. Kao.** 1999. Initiation of genomic positive strand synthesis from DNA and RNA templates by a viral RNA-dependent RNA polymerase. *J. Virol.* 73: 6415—6423.
- Sivakumaran, K., C. H. Kim, R. Jr. Tayon, and C. C. Kao.** 1999. RNA sequence and secondary structural determinants in a minimal viral promoter that directs replicase recognition and initiation of genomic plus-strand RNA synthesis. *J Mol Biol.* 294(3): 667-682.
- Skern, T., I. Fita and A. Guarne.** 1998. A structural model of picornavirus leader proteinases based on papain and bleomycin hydrolase. *J. Gen. Virol.* 79: 301-307.
- Snijder, E. J., A. L. M. Wassenaar, and W. J. M. Spaan.** 1992. The 5' end of the equine arteritis virus replicase gene encodes a papain-like cysteine protease. *J. Virol.* 66: 7040-7048.
- Spangberg, K., L. Goobar-Larsson, M. Wahren-Herlenius, and S. Schwartz.** 1999. The La protein from human liver cells interacts specifically with the U-rich region in the hepatitis C virus 3' untranslated region. *J Hum Virol.* 2(5): 296-307.
- Strauss, E. G., and J. H. Strauss.** 1986. Structure and replication of the alphavirus genome, p. 35-90. In S. Schlesinger and M. J. Schlesinger (ed.), *The Togaviridae and Flaviviridae*. Plenum publishing Corp., New York.
- Strauss, E. G., R. J. de Groot, R. Levinson, and J. H. Strauss.** 1992. Identification of the active site residues in the nsP2 proteinase of Sindbis virus. *Virology* 191: 932-940.
- Strauss, J. H., and E. G. Strauss.** 1994. The alphaviruses: Gene expression, replication, evolution. *Microbiol. Rev.* 58: 491-562. Review.
- Sullivan, M. L., and P. Ahlquist.** 1999. A brome mosaic virus intergenic RNA3 replication signal functions with viral replication protein 1a to dramatically stabilize RNA *in vivo*. *J. Virol.* 73(4): 2622-2632.
- Sun, J. H., S. Adkins, G. Faurete, and C. C. Kao.** 1996. Initiation of (-)-strand RNA synthesis catalyzed by the BMV RNA-dependent RNA polymerase: synthesis of oligonucleotides. *Virology* 226(1): 1-12.
- Suomalainen, M., H. Garoff, and M. D. Baron.** 1990. The E2 signal sequence of rubella virus remains part of the capsid protein and confers membrane association *in vitro*. *J. Virol.* 64: 5500-5509.
- Suomalainen, M., P. Liljestrom, and H. Garoff.** 1992. Spike protein-nucleocapsid interactions drive the budding of alphaviruses. *J. Virol.* 66: 4737-4747.
- Svitkin, Y. V., K. Meerovitch, H. S. Lee, J. N. Dholakia, D. J. Kenan, V. I. Agol, and N. Sonenberg.** 1994. Internal translation initiation on poliovirus RNA: further characterization of La function in poliovirus translation *in vitro*. *J. Virol.* 68: 1544-1550.

- Takkinen, K., J. Peranen, and L. Kaariainen.** 1991. Proteolytic processing of Semliki Forest virus-specific non-structural polyprotein. *J. Gen Virol.* 72: 1627-1633.
- Tao, K., N. A. Stearns, J. Dong, Q. L. Wu, and G. G. Sahagian.** 1994. The proregion of cathepsin L is required for proper folding stability, and ER exit. *Arch. Biochem. Biophys.* 311: 19-27.
- Teng, H., J. D. Pinon and S. R. Weiss.** 1999. Expression of murine coronavirus recombinant papain-like proteinase: efficient cleavage is dependent on the lengths of both the substrate and the proteinase polypeptides. *J. Virol.* 73: 2658-2666.
- Terry, G. M., L. Ho-Terry, P. Londesborough, and K. R. Rees.** 1988. Localization of the rubella E1 epitopes. *Arch. Virol.* 98: 189-197.
- Tesh, R. B., and L. Rosen.** 1975. Failure of rubella virus to replicate in mosquitos. *Intervirology.* 5(3-4): 216-219.
- Trudel, M., F. Nadon, C. Sequin, A. Amarouch, P. Payment, and S. Gillam.** 1985. E1 glycoprotein of rubella virus carries an epitope that binds a neutralizing antibody. *J. Virol. Methods* 12: 243-250.
- Trudel, M., M. Ravaoarinoro, and P. Payment.** 1980. Reconstitution of rubella hemagglutinin on liposome. *Can J. Microbiol.* 26: 899-904.
- Tsuchihara, K., T. Tanaka, M. Hijikata, S. Kuge, H. Toyoda, A. Nomoto, N. Yamamoto, and K. Shimotohno.** 1997. Specific interaction of polypyrimidine tract-binding protein with the extreme 3'-terminal structure of the hepatitis C virus genome, the 3'X. *J Virol.* 71(9): 6720-6726.
- Umino, Y., T. A. Sato, S. Katow, T. Matsuno, and A. Sugiura.** 1985. Monoclonal antibodies directed to E1glycoprotein of rubella virus. *Arch Virol.* 83: 33-42.
- Van Bokhoven, H., O. Le Gall, D. Kasteel, J. Verver, J. Wellink, and A. van Kammen.** 1993. *Cis*- and *trans*-acting elements in cowpea mosaic virus RNA replication. *Virology* 195: 377-386.
- Vennema, H., G.-J. Godeke, J. W. A. Rossen, W. F. Voorhout, M. C. Horzinek, D.-J. E. Opstelten, and P. J. M. Rottier.** 1996. Nucleocapsid-independent assembly of coronavirus-like particles by co-expression of viral envelope protein genes. *EMBO J.* 15:2020-2028.
- Vidgren, G., K. Takkinen, N. Kalkkinen, L. Kaarianen, and R. F. Pettersson.** 1987. Nucleotide sequence of the genes coding for the membrane glycoproteins E1 and E2 of rubella virus. *J. Gen. Virol.* 68: 2347-2357.
- Vogel, R. H., S. W. Provencher, C. H. von Bonsdorff, M. Adrian, J. Dubochet.** 1986. Envelope structure of Semliki Forest virus reconstructed from cryo-electron micrographs. *Nature* 320: 533-535.

- Waxham, M. N., and J. S. Wolinsky.** 1983. Immunochemical identification of rubella virus hemagglutinin. *Virology* 126: 194-203.
- Waxham, M. N., and J. S. Wolinsky.** 1985a. A model of the structural organization of rubella virions. *Rev. Inf. Dis.* 7 (Suppl. 1): S133-S139.
- Waxham, M. N., and J. S. Wolinsky.** 1985b. Detailed immunologic analysis of the structural polypeptides of rubella virus using monoclonal antibodies. *Virology* 143: 153-165.
- Weiland, J. J., and T. W. Dreher.** 1993. *Cis*-preferential replication of the turnip yellow mosaic virus RNA genome. *Proc. Natl. Acad. Sci. USA* 90: 6095-6099.
- White, C. L., M. Thomson, and N. J. Dimmock.** 1998. Deletion analysis of a defective interfering Semliki Forest virus RNA genome defines a region in the nsP2 sequence that is required for efficient packaging of the genome into virus particles. *J. Virol.* 72(5): 4320-4326.
- White, K. A., J. B. Bancroft, and G. A. Mackie.** 1992. Coding capacity determines *in vivo* accumulation of defective RNA of clover yellow mosaic virus. *J. Virol.* 66: 3069-3076.
- Wimmer, E., C. U. T. Hellen, and X. Cao.** 1993. Genetics of poliovirus. *Annu. Rev. Genet.* 27: 353-436.
- Wolinsky, J. S.** 1996. Rubella. p899-921. In B.N. Fields, D.M. Knipe, P.M. Howley, *et al.* (ed), *Fields Virology*, third edition. Lipincott-Raven Publishers, Philadelphia.
- Wolinsky, J. S., M. McCarthy, O. Allen-Cannady, W. T. Moore, R. Jin, S. N. Cao, A. lovett, and D. Simmons.** 1991. Monoclonal antibody-defined epitope map of expressed rubella virus protein domains. *J. Virol.* 65: 3986-3994.
- Xu, J., E. Mendez, P. R. Caron, C. Lin, M. A. Murcko, M. S. Collett, and C. M. Rice.** 1997. Bovine viral diarrhea virus NS3 serine proteinase: polyprotein cleavage sites, cofactor requirements, and molecular model of an enzyme essential for pestivirus replication. *J. Virol.* 71: 5312-5322.
- Yang, D., D. Hwang, Z. Qiu, and S. Gillam.** 1998. Effects of mutations in the rubella virus E1 glycoprotein on E1-E2 interaction and membrane fusion activity. *J. Virol.* 72: 8747-8755.
- Yao, J., and S. Gillam.** 1999. Mutational analysis, using a full-length rubella virus cDNA clone, of rubella virus E1 transmembrane and cytoplasmic domains required for virus release. *J. Virol.* 73: 4622-4630.
- Yao, J., and S. Gillam.** 2000. A single-amino-acid substitution of a tyrosine residue in the rubella virus E1 cytoplasmic domain blocks virus release. *J. Virol.* 74(7): 3029-3036.
- Yao, J., D. Yang, P. Chong, D. Hwang, Y. Liang, and S. Gillam.** 1998. Proteolytic processing of rubella virus nonstructural proteins. *Virology* 246(1): 74-82.
- Yu, W., and J. L. Leibowitz.** 1995. Specific binding of host cellular proteins to multiple sites within the 3' end of mouse hepatitis virus genomic RNA. *J. Virol.* 69(4): 2016-2023.

Zhou, H., and A. O. Jackson. 1996. Analysis of cis-acting elements required for replication of barley stripe mosaic virus RNAs. *Virology* 219(1): 150-160.